

**Corrosion of Carbon Steel in Stirred Two
Phase Media of Brine-Gas oil and Brine-CO₂
and Prevention by Cathodic Protection**

A Thesis

**Submitted to the College of Engineering of Alnahrain University in
Partial Fulfillment of the Requirements for the
Degree of Master of Science
in
Chemical Engineering**

by

Sahir Mohammed Aziz

(B.Sc. in Chemical Engineering 2011)

**Sha'ban
June**

**1435
2014**

تأكل الفولاذ الكربوني تحت ظروف الخلط في وسط ثنائي
الطور لمحلول ملحي مع زيت الغاز وثنائي أوكسيد الكربون
والسيطرة عليه بالحماية الكاثودية

رسالة

مقدمة إلى كلية الهندسة في جامعة النهريين
و هي جزء من متطلبات نيل درجة ماجستير علوم
في الهندسة الكيمياءوية

من قبل

ساهر محمد عزيز

(بكالوريوس علوم في الهندسة الكيمياءوية ٢٠١١)

شعبان
حزيران

١٤٣٥
٢٠١٤

Certification

I certify that this thesis entitled "Corrosion and its control of carbon steel in petroleum-brine mixture under flow conditions" was prepared by **Sahir Mohammed Aziz** under my supervision at Alnahrain University / College of Engineering in partial fulfillments of the requirements for the degree of Master of Science in Chemical Engineering.

Signature:

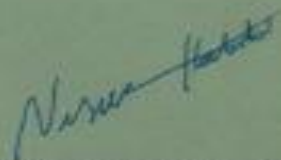


Name: **Asst. Prof. Dr. Basim O. Hasan**

(Supervisor)

Date: 1/6/2014

Signature:



Name: **Asst. Prof. Dr. Naseer A. Al-Habobi**

(Head of Department)

Date: 1/6/2014

Committee Certificate

Examining Committee, after reading this thesis "Corrosion of Carbon
Saturated Two Phase Media of Brine-Gas oil and Brine-CO₂ and
its Protection by Cathodic Protection" and examining the student "Sahir
Abdul Aziz" in its content, find it is adequate as a thesis for the degree of
Master of Science in Chemical Engineering.

I. K. Salih

Asst. Prof. Dr. Issam K. Salih

Chairman

7/7/2014

B. A.

Dr. Basma Abbas
Member

Yasser L. Abdulaziz

Dr. Yasser L. Abdulaziz
Member

7/7/2014

Basim O. Hasan

Asst. Prof. Dr. Basim O. Hasan

Supervisor and Member

2/7/2014

Approved by the College of Engineering/ Alnahrain University

Jassim Abbood Abbas Aldabbagh

Prof. Dr. Jassim Abbood Abbas Aldabbagh

Dean, College of Engineering /Alnahrain University

1 / 2014

Abstract

Corrosion tests of carbon steel (CS) in single and two phase media of two immiscible liquids (CaCO₃ solution-gasoil mixture) and liquid-gas (CaCO₃ solution -CO₂ gas) under different operating conditions of temperature, agitation velocity, phase fractions, gas flow rate, and immersion time were carried out using weight loss method and electrochemical polarization technique. Flat blade disc turbine mixer was used to simulate the two phase flow conditions.

The ranges of operating parameters in two immiscible phase tests were agitation velocities of (0 - 1200 rpm), temperature of (25- 45 °C), (1-10 vol %) gas oil. The effect of presence of acids such as HCl and H₂SO₄ on corrosion rate was also investigated under different conditions.

Corrosion rate (i_L) measurements in CO₂ saturated solution were also attained in different operating conditions of temperatures(25- 45 °C), agitation velocity (0-800 rpm), salts concentrations (2.5×10^{-3} to 9.9×10^{-3} M), CO₂ flow rate (0.142 to 1.132 m³/h), and immersion time by determining the limiting current density.

The pH values, oxygen solubility, and electrical conductivity of tested solutions were measured under all to interpret the obtained result.

The results revealed that increasing agitation velocity and temperature leads to an increase of the corrosion rate in single phase brine solution. The corrosion rate in brine-gasoil mixture is irregularly varied with concentration of gasoil and agitation velocity. The limiting current density in single phase CaCO₃ increases with the increase in agitation velocity, concentration of brine, and temperature. The corrosion rate in two phase brine-CO₂ mixture decreases with the increase of agitation velocity flow rate of CO₂, temperature, and immersion

time. The corrosion potential of Carbon steel under various conditions were determined and discussed.

Cathodic protection was used to protect carbon steel in brine-CO₂ mixture by using zinc as sacrificial anode under different operating conditions of flow rate of CO₂, agitation velocity, and temperature. Good corrosion protection efficiency was attained.

List of Contents

Contents	Page
Abstract	I
List of Contents	III
Nomenclature	VII
Greek Symbols	VIII
Abbreviations	IX
List of Tables	IX
List of Figures	XIV

Chapter One : Introduction

Introduction	1
Aim of the work	4

Chapter Two: Corrosion in Petroleum Industry

2.1	Corrosion Theory	5
2.2	Corrosion Cell	5
2.2.1	Corrosion Cell Parts	5
2.2.2	Types of Cells	7
2.3	Classification of Corrosion	7
2.3.1	wet Corrosion	8
2.3.2	Dry Corrosion	8
2.4	Factors Effecting Corrosion Rate	9
2.4.1	Diffusion	9
2.4.2	Solution pH	9

2.4.3	Effect of Temperature	10
2.4.4	Effect of velocity	12
2.5	Oxygen Reductions and Transport	14
2.6	Differential oxygen concentration	15
2.7	Limiting Current Density	16
2.8	Polarization	17
2.9	Polarization Types	19
2.9.1	Activation Polarization	19
2.9.2	Concentration Polarization	20
2.9.3	Combined Polarization	21
2.9.4	Resistance Polarization	21
2.10	Cathodic Protection	22
2.11	Sacrificial Anode method	23
2.12	Sacrificial Material	24
2.13	Corrosion in Petroleum Industry	26
2.13.1	Introduction	26
2.13.2	Acidization of oil well	27
2.13.3	Carbon Dioxide (sweet) corrosion	29
2.13.4	Mechanisms CO ₂ Corrosion	30
2.14	Corrosion of iron in by Acids in petroleum industry	32
2.15	Mixing And Agitation	34
2.15.1	Standard Turbine Design	35
2.15.2	Mixing of Liquids	36
2.15.3	Gas-liquid mixing	37
2.16	Literature Review	37

Chapter Three: Experimental Work

3.1	Introduction	41
3.2	Material Analysis	42
3.3	The Solutions	42
3.4	Materials	43
3.5	Experimental Apparatus	44
3.6	Agitation System	46
3.7	Experimental Procedures	48
3.7.1	Weight Loss Experiments	48
3.7.2	Working Solution Preparation	49
3.7.3	Polarization Experiments	50
3.7.4	Corrosion control experiments	51

Chapter Four : Results

4.1	Introduction	52
4.2	Corrosion rate in CaCO_3 solution	52
4.3	Corrosion rate in two phase mixture	53
4.4	Corrosion rate of two phase mixture in presence of acids	59
4.5	Corrosion rate in two phase system (CaCO_3 - CO_2)	66
4.6	Cathodic Protection Results	66
4.6.1	Corrosion Rate Results with sacrificial anode.	66
4.6.2	Protection Potential with time	68

Chapter Five: Discussion

5.1	Introduction	69
5.2	Corrosion rate in single phase CaCO_3	69
5.3	Corrosion rate in two phase brine – gasoil	70

5.4	Corrosion rate of two phase mixture in presence of acids	72
5.5	Polarization results	78
5.5	Cathodic polarization of brine (CaCO ₃) solution	78
5.5.1	Corrosion Rate	78
5.5.1	Corrosion Potential	82
5.6	Cathodic polarization of CaCO ₃ in presence CO ₂	86
5.6.1	Corrosion rate	86
5.6.2	Corrosion Potential	94
5.7	Cathodic Protection Results	97
5.7.1	Protection Potential	98
5.7.2	Corrosion rates in presence of sacrificial anode	103
Chapter Six	Conclusions and Recommendations	
6.1	Conclusions	107
6.2	Recommendations	108
References		109
 Appendices		
Appendix -A-	Physical Properties of Water	A-1
Appendix -B-	Measured Experimental Value of pH,...	B-1
Appendix -C-	Polarization Curves	C-1
Appendix -D-	Cathodic Protection Data	D-1

Nomenclature

Symbol	Meaning	Units
A	Surface area of specimen	m^2
C_b	Bulk concentration	ppm (mg/L)
d	diameter of specimen	m
L	Length of specimen	m
D	Diffusivity	m^2/s
D_a	Diameter of impeller	m
D_t	Diameter of tank	m
H	Height of tank	m
J	Width of baffles	m
W	Width of impeller	m
N_i	Rotational speed of impeller	rev./s
E	Electrode potential	V
E_a	Activation energy	kJ/mol
$E_{corr.}$	Corrosion potential	V
F	Faraday No. (96487)	Columb/equivalent
I	Current	A
i	current density	A/m^2
$i_{corr.}$	Corrosion current density	A/m^2
i_L	Limiting current density	A/m^2
k	Mass transfer coefficient	m/s
N_{Fe}	molar flux of iron	mole/ $m^2.s$
N_{O_2}	Molar flux of oxygen	mole / $m^2.s$

Re	Reynolds number	dimensionless
t	Immersion time	h.
T	Temperature	°C
u	Agitation velocity	rpm
Z	Number of electrons transferred	...
ΔW	Weight loss	g

Greek symbols

Symbol	Meaning	Units
μ	Fluid viscosity	kg/m. s
ρ	Fluid density	kg/m ³
δ	Thickness of diffusion layer	m
η	Polarization overpotential	V
η^T	Total overpotential	V
η^A	Activation overpotential	V
η^C	Concentration overpotential	V
η^R	Resistance overpotential	V
E_{eq}	The equilibrium potential	V
E_i	The polarized (current flowing) potential	V

Abbreviations

Abbreviation	Meaning
CR	Corrosion rate
CS	Carbon steel

CD	Cathodic Protection
LCD	Limiting current density
SCE	Standard calomel electrode
RCE	Rotating cylinder electrode
gmd	Gram per square meter per day
WL	Weight loss
% vol.	Percentage volume

List of Tables

Table	Title	Page
2-1	Design Equations of Agitator (Vessel)	35
3-1	Chemical composition of carbon steel used	42
3-2	Chemical composition of zinc used	42
4-1	Corrosion rate of carbon steel in 2.5×10^{-3} M CaCO_3 at 35°C for different velocities.	55
4-2	Corrosion rate of carbon steel in 2.5×10^{-3} M CaCO_3 + 1% (v/v) Gasoil at 35°C	55
4-3	Corrosion rate of carbon steel in 2.5×10^{-3} M CaCO_3 + 2% (v/v) Gasoil at 35°C .	55
4-4	Corrosion rate of carbon steel in 2.5×10^{-3} M CaCO_3 + 5% (v/v) Gasoil at 35°C .	56
4-5	Corrosion rate of carbon steel in 2.5×10^{-3} M CaCO_3 + 2% (v/v) Gasoil + 2% (v/v) HCl at 35°C .	56
4-6	Corrosion rate of carbon steel in 2.5×10^{-3} M CaCO_3 + 5% (v/v) Gasoil + 2% (v/v) HCl at 35°C .	56

4-7	Corrosion rate of carbon steel in 2.5×10^{-3} M CaCO_3 + 10% (v/v) Gasoil + 2% (v/v) HCl at 35°C .	57
4-8	Corrosion rate of carbon steel in 2.5×10^{-3} M CaCO_3 + 5% (v/v) Gasoil + 2% (v/v) HCl at 25°C .	57
4-9	Corrosion rate of carbon steel in 2.5×10^{-3} M CaCO_3 + 5% (v/v) Gasoil + 2% (v/v) HCl at 45°C .	57
4-10	Corrosion rate of carbon steel in 2.5×10^{-3} M CaCO_3 + 5% (v/v) Gasoil + 2% (v/v) H_2SO_4 at 35°C .	58
4-11	Corrosion rate of carbon steel in 2.5×10^{-3} M CaCO_3 + 10% (v/v) Gasoil + 2% (v/v) H_2SO_4 at 35°C .	58
4-12	Corrosion rate of carbon steel in 2.5×10^{-3} M CaCO_3 + 5% Gasoil + 2% H_2SO_4 at different temperatures and velocity 300 rpm.	58
4-13	Corrosion of carbon steel in 2.5×10^{-3} M CaCO_3 at different velocity and $T=35^\circ\text{C}$.	61
4-14	Corrosion of carbon steel in 9.9×10^{-3} M CaCO_3 at different velocities and $T=35^\circ\text{C}$.	61
4-15	Corrosion of carbon steel in different salt concentrations at 35°C and velocity of 0 rpm.	61
4-16	Corrosion of carbon steel in 9.99×10^{-3} M CaCO_3 at different temperatures and velocity of 0 rpm.	62
4-17	Corrosion of carbon steel in 9.99×10^{-3} M CaCO_3 at different temperatures and velocity of 400 rpm.	62
4-18	Corrosion of carbon steel in 9.99×10^{-3} M CaCO_3 at 35°C for different exposure times at velocity of 0 rpm.	62
4-19	Corrosion of carbon steel in 9.99×10^{-3} M CaCO_3 at 35°C for different exposure times at velocity of 400	63

4-20	Corrosion of carbon steel in 9.99×10^{-3} M CaCO_3 at 35 °C for different exposure times at velocity of 1200 rpm.	63
4-21	Corrosion of carbon steel in 9.99×10^{-3} M CaCO_3 with different flow rate of CO_2 at T= 35 °C, and u= 0 rpm	63
4-22	Corrosion of carbon steel in 9.99×10^{-3} M CaCO_3 with flow rate of $\text{CO}_2=0.283\text{m}^3/\text{h}$ at different velocities and T=35 °C.	64
4-23	Corrosion of carbon steel in 9.99×10^{-3} M CaCO_3 with flow rate of $\text{CO}_2= 1.132\text{m}^3/\text{h}$ at different.	64
4-24	Corrosion of carbon steel in 9.99×10^{-3} M CaCO_3 with flow rate of $\text{CO}_2= 0.283\text{m}^3/\text{h}$ for immersion different exposure times at T= 25 °C, and u= 0 rpm.	65
4-25	Corrosion of carbon steel in 9.99×10^{-3} M CaCO_3 with flow rate of $\text{CO}_2= 0.283\text{m}^3/\text{h}$ for immersion different exposure times at T= 35 °C, and u= 0 rpm.	65
4-26	Corrosion of carbon steel in 9.99×10^{-3} M CaCO_3 with flow rate of $\text{CO}_2= 0.283\text{m}^3/\text{h}$ for immersion different exposure times at T= 45 °C, and u= 0 rpm.	65
4-27	Corrosion of carbon steel in 9.99×10^{-3} M CaCO_3 with flow rate of $\text{CO}_2= 0.283\text{m}^3/\text{h}$ for immersion different exposure times at T= 35 °C, and u= 200 rpm.	66
4-28	Corrosion of carbon steel in 9.99×10^{-3} M CaCO_3 with flow rate of $\text{CO}_2= 0.283\text{m}^3/\text{h}$ for immersion different exposure times at T= 35 °C, and u= 800 rpm.	66

5-29	Corrosion of carbon steel in 9.99×10^{-3} M CaCO_3 with flow rate of $\text{CO}_2 = 0.283 \text{ m}^3/\text{h}$ for different temperatures, and $u = 0$ rpm.	66
5-30	Corrosion of carbon steel in 9.99×10^{-3} M CaCO_3 with flow rate of $\text{CO}_2 = 1.132 \text{ m}^3/\text{h}$ for different temperatures, and $u = 0$ rpm.	67
5-31	corrosion rate of carbon steel, zinc and protection in 9.99×10^{-3} M CaCO_3 at different temperature for immersion time of 1.5 h, $u = 0$ rpm and $Q_{\text{CO}_2} = 0.283 \text{ m}^3/\text{h}$.	67
5-32	corrosion rate of carbon steel, zinc and protection in 9.99×10^{-3} M CaCO_3 at different velocity for immersion time of 1.5 h, $T = 35^\circ\text{C}$ and $Q_{\text{CO}_2} = 0.283 \text{ m}^3/\text{h}$.	67
5-33	corrosion rate of carbon steel, zinc and protection in 9.99×10^{-3} M CaCO_3 at different flow rate for immersion time of 1.5 h, $T = 35^\circ\text{C}$, and $u = 200$ rpm.	68
A-1	Physical Properties of Water at Atmospheric	A-1
B-1	Measured oxygen solubility at different CaCO_3 concentrations and temperatures and $u = 0$ rpm.	B-1
B-2	Measured oxygen solubility in 9.9×10^{-3} M CaCO_3 with addition of CO_2 bubbles at different velocity and $T = 35^\circ\text{C}$, $Q_{\text{CO}_2} = 0.283 \text{ m}^3/\text{h}$.	B-1
B-3	Measured conductivity values of different concentration of CaCO_3 solution at different temperature.	B-1
B-4	Measured conductivity values of CaCO_3 - gasoil, acid mixtures at different concentrations and $T = 35^\circ\text{C}$, $u = 200$ rpm.	B-2

B-6	Measured conductivity values of CaCO ₃ solution– CO ₂ gas at different temperature and Q _{CO₂} = 0.283 m ³ /h and u= 0 rpm.	B-2
B-7	Measured conductivity values of CaCO ₃ – CO ₂ gas at different flow rate of CO ₂ , velocity and T= 35°C	B-2
B-8	Measured pH values of different concentration of CaCO ₃ solution at T= 35°C and u= 0rpm.	B-2
B-9	Measured pH values for CaCO ₃ and CaCO ₃ - gasoil, acid mixtures at different concentrations and T= 35 °C and u=200 rpm.	B-3
B-10	Measured pH values for CaCO ₃ - CO ₂ gas mixtures at different flow rate of CO ₂ , and temperatures	B-3
D-1	Potential vs. time for cathodic protection of CaCO ₃ – Q _{CO₂} = 0.283 m ³ /h at T= 25°C and u= 0 rpm.	D-1
D-2	Potential vs. time for cathodic protection of CaCO ₃ – Q _{CO₂} = 0.283 m ³ /h at T= 35°C and u= 0 rpm.	D-1
D-3	Potential vs. time for cathodic protection of CaCO ₃ – Q _{CO₂} = 0.283 m ³ /h at T= 45°C and u= 0 rpm.	D-2
D-4	Potential vs. time for cathodic protection of CaCO ₃ – Q _{CO₂} = 0.283 m ³ /h at T= 35°C and u= 200 rpm	D-3
D-5	Potential vs. time for cathodic protection of CaCO ₃ – Q _{CO₂} = 0.566 m ³ /h at T= 35°C and u= 200 rpm	D-3
D-6	Potential vs. time for cathodic protection of CaCO ₃ – Q _{CO₂} = 1.132 m ³ /h at T= 35°C and u= 200 rpm	D-3
D-7	Potential vs. time for cathodic protection of CaCO ₃ – Q _{CO₂} = 0.283 m ³ /hat T= 35°C and u= 400 rpm	D-4
D-8	Potential vs. time for cathodic protection of CaCO ₃ – Q _{CO₂} = 0.283 m ³ /hat T= 35°C and u= 800 rpm	D-5

List of Figures

Figure	Title	Page
2- 1	Corrosion Cell	6
2-2	Effect of pH on corrosion rate of iron	10
2-3	Effect of temperature on corrosion of iron in water containing dissolved oxygen	11
2- 4	Effect of Velocity on i_L	13
2- 5	Effect of Velocity on the CR	13
2- 6	Principle of cathodic protection with sacrificial anodes.	23
2- 7	Corrosion in every aspect of oil industry, Oil well stimulation	27
2- 8	The CO ₂ corrosion mechanism. CO ₂ dissolves in the condensed aqueous liquid phase diffuses to the surface and dissolves iron by an electrochemical mechanism	32
2- 9	Measurements of Turbine	39
3-1	Carbon steel specimen	44
3-2	Circular Disk Turbine (four- blades).	46
3- 3	Dimensions of Tank and Disk Turbine (Six- Blades Turbine).	47
3- 4	Experimental rig picture.	47
3-5	Schematic illustrates of experimental apparatus.	48
3-6	Carbon steel and Zinc specimens.	52
4-1	Typical Polarization Curve	60
5-1	Variation of CR with velocity in single phase CaCO ₃ at 35 °C.	70
5-2	Carbon steel specimens (a) before (b) after exposed corrosion (c) after cleaning corrosion attack.	70
5-3	Variation of CR with velocity in two phase CaCO ₃ + gasoil at 35°C.	72

5-4	Variation of CR with velocity in two phase brine- gasoil in presence of Hcl.	73
5-5	Variation of CR with velocity in two phase brine- gasoil in presence of Hcl at different temperature.	75
5-6	Variation of CR with velocity in two phase brine- gasoil in presence of H ₂ SO ₄ .	76
5-7	Variation of CR with temperature in two phase brine- gasoil in presence of H ₂ SO ₄ .	77
5-8	Specimen of CS (a) before (b) after exposure to corrosion in presence of HCl acid.	78
5-9	Effect of velocity on i_L in brine CaCO ₃ of different concentrations	79
5-10	Effect of CaCO ₃ concentration on i_L .	80
5-11	Variation of temperature on i_L in 9.9×10^{-3} M CaCO ₃	81
5-12	Variation of i_L with time at 35 °C and different velocities in 9.9×10^{-3} M CaCO ₃	82
5-13	Variation of velocity on corrosion potential in brine CaCO ₃ solution.	84
5-14	Effect of salt concentration on corrosion potential.	85
5-15	Variation of temperature on corrosion potential in 9.9×10^{-3} M CaCO ₃	86
5-16	Variation of time on corrosion potential in 9.9×10^{-3} M CaCO ₃	86
5-17	Carbon steel specimens (a) before (b) after cathodic polarization (c) after cleaning cathodic polarization attack (d) corrosion product layer on the specimen at 45 °C.	88
5-18	Optical microscope examination (10 X, 20Xand 50X) of carbon steel specimen after exposure.	89
5-19	Variation of flow rate of CO ₂ on i_L in brine CaCO ₃	91
5-20	Effect of velocity on i_L in brine CaCO ₃ - CO ₂ solution.	92

5-21	Variation of i_L with time at different temperatures in brine $\text{CaCO}_3\text{-CO}_2$	93
5-22	Variation of i_L with time at velocity in brine $\text{CaCO}_3\text{-CO}_2$	94
5-23	Effect of temperature on i_L in brine $\text{CaCO}_3\text{-CO}_2$	108
5-24	Variation of flow rate on corrosion potential in $\text{CaCO}_3\text{-CO}_2$ solution.	109
5-25	Variation of velocity on corrosion potential in brine $\text{CaCO}_3\text{-CO}_2$ solution.	95
5-26	Variation of time on E_C in $\text{CaCO}_3\text{-CO}_2$ at different temperatures	96
5-27	Variation of time on E_C in $\text{CaCO}_3\text{-CO}_2$ at different velocities	96
5-28	variation of temperature on corrosion potential in brine $\text{CaCO}_3\text{-CO}_2$	96
5-29	Carbon steel specimens (a) before (b) after cathodic polarization $\text{CaCO}_3\text{-CO}_2$ (c) after cleaning cathodic polarization attack.	97
5-30	Carbon steel specimens (a) before (b) after cathodic polarization $\text{CaCO}_3\text{-CO}_2$ after 2 h at 35°C (c) after cathodic polarization $\text{CaCO}_3\text{-CO}_2$ after 2 h at 45°C .	97
5-31	Potential vs. time for cathodic protection of $\text{CaCO}_3\text{-CO}_2$ at $T= 35^\circ\text{C}$ and $u= 0$ rpm.	99
5-32	Potential vs. time for cathodic protection of $\text{CaCO}_3\text{-CO}_2$ at $T= 25^\circ\text{C}$ and $u= 0$ rpm.	100
5-33	Potential vs. time for cathodic protection of $\text{CaCO}_3\text{-CO}_2$ at $T= 45^\circ\text{C}$ and $u= 0$ rpm.	100
5-34	Potential vs. time for cathodic protection of $\text{CaCO}_3\text{-CO}_2$ at $T= 35^\circ\text{C}$ and $u= 200$ rpm.	101
5-35	Potential vs. time for cathodic protection of $\text{CaCO}_3\text{-CO}_2$ at $T= 35^\circ\text{C}$ and $u= 400$ rpm	101
5-36	Potential vs. time for cathodic protection of $\text{CaCO}_3\text{-CO}_2$ at $T= 35^\circ\text{C}$ and $u= 800$ rpm.	101

5-37	Potential vs. time for cathodic protection of CaCO ₃ –CO ₂ at Q _{CO2} = 0.566 m ³ /h and u= 200 rpm.	102
5-38	Potential vs. time for cathodic protection of CaCO ₃ –CO ₂ at Q _{CO2} = 1.132 m ³ /h and u= 200 rpm	102
5-39	Effect of temperature on CR of free corrosion of CS and protection with zinc	104
5-40	Effect of temperature on CR of zinc coupled with CS	104
5-41	Effect of velocity on CR of free corrosion of CS and protection with zinc	105
5-42	Effect of velocity on CR of zinc coupling with CS	105
5-43	Effect of flow rate on CR of free corrosion of CS and protection with zinc.	106
5-44	Effect of flow rate on CR of zinc coupling with CS	106
5-45	Carbon steel specimens (a) before (b) after corrosion in CaCO ₃ -CO ₂ (c) specimen of CS and Zn after cathodic protection	106
C-1	Polarization curve in 2.5 × 10 ⁻³ M CaCO ₃ at 35°C and 0 rpm	C-1
C-2	Polarization curve in 2.5 × 10 ⁻³ M CaCO ₃ at 35°C and 200 rpm	C-1
C-3	Polarization curve in 2.5 × 10 ⁻³ M CaCO ₃ at 35°C and 400 rpm	C-2
C-4	Polarization curve in 2.5 × 10 ⁻³ M CaCO ₃ at 35°C and 800 rpm	C-2
C-5	Polarization curve in 2.5 × 10 ⁻³ M CaCO ₃ at 35°C and 1200 rpm	C-3
C-6	Polarization curve in 9.9 × 10 ⁻³ M CaCO ₃ at 35°C and 0 rpm	C-3
C-7	Polarization curve in 9.9 × 10 ⁻³ M CaCO ₃ at 35°C and 200 rpm	C-4
C-8	Polarization curve in 9.9 × 10 ⁻³ M CaCO ₃ at 35°C and 400 rpm	C-4
C-9	Polarization curve in 9.9 × 10 ⁻³ M CaCO ₃ at 35°C and 800 rpm	C-5
C-10	Polarization curve in 9.9 × 10 ⁻³ M CaCO ₃ at 35°C and 1200 rpm	C-5
C-11	Polarization curve in 4.99×10 ⁻³ M CaCO ₃ at 35°C and 0 rpm	C-6
C-12	Polarization curve in 9.9 × 10 ⁻³ M CaCO ₃ at 45°C and 0 rpm	C-6
C-13	Polarization curve in 9.9 × 10 ⁻³ M CaCO ₃ at 55°C and 0 rpm	C-7

C-14	Polarization curve in 9.9×10^{-3} M CaCO_3 at 45°C and 400 rpm	C-7
C-15	Polarization curve in 9.9×10^{-3} M CaCO_3 at 55°C and 400 rpm	C-7
C-16	Cathodic polarization curves in 9.9×10^{-3} M CaCO_3 at 0 rpm at 35°C for 2h.	C-8
C-17	Cathodic polarization curves in 9.9×10^{-3} M CaCO_3 at 400 rpm at 35°C for 2h.	C-8
B-18	Cathodic polarization curves in 9.9×10^{-3} M CaCO_3 at 1200 rpm at 35°C for 2h.	C-8
C-19	Cathodic polarization curve in 9.9×10^{-3} M CaCO_3 at different flow rate of CO_2 and 35°C and 0 rpm.	C-9
C-20	Cathodic polarization Curves in 9.9×10^{-3} M CaCO_3 + $Q_{\text{CO}_2}=0.283\text{m}^3/\text{h}$ at 0 rpm at 25°C for 2h.	C-9
C-21	Cathodic polarization curves in 9.9×10^{-3} M CaCO_3 + $Q_{\text{CO}_2}=0.283$ m^3/h at 0 rpm at 35°C for 2h.	C-10
C-22	Cathodic polarization curves in 9.9×10^{-3} M CaCO_3 + $Q_{\text{CO}_2}=0.283$ m^3/h at 200 rpm at 35°C for 2h.	C-10
C-23	Cathodic polarization curves in 9.9×10^{-3} M CaCO_3 + $Q_{\text{CO}_2}=0.283$ m^3/h at 800 rpm at 35°C for 2h.	C-11
C-24	Cathodic polarization curves in 9.9×10^{-3} M CaCO_3 + $Q_{\text{CO}_2}=0.283$ m^3/h at 0 rpm at 45°C for 2h.	C-11
C-25	Cathodic polarization curve in 9.9×10^{-3} M CaCO_3 at different rotational velocity, $Q_{\text{CO}_2}= 0.283\text{m}^3/\text{h}$, and 35°C .	C-12
C-26	Cathodic polarization curve in 9.9×10^{-3} M CaCO_3 at different rotational velocity, $Q_{\text{CO}_2}= 1.132\text{m}^3/\text{h}$, and 35°C .	C-12
C-27	Cathodic polarization curve in 9.9×10^{-3} M CaCO_3 at different temperature, $Q_{\text{CO}_2}= 0.283 \text{m}^3/\text{h}$, and 0 rpm.	C-13
C-28	Cathodic polarization curve in 9.9×10^{-3} M CaCO_3 at different temperature, $Q_{\text{CO}_2}= 0.283 \text{m}^3/\text{h}$, and 0 rpm.	C-13

Appendix -A-

Physical properties of water

Table A-1 Physical Properties of Water at Atmospheric Pressure [Perry and Chilton, 1997].

T (°C)	ρ (kg/m³)	$\mu \times 10^4$ (kg/m.s.)
0.00	999.8	17.9
4.44	999.8	15.5
10.0	999.2	13.1
15.56	998.6	11.2
21.11	997.4	9.80
26.67	995.8	8.60
32.22	994.9	7.65
37.78	993.0	6.82
43.33	990.6	6.16
54.44	985.7	5.13
60.0	983.3	4.71

Appendix -B-

Measured Experimental Value of pH, conductivity, and oxygen solubility

Table B-1 Measured oxygen solubility at different CaCO₃ concentrations and temperatures and u= 0 rpm.

CaCO ₃ concentrations in M	C _b , ppm		
	25 °C	35 °C	45 °C
9.99×10^{-4}	7.80	7.32	6.22
2.5×10^{-3}	6.95	6.15	4.40
4.99×10^{-3}	6.85	5.84	4.05
9.99×10^{-3}	6.2	5.23	4.72

Table B-2 Measured oxygen solubility in 9.9×10^{-3} M CaCO₃ with addition of CO₂ bubbles at different velocity and T=35 °C, Q_{CO2}=0.283 m³/h.

u, rpm T, °C	C _b , ppm		
	25 °C	35 °C	45 °C
0	1.8	0.13	0.11
200	2.6	0.9	0.18
400	3.4	1.9	0.35
800	3.95	2.14	1.05

Table B-3 measured conductivity values of different concentration of CaCO₃ solution at different temperature.

Solution T, °C	Conductivity, μS		
	25 °C	35 °C	45 °C
2.5×10^{-3}	41.5	44.5	47.1
4.99×10^{-3}	42.9	45.9	49.4
9.99×10^{-3}	45.7	48.3	52.1

Table B-4 Measured conductivity values of CaCO₃ - gasoil, acid mixtures at different concentrations and T= 35 °C, u=200 rpm.

Solutions concentration	Conductivity, μS
2.5×10 ⁻³ M CaCO ₃ + 2% gasoil	15.26
2.5×10 ⁻³ M CaCO ₃ + 2% gasoil+ 2% HCl	188.5
2.5×10 ⁻³ M CaCO ₃ + 5% gasoil+ 2% HCl	169
2.5×10 ⁻³ M CaCO ₃ + 5% gasoil+ 2% H ₂ SO ₄	94.8

Table B-5 Measured conductivity values of CaCO₃ solution– CO₂ gas at different temperature and Q_{CO2} = 0.283 m³/h and u= 0 rpm.

T, °C	25 °C	35 °C	45 °C
Conductivity, μS	1270	1165	986

Table B-6 Measured conductivity values of CaCO₃ – CO₂ gas at different flow rate of CO₂, velocity and T= 35°C

u, rpm Q, m ³ /h	Conductivity, μS			
	0.142	0.283	0.566	1.132
0	789	1165	1083	1126
200	855	1197	1090	1131
400	976	1130	1098	1123
800	1045	1122	1103	1108

Table B-7 Measured pH values of different concentration of CaCO₃ solution at T= 35°C and u= 0rpm.

CaCO ₃ concentrations in M	pH
2.5×10 ⁻³	8.84
4.99×10 ⁻³	9.35
9.99×10 ⁻³	9.43

Table B-8 Measured pH values for CaCO₃ and CaCO₃- gasoil, acid mixtures at different concentrations and T= 35 °C and u=200 rpm.

Solutions concentration	pH
gasoil	7.5
2.5×10 ⁻³ MCaCO ₃ + 1% gasoil	8.52
2.5×10 ⁻³ MCaCO ₃ + 2% gasoil	8.32
2.5×10 ⁻³ MCaCO ₃ + 5% gasoil	8.02
2.5×10 ⁻³ MCaCO ₃ + 2% gasoil+ 2% HCl	0.29
2.5×10 ⁻³ MCaCO ₃ + 5% gasoil+ 2% HCl	0.34
2.5×10 ⁻³ MCaCO ₃ + 5% gasoil+ 2% H ₂ SO ₄	0.55
2.5×10 ⁻³ MCaCO ₃ + 10% gasoil+ 2% H ₂ SO ₄	0.58

Table B-9 Measured pH values for CaCO₃- CO₂ gas mixtures at different flow rate of CO₂, and temperatures.

Q, m ³ /h T, °C	pH		
	25 °C	35 °C	45 °C
0.142	5.75	5.83	6.10
0.283	5.78	5.84	6.14
0.566	5.80	5.85	6.14
1.132	6.14	5.85	6.26

Appendix -D-

Cathodic Protection Data

Table D-1 Potential vs. time for cathodic protection of $\text{CaCO}_3 - Q_{\text{CO}_2} = 0.283 \text{ m}^3/\text{h}$ at $T = 25^\circ\text{C}$ and $u = 0 \text{ rpm}$.

Time(min)	E (V)	Time(min)	E (V)
0	-0.57	0	-0.768
1	-0.574	1	-0.78
2	-0.58	2	-0.792
3	-0.587	3	-0.8
5	-0.592	4	-0.807
7	-0.598	5	-0.813
9	-0.61	6	-0.814
11	-0.623	7	-0.82
13	-0.629	9	-0.825
15	-0.636	11	-0.829
20	-0.645	13	-0.831
25	-0.651	15	-0.833
30	-0.652	17	-0.836
35	-0.654	22	-0.839
45	-0.654	27	-0.843
55	-0.655	32	-0.845
65	-0.655	37	-0.846
75	-0.655	47	-0.848
90	-0.655	57	-0.852
		67	-0.855
		77	-0.859
		90	-0.861

Table D-2 Potential vs. time for cathodic protection of $\text{CaCO}_3 - Q_{\text{CO}_2} = 0.283 \text{ m}^3/\text{h}$ at $T = 35^\circ\text{C}$ and $u = 0 \text{ rpm}$

Time(min)	E (V)	Time(min)	E (V)
0	-0.614	0	-0.715
1	-0.615	1	-0.722
2	-0.622	2	-0.73
3	-0.624	3	-0.741
4	-0.629	4	-0.749
5	-0.632	6	-0.76
6	-0.633	8	-0.776
7	-0.634	10	-0.791
8	-0.637	12	-0.802

9	-0.64	14	-0.815
10	-0.641	19	-0.833
12	-0.642	24	-0.847
14	-0.642	29	-0.857
16	-0.646	34	-0.862
18	-0.648	44	-0.87
20	-0.648	54	-0.877
25	-0.648	64	-0.881
30	-0.648	74	-0.888
35	-0.648	84	-0.888
40	-0.649	90	-0.888
50	-0.649		
60	-0.651		
70	-0.652		
80	-0.653		
90	-0.653		

Table D-3 Potential vs. time for cathodic protection of CaCO_3 – $Q_{\text{CO}_2} = 0.283 \text{ m}^3/\text{h}$ at $T = 45^\circ\text{C}$ and $u = 0 \text{ rpm}$

Time(min)	E (V)	Time(min)	E (V)
0	-0.612	0	-0.737
1	-0.617	1	-0.753
2	-0.621	2	-0.771
3	-0.623	3	-0.775
4	-0.626	4	-0.782
5	-0.628	5	-0.786
6	-0.63	7	-0.79
8	-0.631	9	-0.794
10	-0.633	11	-0.796
12	-0.635	13	-0.796
14	-0.638	15	-0.797
16	-0.639	20	-0.797
21	-0.64	25	-0.797
26	-0.64	35	-0.798
31	-0.64	45	-0.803
36	-0.641	55	-0.808
41	-0.641	65	-0.82
51	-0.642	75	-0.822
61	-0.644	85	-0.822
71	-0.647	90	-0.822

81	-0.648		
90	-0.649		

Table D-4 Potential vs. time for cathodic protection of $\text{CaCO}_3 - Q_{\text{CO}_2} = 0.283 \text{ m}^3/\text{h}$ at $T = 35^\circ\text{C}$ and $u = 200 \text{ rpm}$

Time(min)	E (V)	Time(min)	E (V)
0	-0.392	0	-0.773
1	-0.396	1	-0.791
2	-0.443	2	-0.81
3	-0.423	3	-0.82
4	-0.43	4	-0.822
6	-0.488	5	-0.824
8	-0.489	6	-0.825
10	-0.49	7	-0.824
12	-0.472	8	-0.826
14	-0.475	10	-0.825
16	-0.492	12	-0.826
20	-0.516	14	-0.826
25	-0.672	16	-0.827
30	-0.673	18	-0.829
35	-0.673	23	-0.83
40	-0.673	28	-0.831
45	-0.674	33	-0.832
50	-0.674	38	-0.831
60	-0.672	43	-0.832
70	-0.672	48	-0.835
80	-0.672	58	-0.837
90	-0.673	68	-0.839
		78	-0.841
		90	-0.845

Table D-5 Potential vs. time for cathodic protection of $\text{CaCO}_3 - Q_{\text{CO}_2} = 0.566 \text{ m}^3/\text{hat}$ $T = 35^\circ\text{C}$ and $u = 200 \text{ rpm}$

Time(min)	E (V)	Time(min)	E (V)
0	-0.639	0	-0.68
1	-0.666	1	-0.8
2	-0.675	2	-0.81
3	-0.673	3	-0.813
4	-0.673	4	-0.81
5	-0.672	5	-0.807
6	-0.671	6	-0.805

8	-0.67	8	-0.801
10	-0.669	10	-0.801
12	-0.669	12	-0.802
14	-0.669	14	-0.803
16	-0.669	16	-0.805
21	-0.669	21	-0.809
26	-0.668	26	-0.812
31	-0.667	31	-0.813
36	-0.667	36	-0.815
41	-0.666	41	-0.818
51	-0.666	51	-0.822
61	-0.666	61	-0.828
71	-0.665	71	-0.833
81	-0.666	81	-0.836
90	-0.666	90	-0.839

Table D-6 Potential vs. time for cathodic protection of $\text{CaCO}_3 - Q_{\text{CO}_2} = 1.132 \text{ m}^3/\text{hat}$ $T = 35^\circ\text{C}$ and $u = 200 \text{ rpm}$

Time(min)	E (V)	Time(min)	E (V)
0	-0.672	0	-0.76
1	-0.677	1	-0.821
2	-0.683	2	-0.857
3	-0.684	3	-0.864
4	-0.683	4	-0.863
5	-0.682	5	-0.86
7	-0.681	6	-0.857
9	-0.68	7	-0.855
11	-0.68	9	-0.851
13	-0.68	11	-0.849
15	-0.679	13	-0.848
20	-0.678	15	-0.848
25	-0.677	17	-0.849
30	-0.677	22	-0.85
35	-0.676	27	-0.851
40	-0.675	32	-0.854
50	-0.674	37	-0.855
60	-0.674	42	-0.859
70	-0.674	52	-0.863
80	-0.674	62	-0.866
90	-0.674	72	-0.872
		82	-0.875

		90	-0.875
--	--	----	--------

Table D-7 Potential vs. time for cathodic protection of $\text{CaCO}_3 - Q_{\text{CO}_2} = 0.283 \text{ m}^3/\text{hat}$ $T = 35^\circ\text{C}$ and $u = 400 \text{ rpm}$

Time(min)	E (V)	Time(min)	E (V)
0	-0.392	0	-0.737
1	-0.578	1	-0.792
2	-0.612	2	-0.821
3	-0.655	3	-0.824
4	-0.67	4	-0.823
5	-0.673	5	-0.822
6	-0.676	6	-0.823
7	-0.677	7	-0.821
9	-0.676	9	-0.818
11	-0.676	11	-0.821
13	-0.675	13	-0.828
15	-0.676	15	-0.829
17	-0.675	17	-0.831
19	-0.675	22	-0.832
21	-0.674	27	-0.834
26	-0.674	32	-0.835
31	-0.673	37	-0.837
36	-0.674	42	-0.837
41	-0.673	47	-0.839
46	-0.673	52	-0.842
51	-0.673	62	-0.846
61	-0.673	72	-0.851
71	-0.673	82	-0.855
81	-0.673	90	-0.857
90	-0.673		

Table D-8 Potential vs. time for cathodic protection of $\text{CaCO}_3 - Q_{\text{CO}_2} = 0.283 \text{ m}^3/\text{hat}$ $T = 35^\circ\text{C}$ and $u = 800 \text{ rpm}$

Time(min)	E (V)	Time(min)	E (V)
0	-0.608	0	-0.705
1	-0.632	1	-0.746
2	-0.652	2	-0.793
3	-0.671	3	-0.796
4	-0.674	4	-0.795

5	-0.676	5	-0.794
6	-0.677	7	-0.796
8	-0.678	9	-0.797
10	-0.68	11	-0.799
12	-0.68	13	-0.801
14	-0.679	15	-0.802
16	-0.679	17	-0.802
18	-0.678	19	-0.802
23	-0.678	24	-0.805
28	-0.677	29	-0.806
33	-0.677	34	-0.807
38	-0.677	39	-0.808
43	-0.677	44	-0.81
48	-0.677	49	-0.813
58	-0.676	59	-0.816
68	-0.677	69	-0.82
78	-0.677	79	-0.822
90	-0.677	90	-0.825

Appendix -C-

Polarization Curves

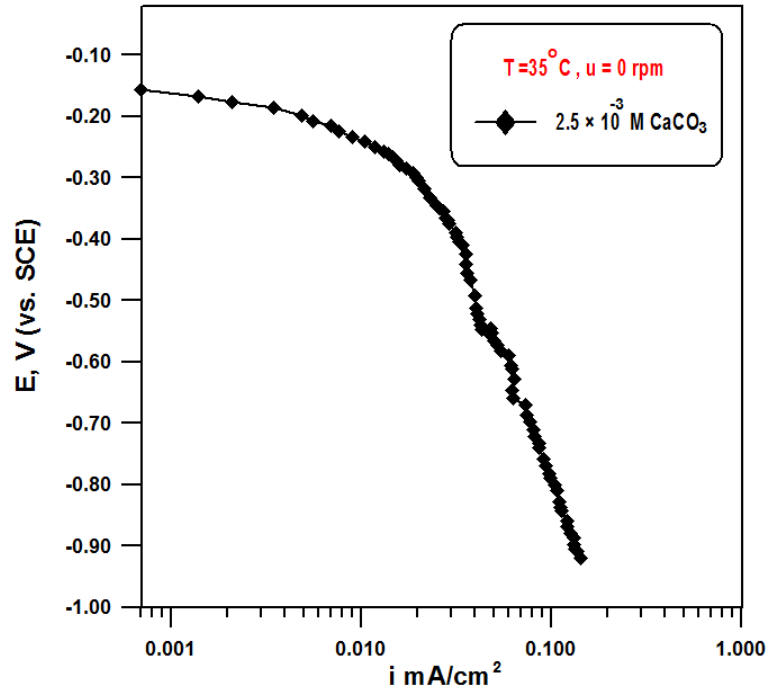


Figure C-1 Polarization curve in $2.5 \times 10^{-3} \text{ M CaCO}_3$ at 35°C and 0 rpm

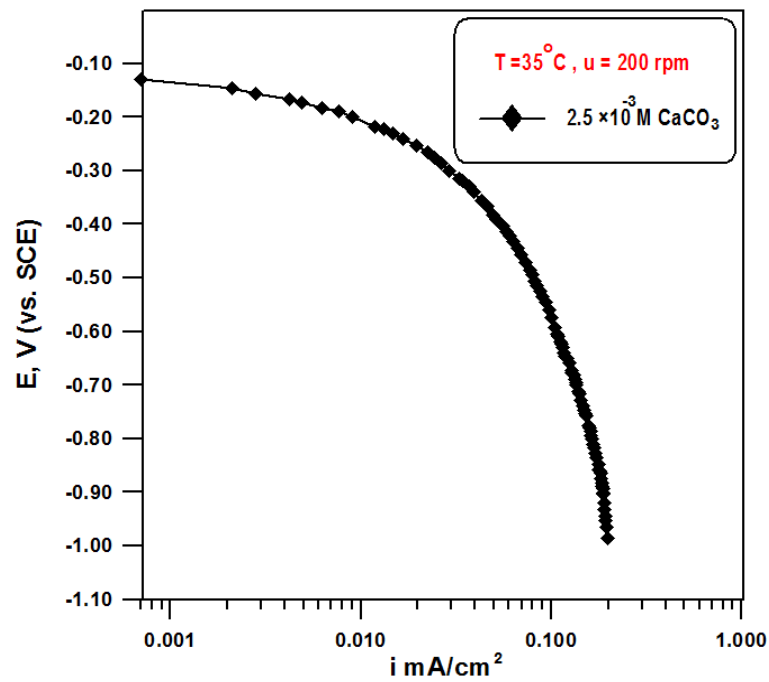


Figure C-2 Polarization curve in $2.5 \times 10^{-3} \text{ M CaCO}_3$ at 35°C and 200 rpm

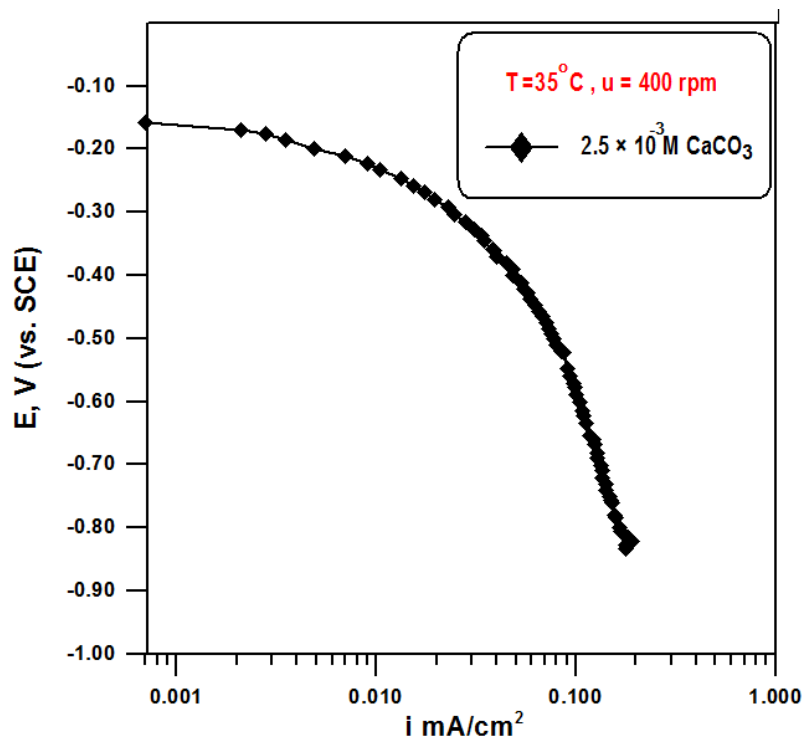


Figure C-3 Polarization curve in $2.5 \times 10^{-3}\text{ M CaCO}_3$ at 35°C and 400 rpm

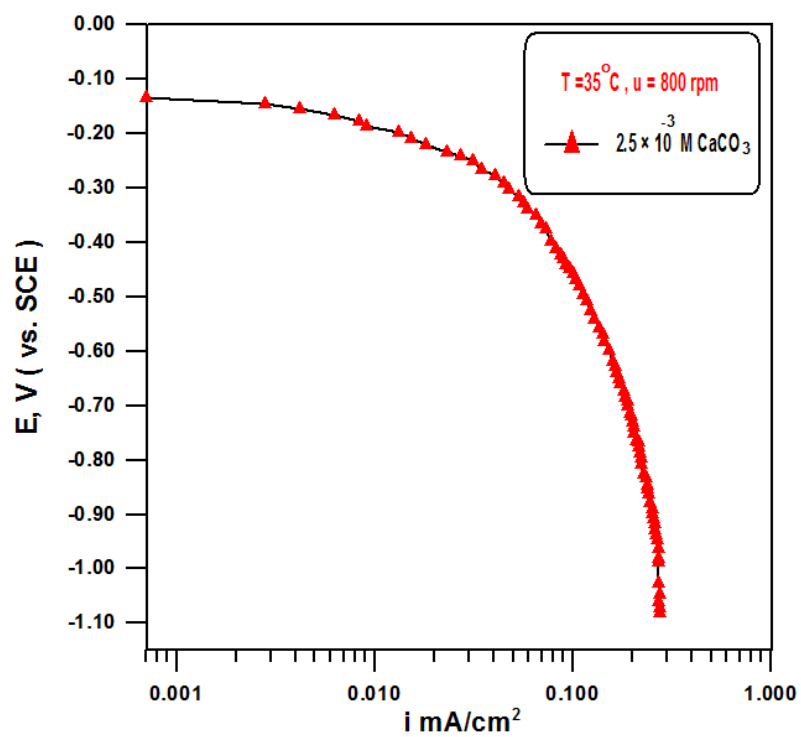


Figure C-4 Polarization curve in $2.5 \times 10^{-3}\text{ M CaCO}_3$ at 35°C and 800 rpm

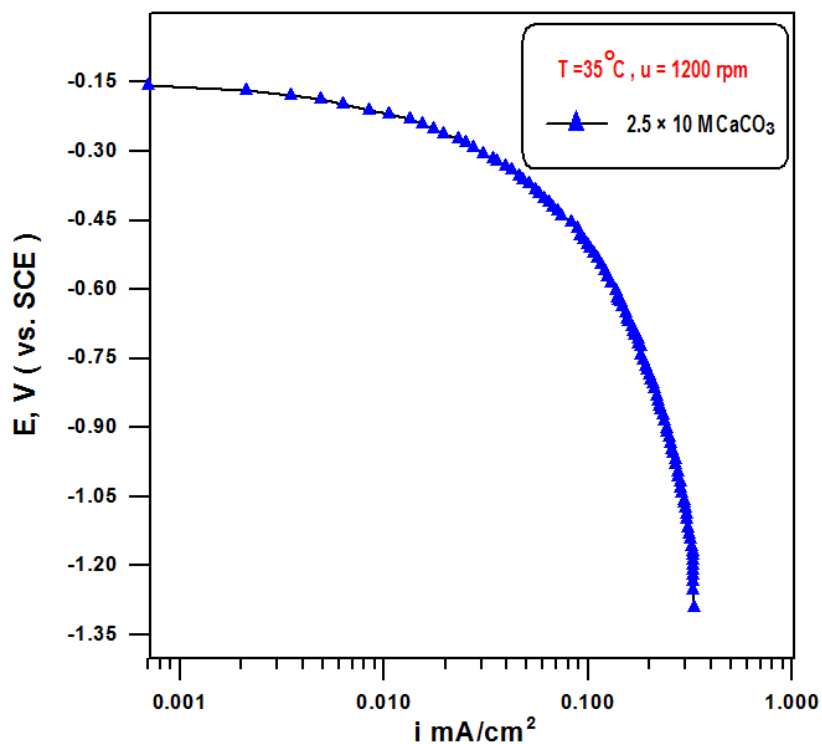


Figure C-5 Polarization curve in $2.5 \times 10^{-3} \text{ M CaCO}_3$ at 35°C and 1200 rpm

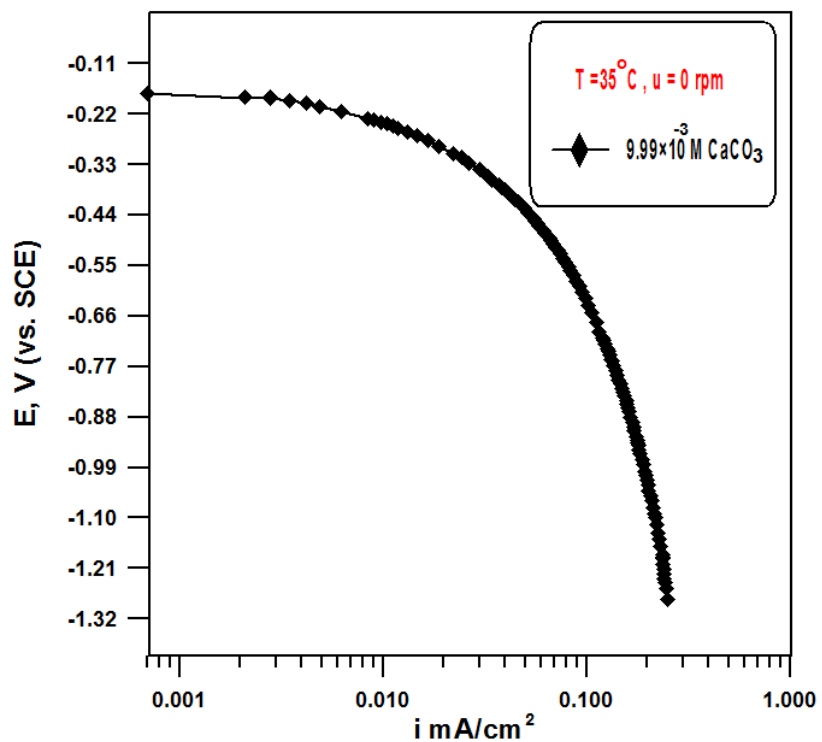


Figure C-6 Polarization curve in $9.9 \times 10^{-3} \text{ M CaCO}_3$ at 35°C and 0 rpm

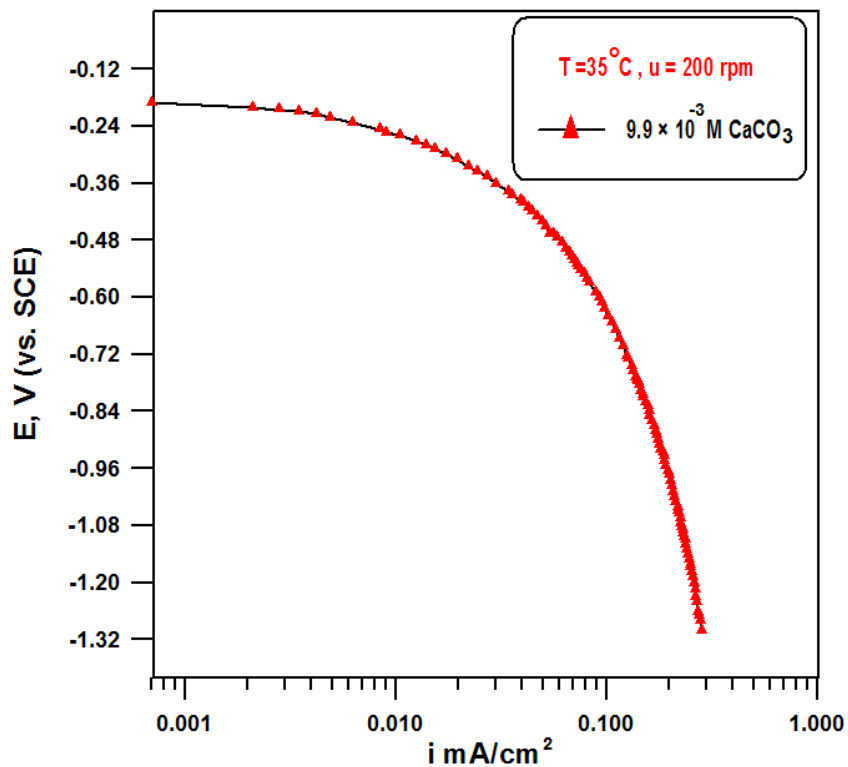


Figure C-7 Polarization curve in 9.9×10^{-3} M CaCO_3 at 35°C and 200 rpm

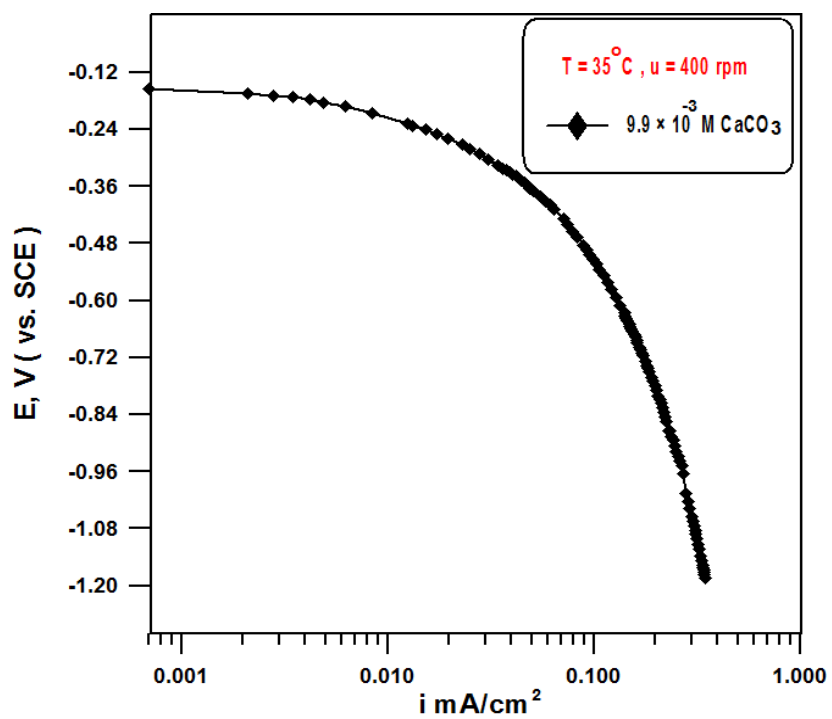


Figure C-8 Polarization curve in 9.9×10^{-3} M CaCO_3 at 35°C and 400 rpm.

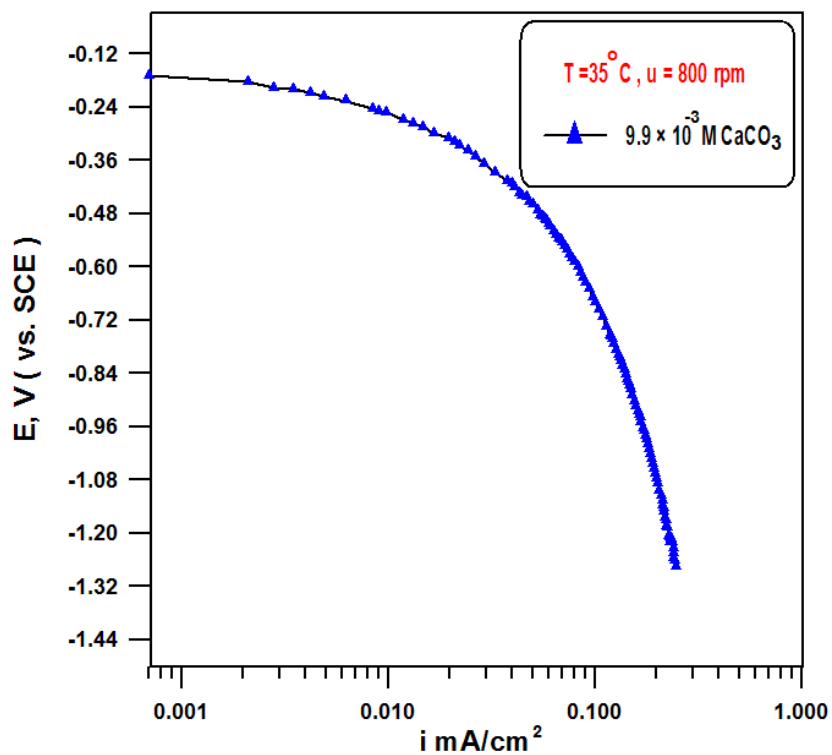


Figure C-9 Polarization curve in $9.9 \times 10^{-3}\text{ M CaCO}_3$ at 35°C and 800 rpm

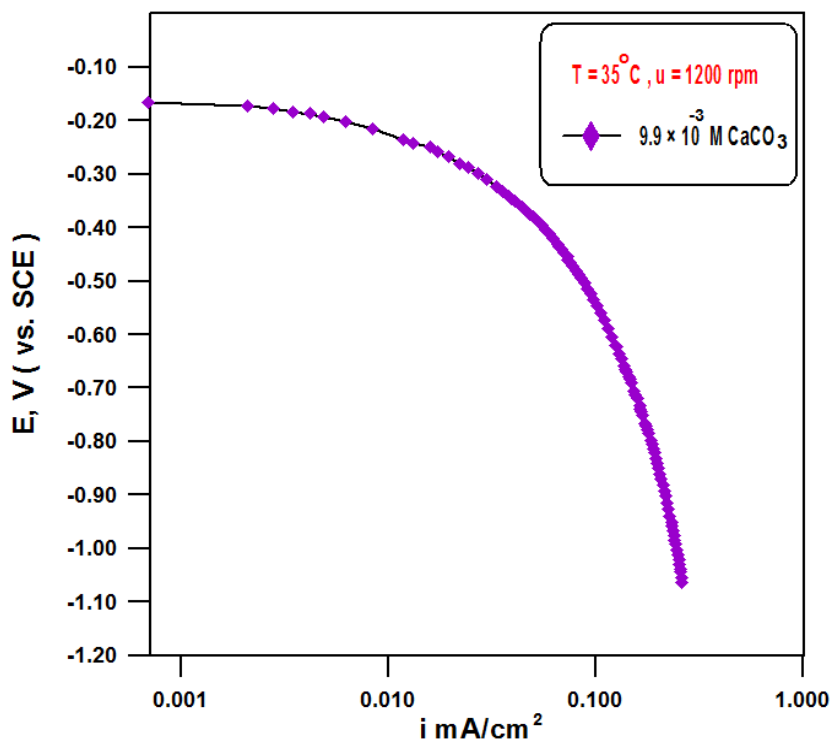


Figure C-10 Polarization curve in $9.9 \times 10^{-3}\text{ M CaCO}_3$ at 35°C and 1200 rpm

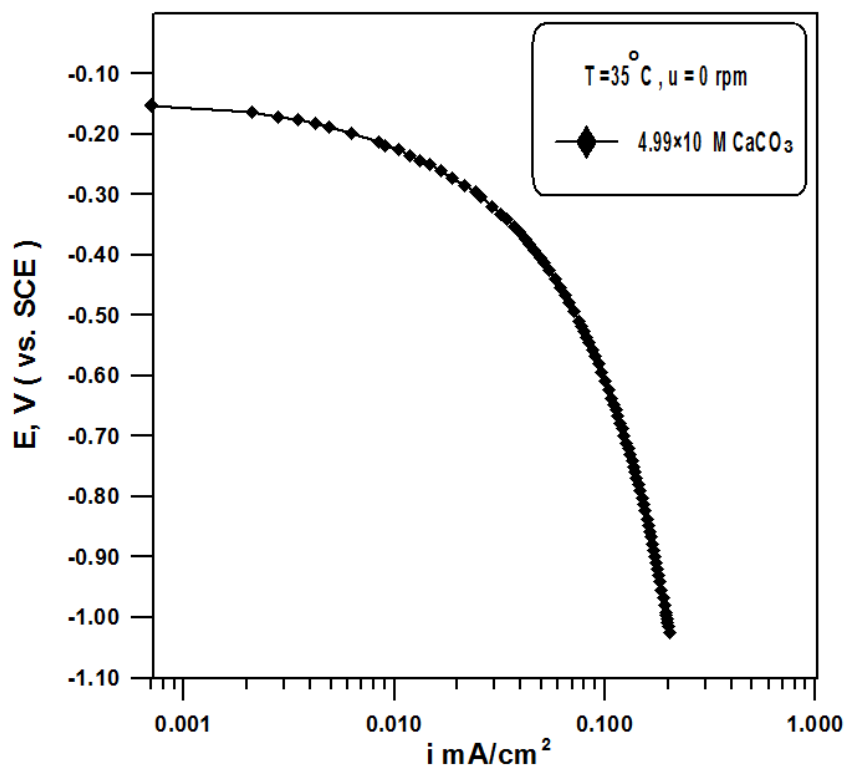


Figure C-11 Polarization curve in 4.99×10^{-3} M CaCO_3 at 35°C and 0 rpm

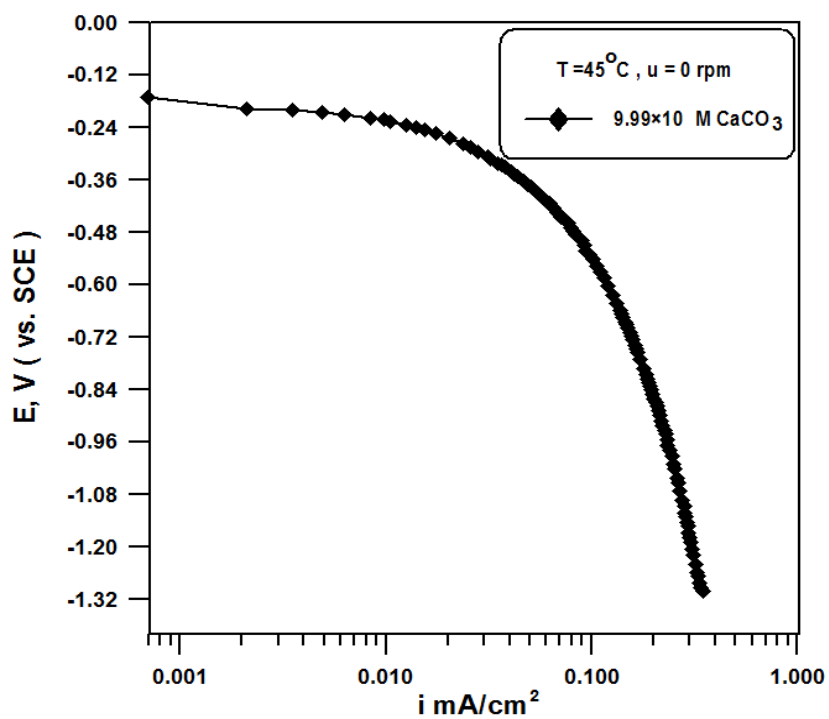


Figure C-12 Polarization curve in 9.9×10^{-3} M CaCO_3 at 45°C and 0 rpm

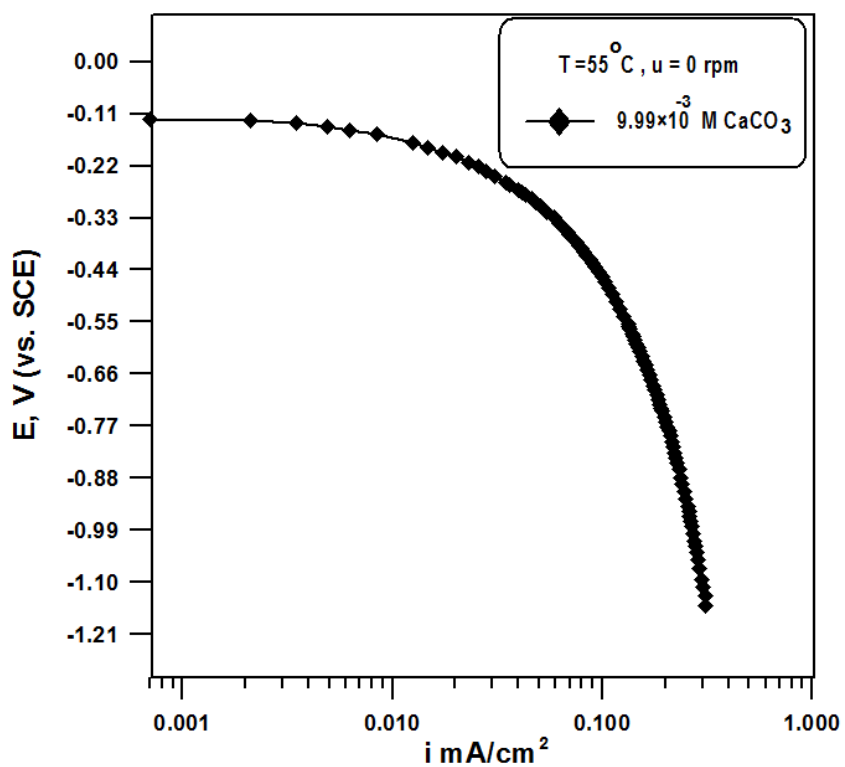


Figure C-13 Polarization curve in 9.9×10^{-3} M CaCO_3 at 55°C and 0 rpm

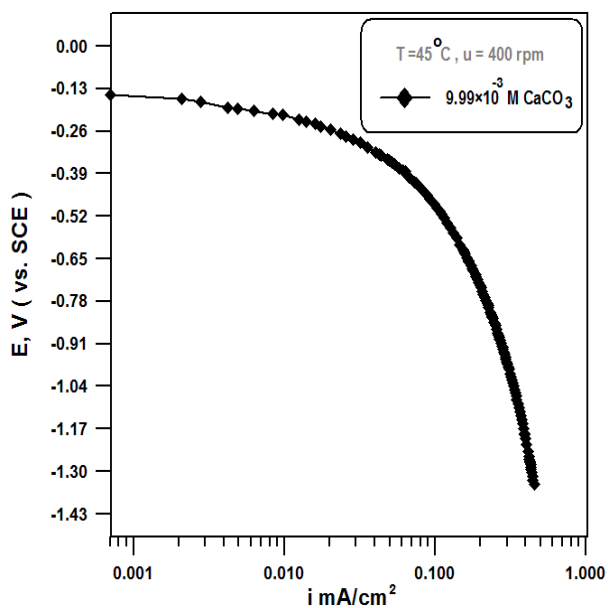


Figure C-14 Polarization curve in 9.9×10^{-3} M CaCO_3 at 45°C and 400 rpm

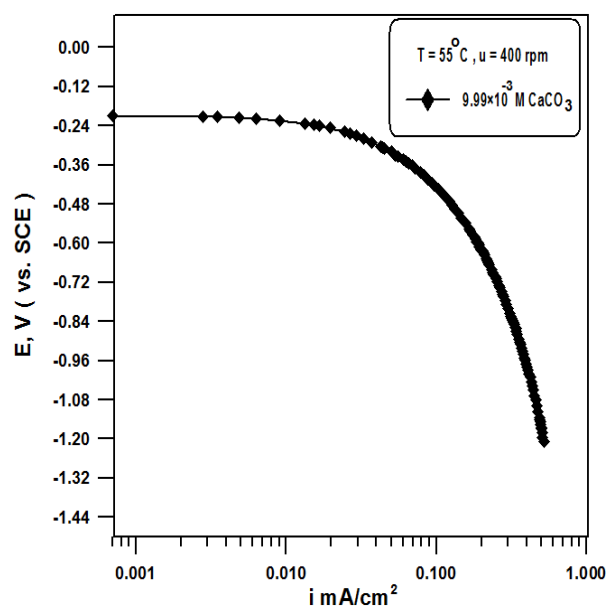


Figure C-15 Polarization curve in 9.9×10^{-3} M CaCO_3 at 55°C and 400 rpm

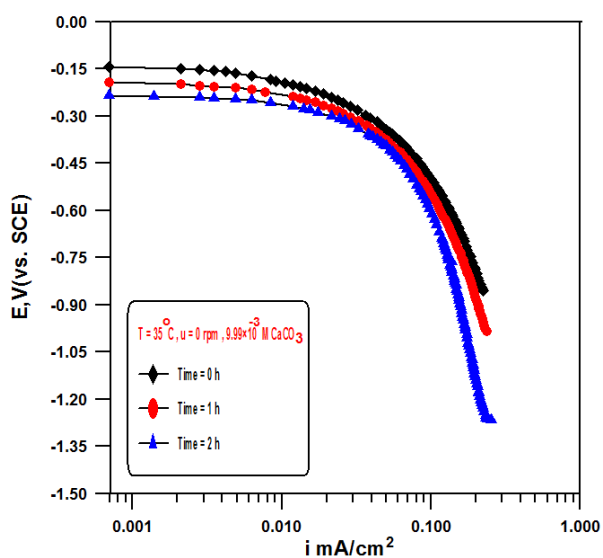


Figure C-16 Cathodic polarization curves in 9.9×10^{-3} M CaCO_3 at 0 rpm at 35 °C for 2h

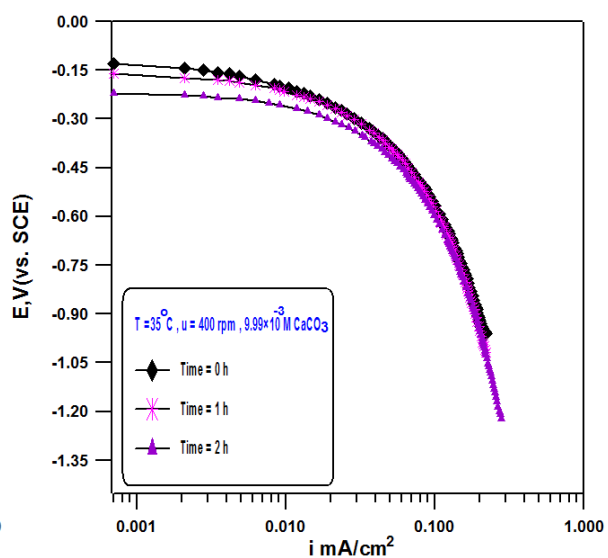


Figure C-17 Cathodic polarization curves in 9.9×10^{-3} M CaCO_3 at 400 rpm at 35 °C for 2h

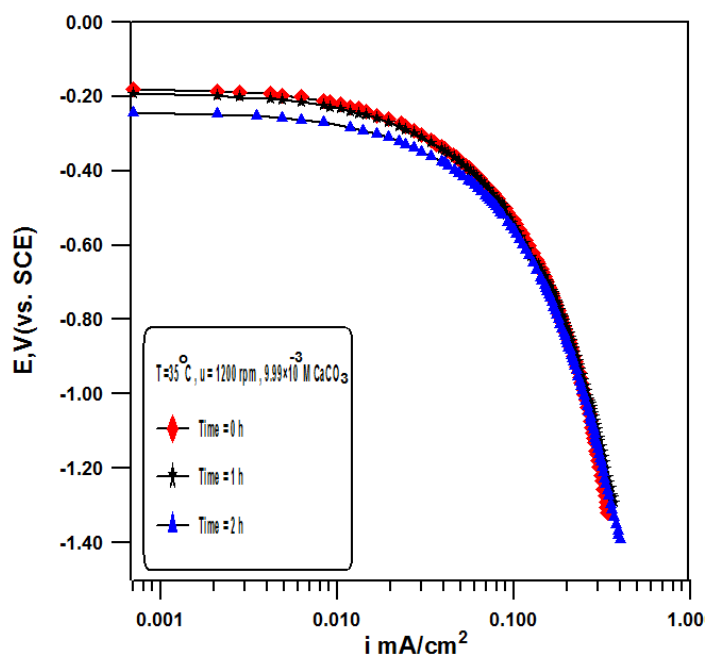


Figure C-18 Cathodic polarization curves in 9.9×10^{-3} M CaCO_3 at 1200 rpm at 35 °C for 2h

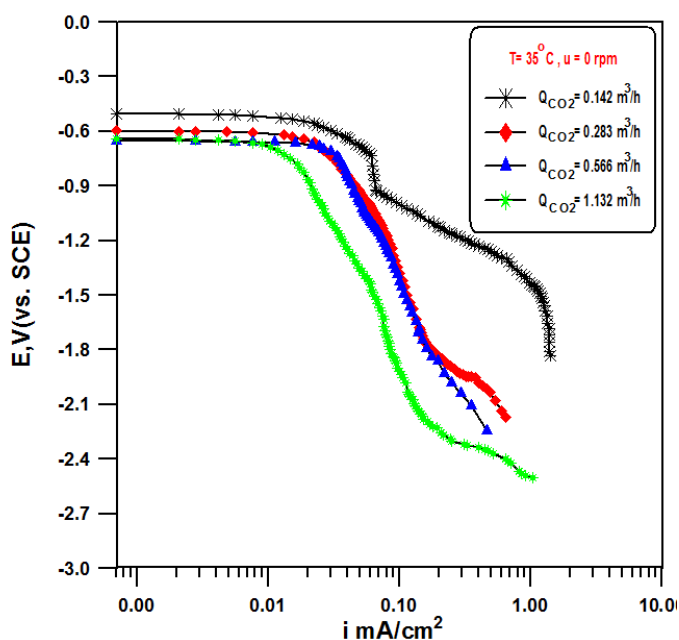


Figure C-19 Cathodic polarization curve in $9.9 \times 10^{-3} \text{ M CaCO}_3$ at different flow rate of CO_2 and 35°C and 0 rpm

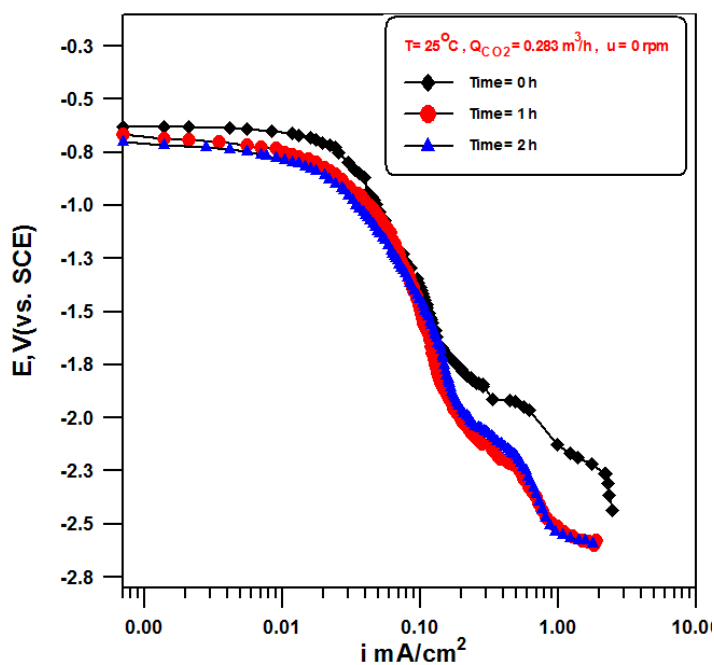


Figure C-20 Cathodic polarization Curves in $9.9 \times 10^{-3} \text{ M CaCO}_3 + Q_{\text{CO}_2} = 0.283 \text{ m}^3/\text{h}$ at 0 rpm at 25°C for 2 h

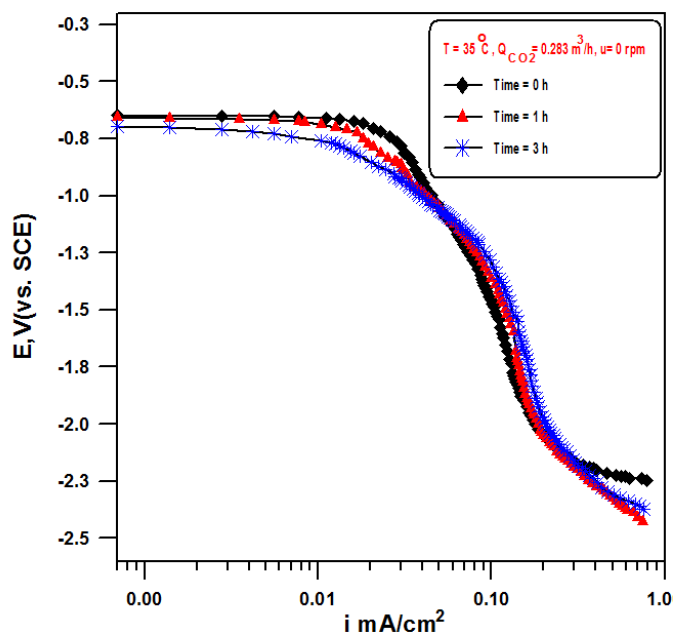


Figure C-21 Cathodic polarization curves in $9.9 \times 10^{-3} \text{ M CaCO}_3 + Q_{\text{CO}_2} = 0.283 \text{ m}^3/\text{h}$ at 0 rpm at 35°C for 2h

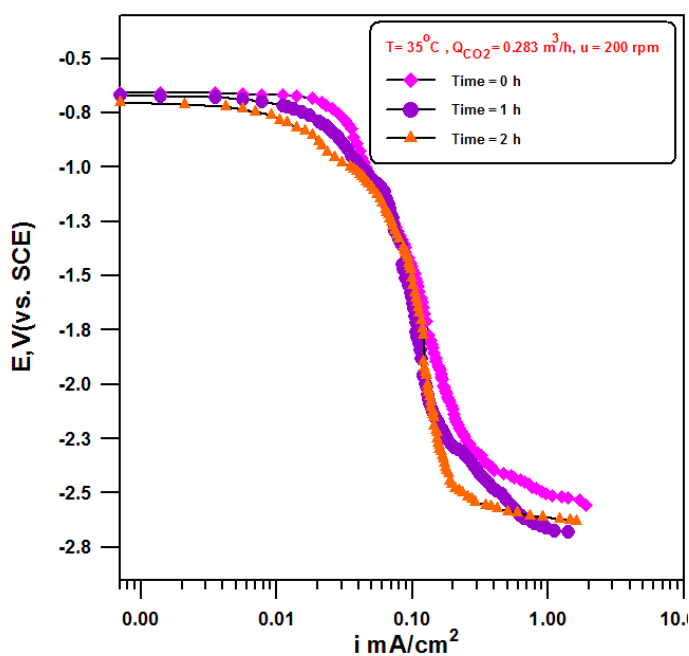


Figure C-22 Cathodic polarization curves in $9.9 \times 10^{-3} \text{ M CaCO}_3 + Q_{\text{CO}_2} = 0.283 \text{ m}^3/\text{h}$ at 200 rpm at 35°C for 2h

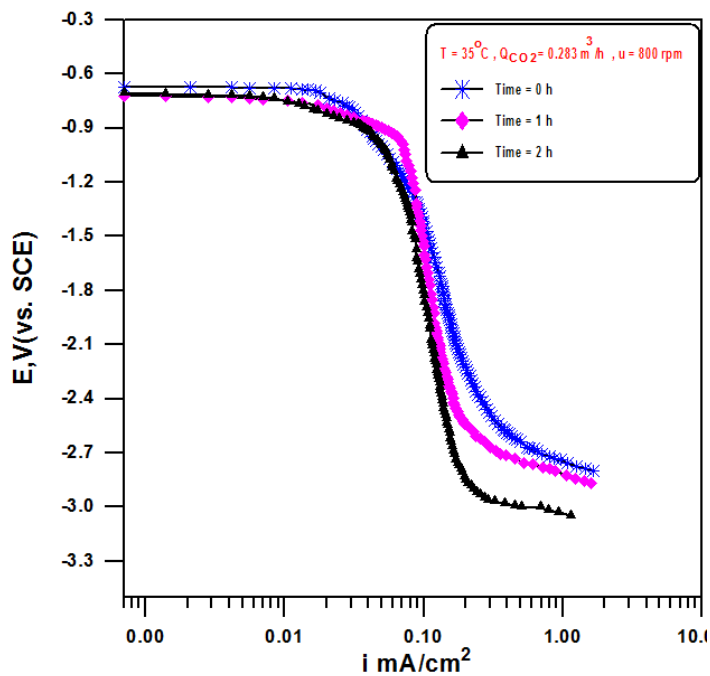


Figure C-23 Cathodic polarization curves in $9.9 \times 10^{-3} \text{ M CaCO}_3 + Q_{\text{CO}_2} = 0.283 \text{ m}^3/\text{h}$ at 800 rpm at $35 \text{ }^\circ\text{C}$ for 2h

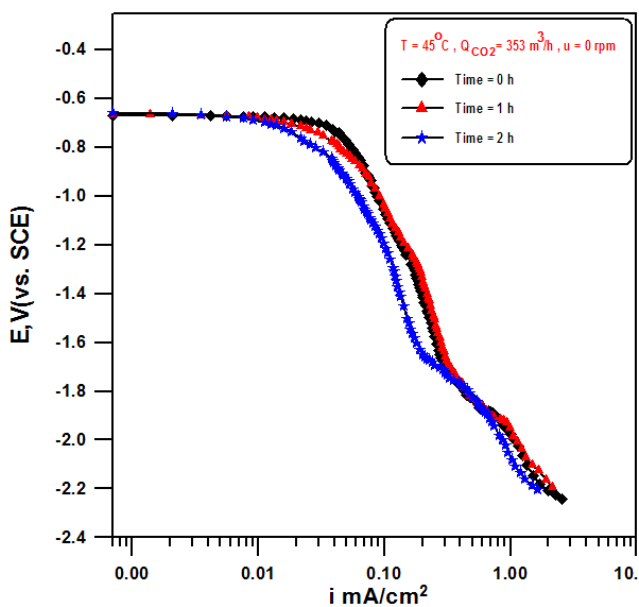


Figure C-24 Cathodic polarization curves in $9.9 \times 10^{-3} \text{ M CaCO}_3 + Q_{\text{CO}_2} = 0.283 \text{ m}^3/\text{h}$ at 0 rpm at $45 \text{ }^\circ\text{C}$ for 2h

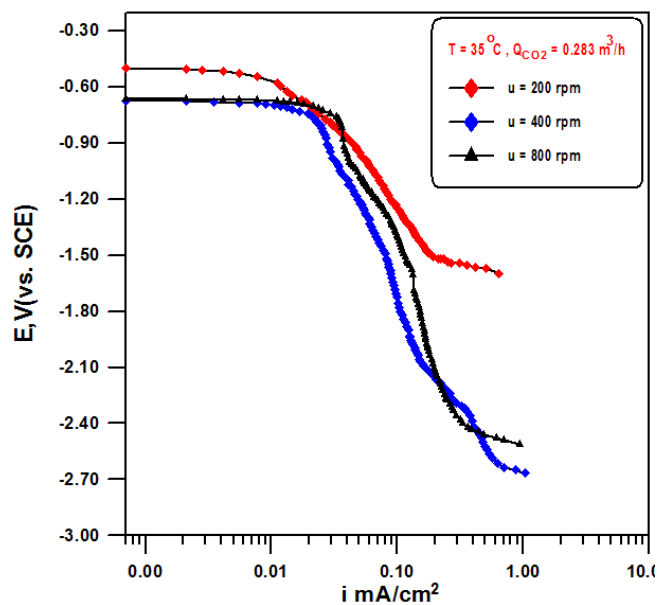


Figure C-25 Cathodic polarization curve in 9.9×10^{-3} M CaCO_3 at different rotational velocity, $Q_{\text{CO}_2} = 0.283 \text{ m}^3/\text{h}$, and 35°C .

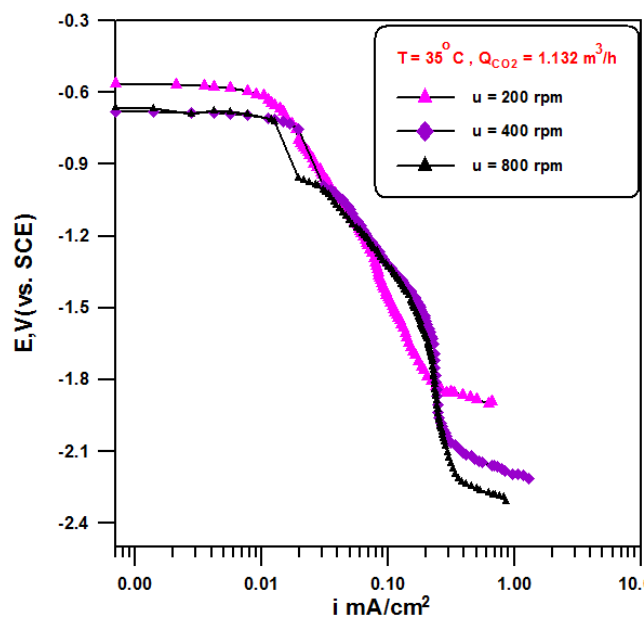


Figure C-26 Cathodic polarization curve in 9.9×10^{-3} M CaCO_3 at different rotational velocity, $Q_{\text{CO}_2} = 1.132 \text{ m}^3/\text{h}$, and 35°C .

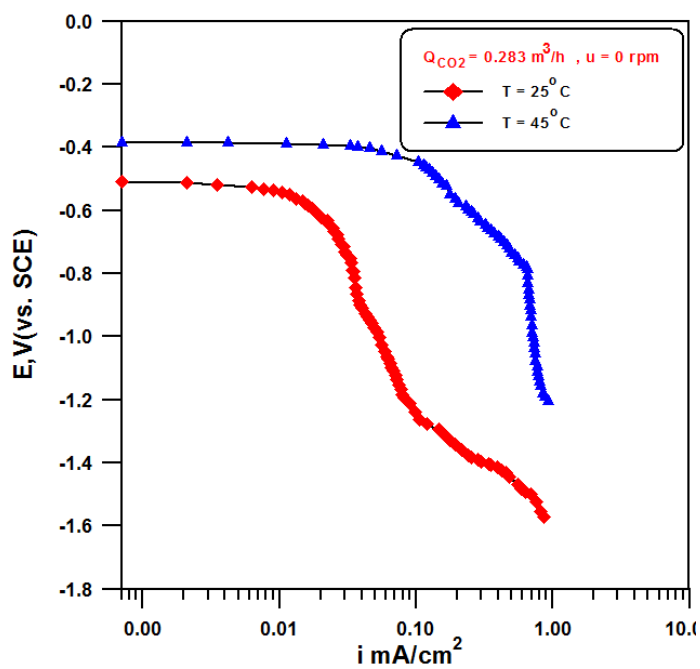


Figure C-27 Cathodic polarization curve in 9.9×10^{-3} M CaCO_3 at different temperature, $Q_{\text{CO}_2} = 0.283 \text{ m}^3/\text{h}$, and 0 rpm.

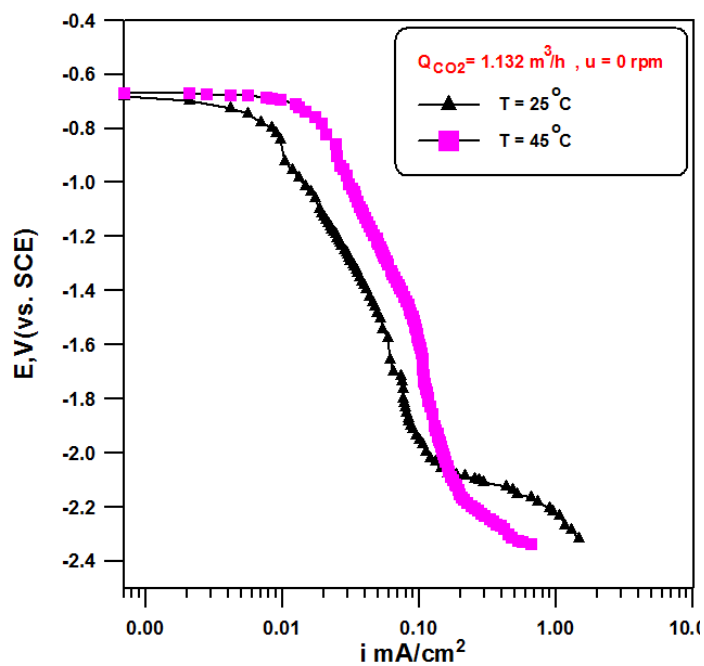


Figure C-28 Cathodic polarization curve in 9.9×10^{-3} M CaCO_3 at different temperature, $Q_{\text{CO}_2} = 1.132 \text{ m}^3/\text{h}$, and 0 rpm.

Chapter Five

Discussion

5.1 Introduction

This chapter discusses the experimental results presented in chapter five for brine, brine-gas oil mixture, acids, and brine-CO₂ gas, for the whole investigated ranges of rotational velocities, temperature, brine concentration, time, and cathodic protection.

5.2 Corrosion rate in single phase CaCO₃ Solution

Fig. 5-1 shows the effect of rotational velocity on corrosion rate of carbon steel (CS) in 2.5×10^{-3} M CaCO₃ at T =35 °C. The figure indicates that the corrosion rate increases with rotational velocity. This trend is in agreement with pervious works [Mahtato et al, 1980, Saliman et. al, 2008, Hasan and Sadek, 2014]. The increase of CR with flow velocity is due to the increased transport of oxygen from bulk of the solution to the metal surface. The rate of oxygen reduction reaction is generally limited by the speed at which oxygen can reach the surface of the metal. Previous studies [Foroulis, 1979; Scheers, 1992; Shreir et.al, 2000, Slaiman and Hasan, 2010] indicated that the greater turbulence due to high velocities results in more uniform O₂ concentration near the surface. Fig. 5.1 reveals that at extremely high velocity the CR tends to decrease. This can be ascribed to the fact that at high velocity the formation of corrosion product is higher which leads to protect and passivate the metal surface [Revie and Uhlig, 2008; Fontana, 1986].

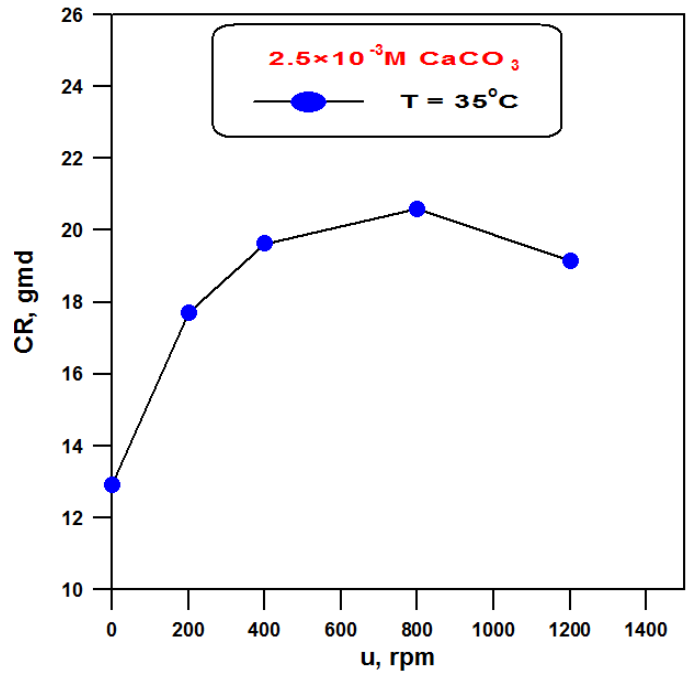


Figure 5-1 Variation of corrosion rate with velocity in 2.5×10^{-3} M CaCO_3 solution at 35°C .

Figure 5-2 shows photos of the specimen of CS before and after exposure to corrosion environment in CaCO_3 solution at $T = 35^\circ\text{C}$. Photo (a) before corrosion (b) after corrosion before cleaning and (c) indicates clear corrosion attack.

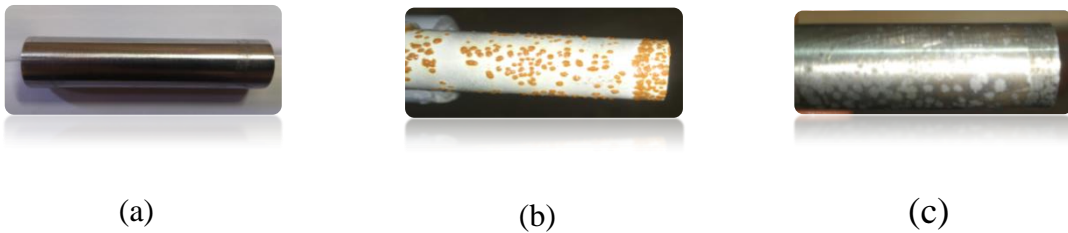


Figure 5-2 Carbon steel specimens (a) before (b) after exposure corrosion (c) after cleaning corrosion attack.

5.3 Corrosion rate in two phase brine – gas oil

Figure 5-3 shows the effect of rotational velocity on corrosion rate of carbon steel (CS) in 2.5×10^{-3} M CaCO_3 solution –gas oil mixture at different

concentrations of gasoil at 35 °C. It is clear that in two phase that, increasing velocity leads to increase the turbulence and increase the number of dispersed phase droplets. Which leads to increase the number of droplets, more intimate contact between the dispersed phase droplets and the metal specimens. Accordingly increasing velocity increases the corrosion rate due to the increasing the O₂ transport to the surface from continuous phases to the metal surface. When further increasing of rotation velocity (mixing velocity) the corrosion rate goes down. This is attributed to the fact that when increasing rotational velocity the shear forces increase leading to break the dispersed phase (gas oil) drops to small droplets which, in turn, increase the contact area between dispersed phase (gas oil) and the metal as well as the probability of striking the metal by gasoil droplets also increases leading to a decrease in the corrosion of carbon steel metal because gasoil is generally less corrosiveness than brine owing to its low electrical conductivity as shown in Table B-4. Some studies for corrosion under two phase dispersion flow, confirmed that the drop impact velocity at the surface affects corrosion rate [Benendetto et. al, 2003; El-Batsh et. al, 2012].

Comparing Figs. 5.1 and 5.3 indicate that corrosion rates in two phase (concentration of gas oil (1, 2, 5%vol.)) is lower than that in single phase of CaCO₃ solution. This is ascribed to the fact that the electrical conductivity of gas oil is lower than that of water (CaCO₃ solution). The solubility of oxygen in gas oil is much higher than that in water, for example, at room temperature the solubility of oxygen in gasoil is 154 cm³/L [Nelson, 1958], while in water it is about 30 cm³/L [Perry and Chilton, 1997; Shreir, 2000]. Also, the figure reveals that as the volume percent of gasoil increases, the corrosion rate increases, this increase is attributed to the fact that the presence of dispersed phase (gas oil) in relatively high percent leads to an increase in the O₂ concentration in the solution

of two-phase (because of high O₂ content of gasoil) therefore the corrosion rate will be higher.

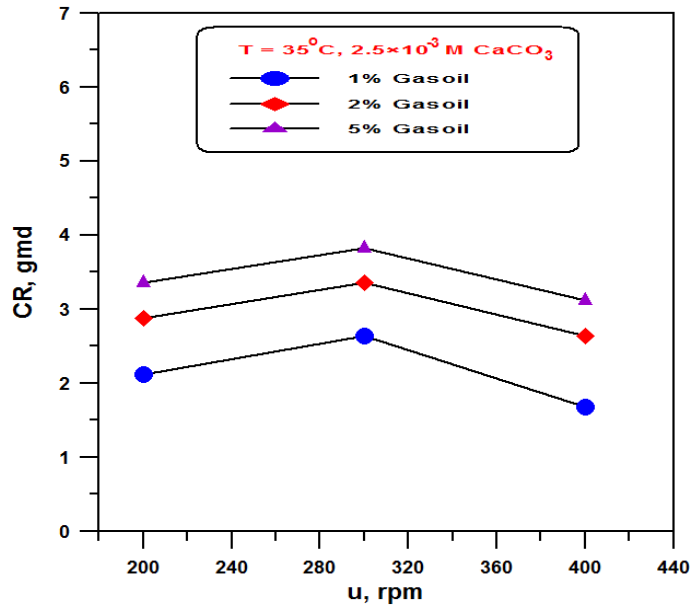


Figure 5-3 Variation of CR with velocity in two phase CaCO₃ + gasoil at 35°C.

The influence of hydrodynamics on corrosion is rather complicated since corrosion is controlled by mass transport through a damped turbulent boundary layer followed by transport through a porous corrosion product layer [Hasan, 2003].

5.4 Corrosion rate of two phase mixture in presence of acids

Figure 5-4 shows the effect of rotational velocity on corrosion rate of carbon steel (CS) in 2.5×10^{-3} M CaCO₃ in the presence of 2% HCl and gas oil at different concentrations under 35 °C. It is clear that increasing the rotation velocity from 200 to 400 rpm leads to an increase in the corrosion rate. This increase is due to the increase in the oxygen transport to metal surface with increase the flow velocity. This agrees with previous studies that found an increases in the corrosion rate of iron in oxygen saturated acid solutions, with

increasing velocity of the solution [Ross et.al, 1966, Hasan and Sadek, 2014]. George and Nesic [2007] stated that the increase in CR with flow velocity in acid solutions is due to the increase in the diffusion of hydrogen ion.

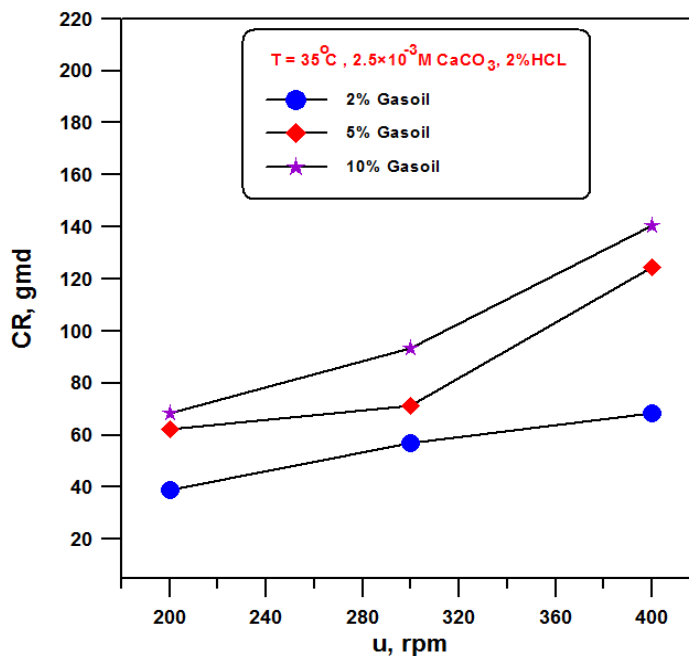


Figure 5-4 Variation of CR with velocity in two phase brine- gasoil in presence of HCl.

The presence of acid in the brine- gas oil mixture makes the process under mixed control, i.e. mass transfer and activation control. In addition the mixture becomes more corrosive, so that, the corrosion rate in 2.5×10^{-3} M CaCO_3 with 2% HCl and gasoil is higher than that in brine solution alone. The increased corrosion rate of iron as pH decreases (i.e. the pH of 2.5×10^{-3} M CaCO_3 is 8.84 and it decreases to 0.29 in 2.5×10^{-3} M CaCO_3 + 2% gasoil+ 2% HCl mixture) is caused by increased hydrogen evolution reaction that leads to greater accessibility of oxygen to the metal surface on dissolution of the surface oxide favors oxygen depolarization [Hasan and Sadek, 2012]. Fig. 5-4 reveals, also, that as the volume percent of gasoil increases (2, 5, and 10%) with HCl content, the corrosion rate increases. This increase is attributed to the fact that the

presence of dispersed phase in relatively high percent leads to the increase in O₂ concentration of acidic two-phase solution because high O₂ content of gasoil therefore the corrosion rate will be higher. The oxygenated acids are characterized by high corrosiveness as has been evidenced by several studies [Shrier, 2000, Hasan and Sadek, 2014]. Previous studies of Alwash et.al [1987] and Turkee [2009] reported that the corrosion rate in aerated acidic solutions increases as the flow increases.

Figure 5-5 shows the effect of rotational velocity on corrosion rate of carbon steel (CS) in 2.5×10^{-3} M CaCO₃ + 2% HCl +5% gasoil at different temperatures of 25, 35, and 45 °C that expressed in gmd with flow velocity. It is clear that increasing the velocity leads to an increase in the corrosion rate. An increase in temperature of acid solutions can affect the corrosion behavior of materials in different ways: (i) the rate of chemical reaction increases with temperature. This issue is here very effective because the system was under activation control because of the presence of acid [Khadom et.al, 2009], (ii) The solubility of some of the reaction products may change resulting in different corrosion reaction products,(iii) viscosity is decreased leading to an increase in the diffusion coefficient of O₂ [Bird et.al, 2002; Brodkey and Hershey 1998]. The study of Niyazi and Serpen [2010] showed that the amount of corrosion increases with HCl concentration, temperature and duration. The rate of corrosion also increases at high temperatures and high HCl concentrations.

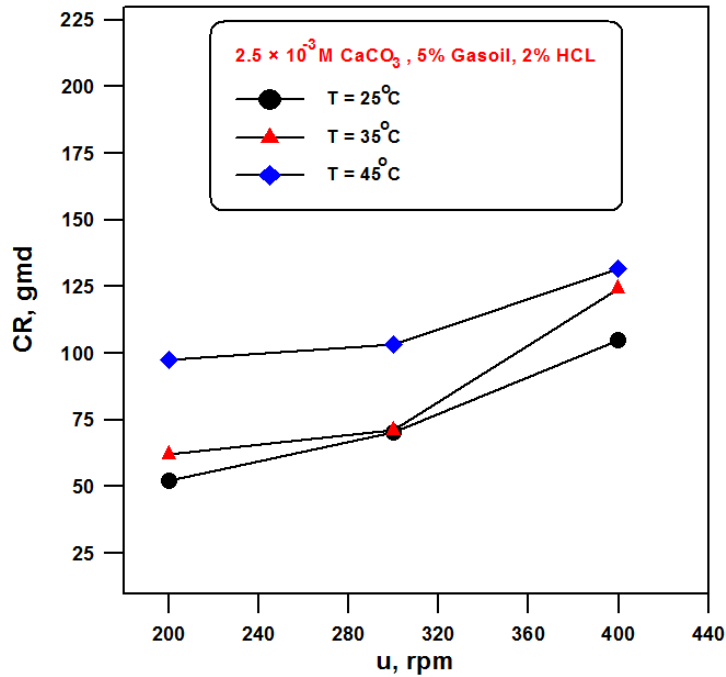


Figure 5-5 Variation of CR with velocity in two phase brine- gasoil in presence of HCl at different temperatures.

Figure 5- 6 shows the variation of corrosion rate with rotation velocity expressed in gmd with velocity at 35 °C in 2.5×10^{-3} M CaCO_3 in the presence 2% H_2SO_4 with different concentration of gas oil. The figure indicates that the corrosion rate increases with rotational velocity. Consequently, the corrosion rate of the carbon steel increases. Also, the figure reveals that as the volume percent of gasoil increases (5 to 10%) with constant volume percent of H_2SO_4 , the corrosion rate increase. This increase is because of high O_2 content of gasoil that will diffuse in the solution due to high turbulence accompanying the agitation; therefore, the corrosion rate will be higher.

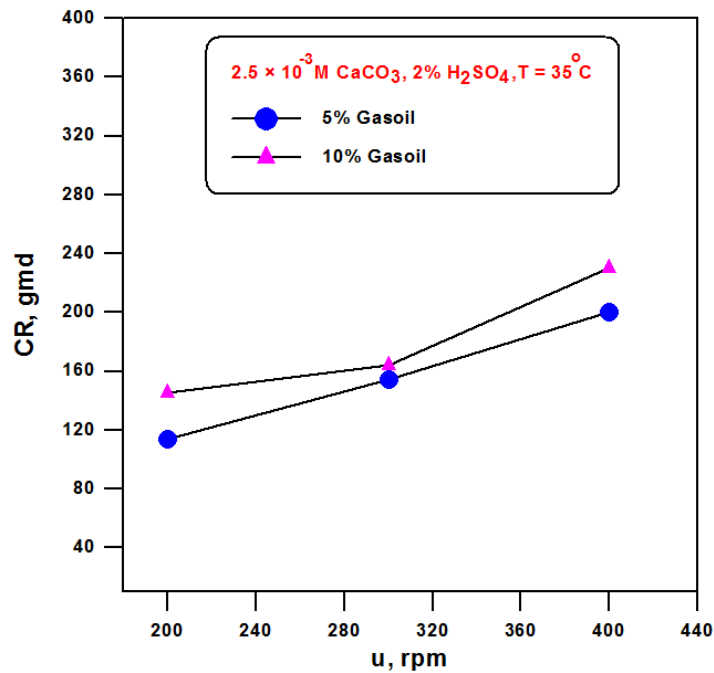


Figure 5-6 Variation of CR with velocity in two phase brine- gasoil in presence of H₂SO₄.

When carbon steel contacts sulfuric acid, the latter is reduced to form H₂ and the iron oxidizes with the formation of ferrous sulfate (FeSO₄), as shown in reaction:



The FeSO₄ adheres to the steel surface and forms a protective layer. This layer prevents the metal against further attack by sulfuric acid. Therefore, the corrosion rate of carbon steel depends on the preservation of the FeSO₄ layer [Zehbour et.al, 2012].

Figure 5-7 shows the variation of corrosion rate with temperature at 300 rpm in 2.5×10^{-3} M CaCO₃ in the presence 2% H₂SO₄ and 5% gas oil that expressed in gmd. It is clear that corrosion rate increases slightly when the temperature increases from 25 °C to 35 °C and increases considerably when the temperature increases to 45°C. The increase in CR with temperature is well

known phenomenon in acid solutions. This behavior can be explained as follows: increasing temperature leads to change two variables. Firstly, increasing temperature accelerates the reaction rate according to Arrhenius equation. Secondly, diffusion rate of dissolved oxygen increases by increasing the molecular diffusion coefficient [Henry and Scott, 1999; Revie and Uhlig, 2008]. However, as the temperature increases the O₂ solubility increases. Zehbour et.al, [2012] in their study on corrosion of carbon steel pipes and tanks by concentrated sulfuric acid, stated that the corrosion mechanism of carbon steel in sulfuric acid is accelerate by several factors such as concentration, temperature, and velocity flow.

Corrosion rate show is considerably increased in brine-acid solution compared with solution containing brine only, the increase high electrical conductivity of two-phase compared to single phase (brine) as shown in Tables B-3 and B-4.

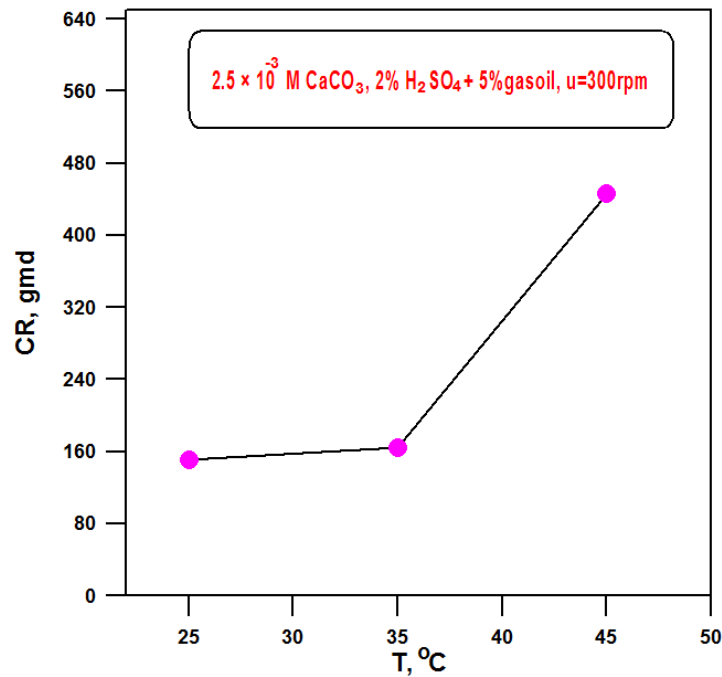


Figure 5-7 Variation of CR with temperature in two phase brine- gasoil in presence of H₂SO₄.

Figure 5-8 shows photos of the specimen of CS before and after exposure to corrosion in brine-gasoil mixture with the presence of HCl acid at $T = 35\text{ }^{\circ}\text{C}$. Photo (b) indicates clear corrosion attack.



Figure 5-8 specimen of CS (a) before (b) after exposure to corrosion in presence of HCl acid.

5.5 Cathodic polarization of brine (CaCO_3) solution

5.5.1 Corrosion rate

Polarization technique was also used to measure the corrosion rate by plotting cathodic polarization curves to obtain the limiting current density (LCD) i_L .

Figure 5-9 shows the variation of oxygen limiting current density (i_L) with rotational velocity in 2.5×10^{-3} and 9.9×10^{-3} M CaCO_3 solutions at $T = 35\text{ }^{\circ}\text{C}$. It is clear that increasing the velocity leads to an increase in the limiting current. The increase in the i_L is due to the increase in the transport of oxygen word to the metal surface [Foroulis, 1979, Mahato et al, 1980; Slaiman and Hasan, 2010]. The influence of velocity on i_L can be understood with the aid of Fig. 2-2. According to this figure increasing velocity, at constant temperature, leads to shift the intersection point between the cathodic curve of O_2 reduction and anodic curve of Fe dissolution. Hence the limiting current density will be increased. Fig. 5-9 reveals that at extremely high velocity the corrosion rate (or i_L) slightly decreases. This support the weight loss results (Fig. 5-1). However, Fig. 5-9 indicates that the limiting current density is higher when the CaCO_3 concentration is high for the whole range of rotational velocity.

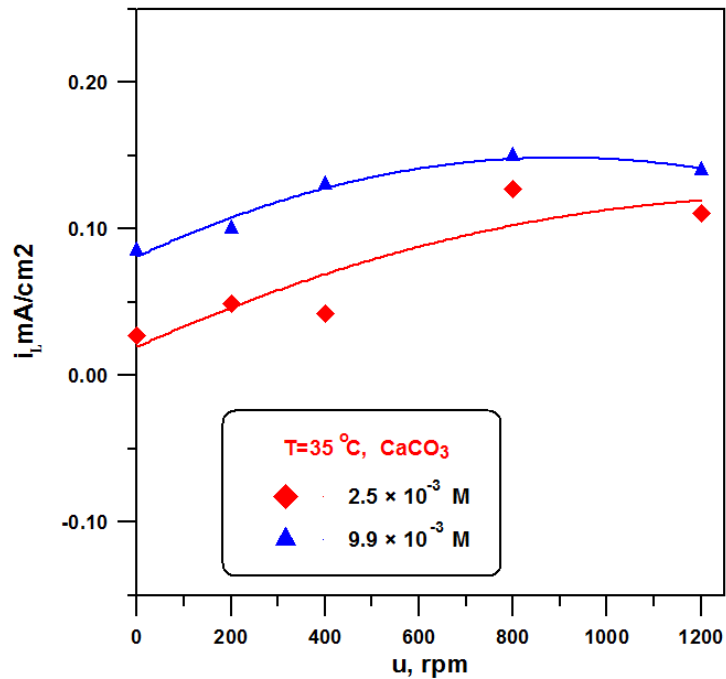


Figure 5-9 Effect of velocity on i_L in brine CaCO_3 of different concentrations

Figure 5-10 shows the effect of calcium carbonate concentrations on the i_L at 35 °C and 0 rpm. It is clear that increasing CaCO_3 concentration from 2.5×10^{-3} to 9.99×10^{-3} M leads to an increase in i_L from 0.027 to 0.0715 mA/cm². This behavior can be attributed to the increased electro-conductivity because of the increased salt content; as listed in Table B-3. The same trend was noticed in previous works for corrosion in NaCl solution, Na_2SO_4 solution [Revie and Uhlig, 2008; Hasan and Sadek, 2014]. The study of Bahar [2002] showed that, in stationary aerated water, the limiting current density increases with increasing NaCl concentration up to 3.5%.

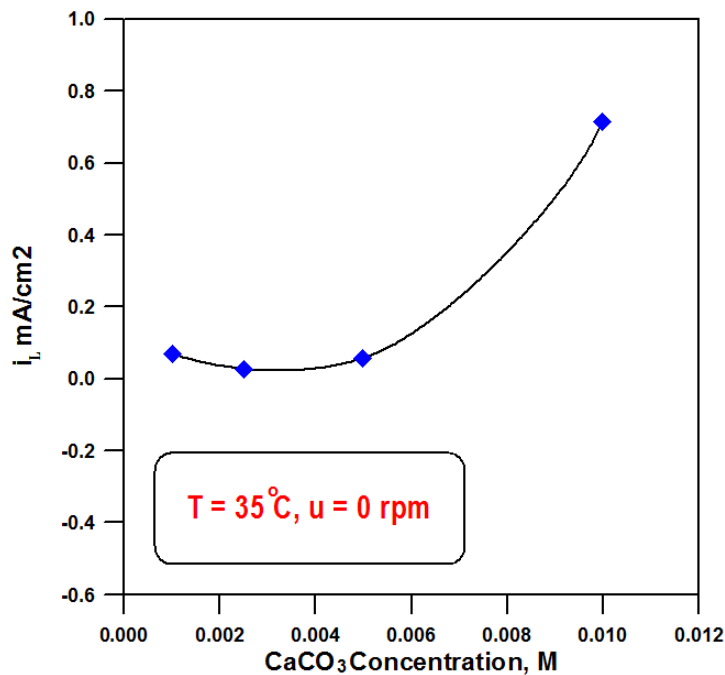


Figure 5-10 Effect of CaCO₃ concentration on i_L .

Figure 5-11 shows the variation of oxygen limiting current density (i_L) with temperatures in 9.9×10^{-3} M CaCO₃ at 0 and 400 rpm. It is clear that increasing the velocity leads to an increase in the limiting current. The increase in the i_L with velocity is due to the increase in the transport of oxygen word to the metal surface [Foroulis, 1979, Mahato et al, 1980]. The effect of temperature on the corrosion rate for mass transfer control systems is represented by changing two parameters affecting the corrosion rate in opposite ways that are the O₂ solubility and diffusivity. Increasing the temperature will increase the rate of oxygen diffusion to the metal surface by decreasing the viscosity of water and by increasing the solution electrical conductivity. All these factors enhance the corrosion rate. On the other hand, increasing temperature decreases the oxygen solubility and there by restrains the corrosion [Mahato et.al, 1980, Shrier, 2000, Slaiman and Hasan, 2010, Hasan and Sadek, 2014].

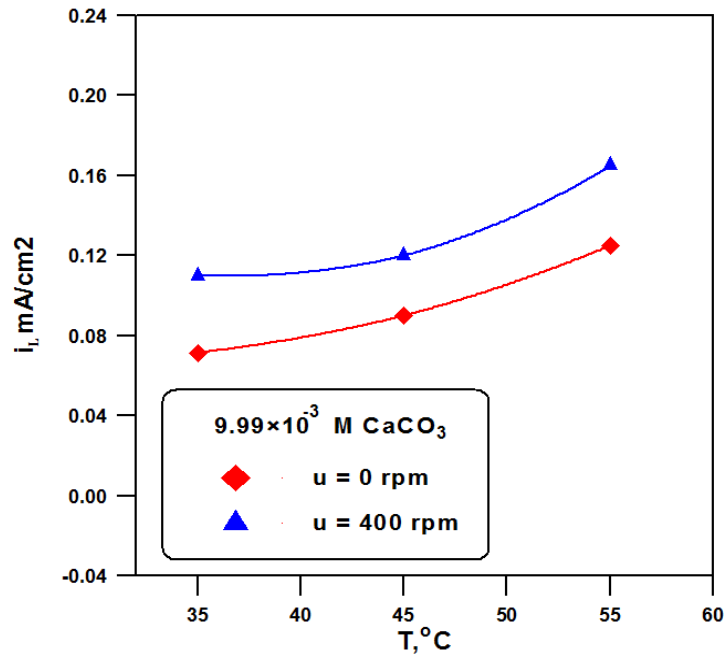


Figure 5-11 variation of temperature on i_L in 9.9×10^{-3} M CaCO_3

Fig. 5-12 illustrates the variation of i_L with time in 9.9×10^{-3} M CaCO_3 at different rotation velocities of 0, 400, and 1200 rpm under 35°C . Examining this figure shows that i_L values decrease with time for all three velocities. The main reason for that is the formation of corrosion products with time [Mahato et al 1968; Slaiman and Hasan, 2010]. In addition, the surface activity decreases with time. Also this figure indicates that for $u=1200$ rpm the decrease in i_L with time is high because high velocity leads to form the corrosion product layer quickly.

The higher the velocity is the higher the decrease in the corrosion rate due to high amount of corrosion products formed which in turn restrains the arrival of dissolved O_2 to the surface. This indicates the important inhibitive effect of this fouling layer to decrease the corrosion. These results agree with the studies of Mahato et. al, [1968 a, b; 1980] and Slaiman and Hasan [2010] for pipe flow these authors indicated that the corrosion rate always decreases with time.

However Slaiman and Hasan [2010] noticed that the formation of corrosion product at low temperature leads to decrease the corrosion rates even at high velocities, but at high temperature and high flow velocities, the formation of corrosion product leads to an increase in the corrosion rate.

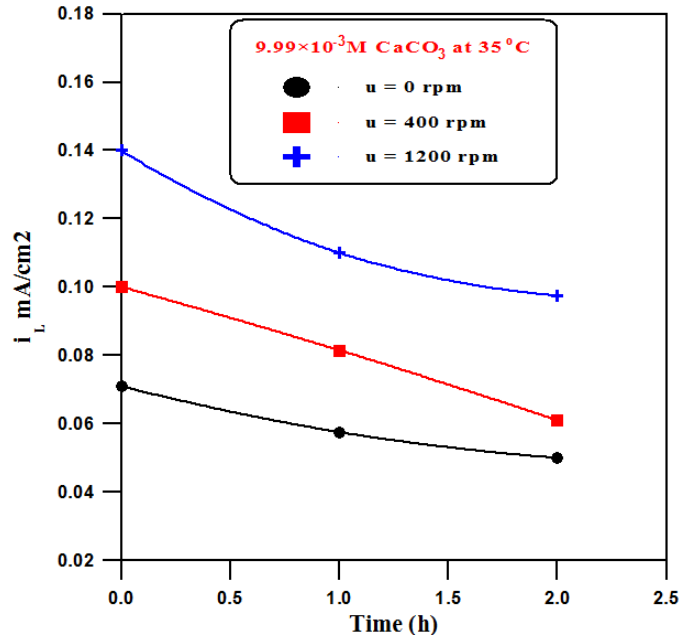


Figure 5-12 Variation of i_L with time at 35 °C and different velocities in 9.9×10^{-3} M CaCO_3

5.5.2 Corrosion Potential

It is generally accepted that the corrosion potential of iron is under mixed control of anodic and cathodic processes [Shreir, 2000; Fontana, 1986]. Therefore, the corrosion potential in aerated and oxygen-saturated solutions is flow dependent since the cathodic process, i.e., oxygen reduction reaction, is mass transfer controlled.

Figure 5-13 illustrates the effect of velocity on the corrosion potential (E_c) in 2.5×10^{-3} and 9.9×10^{-3} M CaCO_3 at $T = 35$ °C. It is clear that the corrosion potential shifts to more positive values with increasing rotation

velocity and then decreases. Some investigators noticed unstable variation of corrosion potential with flow velocity [Foroulis, 1979].

The increase in corrosion potential with flow velocity is mainly due to the increase in the O₂ transport to the surface of metal [Foroulis, 1979; Slaiman and Hasan, 2010; Hasan and Sadek, 2014]. In addition, Fig. 6.13 indicates that in case of high salt concentration brine, the corrosion potential is lower. The increase in salt concentration leads to a decrease in O₂ solubility (Table B-1) and, therefore, shifts the corrosion potential to more negative [Revie and Uhig, 2008; Hasan and Sadek, 2014]. That is in agreement with previous findings of other workers [Nesic et. al, 1995; Hasan 2003; Hasan and Sadek, 2014]. Ross et. al. [1966] stated that the increase of E_{cor} with velocity is due to the increase in oxygen transport to the metal surface and when the system is free from oxygen, the velocity has no effect on E_{corr}.

Figure 5-14 shows the effect of calcium carbonate concentrations on the corrosion potential (E_{corr}) at 35 °C and 0 rpm. It is evident that increasing CaCO₃ concentration from 2.5×10^{-3} to 9.99×10^{-3} M, leads to shift the corrosion potential to more negative. Figure 5-15 shows the variation of corrosion potential (E_{corr}) with temperatures in 9.9×10^{-3} M CaCO₃ at 0 and 400 rpm. It is clear that at a constant velocity the corrosion potential shifts to more positive (more anodic) values with increasing temperature and increase with increase velocity from 0 to 400 rpm.

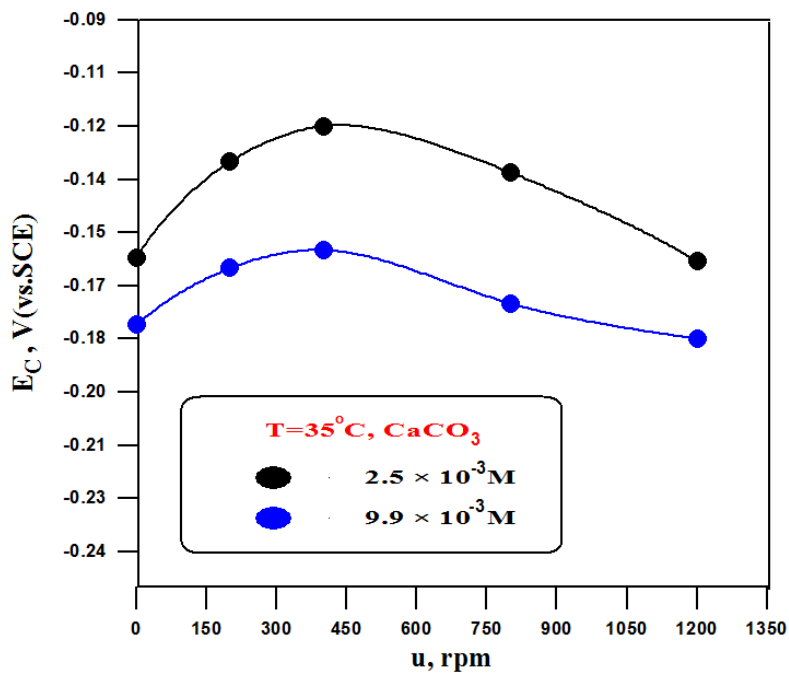


Figure 5- 13 variation of velocity on corrosion potential in brine CaCO_3 solution.

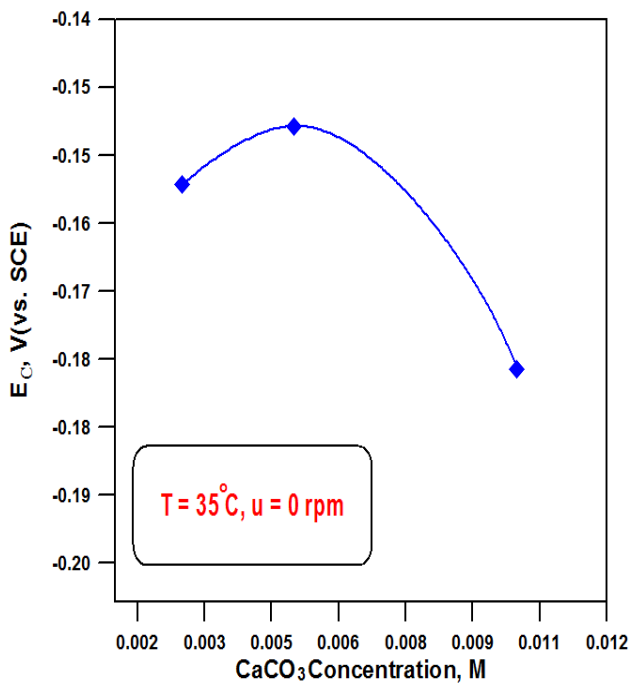


Figure 5-14 Effect of salt concentration on corrosion potential.

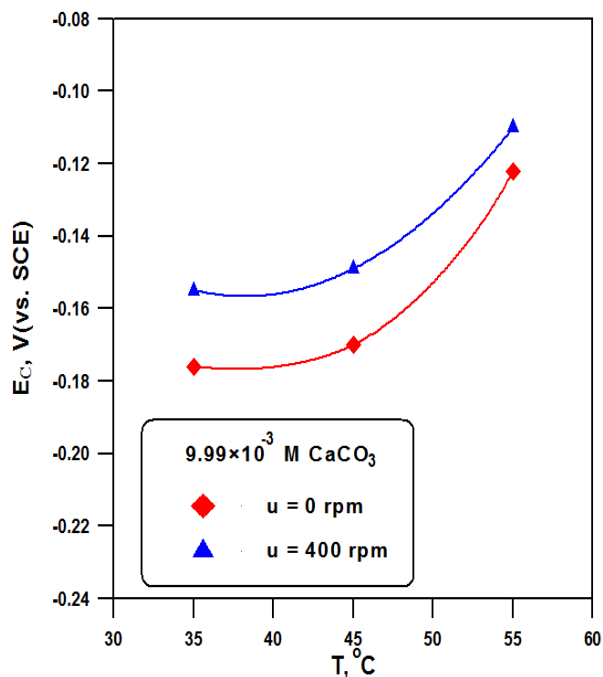


Figure 5-15 variation of temperature on corrosion potential

Figure 5-16 shows the variation of corrosion potential with time in 9.9×10^{-3} M CaCO_3 at different flow velocities of 0, 400, and 1200 rpm and constant temperature of 35°C . The figure indicates that the corrosion potential is shifted to more negative with time. Which may be related to loss of metal activity with time and due to the formation of corrosion product layer which increases the resistance polarization by insulating the metal from the solution shifting its potential to more negative.

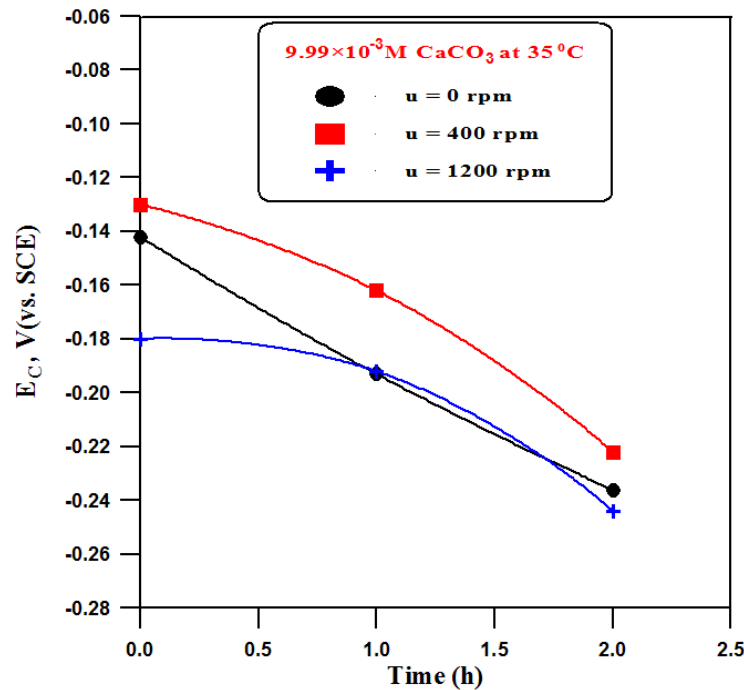


Figure 5-16 variation of time on corrosion potential in 9.9×10^{-3} M CaCO_3

Figure 5-17 shows photos the specimen of CS before and after exposure to cathodic polarization of brine (CaCO_3) solution 35°C . Photo (b) shows the deposition of salt and corrosion product layer on the specimen. Photo c shows the corroded surface after cleaning. Photo d shows the corrosion product layer at temperature 45°C .

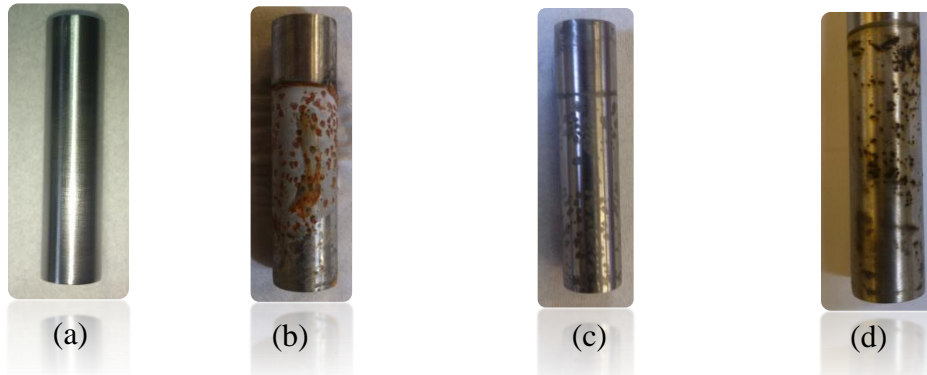


Figure 5-17 Carbon steel specimens (a) before (b) after corrosion (c) after cleaning (d) corrosion product layer on the specimen at 45 °C.

Figure 5-18 shows the surface morphology of corroded specimen obtained using optical microscope after exposure to corrosion environment in brine CaCO_3 solution at $T = 35^\circ\text{C}$.

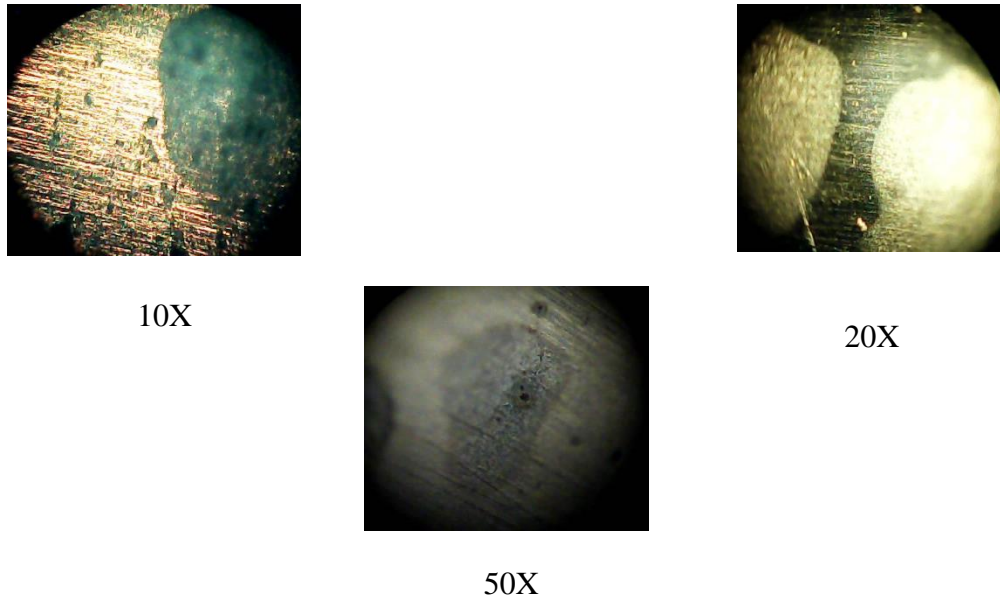


Figure 5-18 Optical microscope examination (10 X, 20X and 50X) of carbon steel specimen after exposure.

5.6 Cathodic polarization of CaCO₃ solution in presence CO₂

5.6.1 Corrosion rate

There is considerable evidence that the dissolution of CO₂ in an aqueous solution will result in dissolved carbon dioxide and dissociated carbonic acid. The limiting current density is for carbonic acid as has been postulated by previous studies concerning CO₂ corrosion [Riesefeld and Biohm, 1950; Postlethwaite et.al, 1996; Kermani and smith, 1997; George and Nestic, 2007]. The corrosion mechanism of carbon steel by carbon dioxide corrosion is a complicated process that is influenced by many factors and conditions i.e. temperature, pH, partial pressure of CO₂, etc. [Kermani and Morshed, 2003].

Figure 5-19 shows the variation of limiting current density (i_L) with volumetric flow rate (pumping rate through the solution) of CO₂ in 9.9×10^{-3} M CaCO₃ at 35 °C under static conditions. It is clear that increasing the flow rate of gas leads to a decrease in the limiting current (corrosion rate). This trend is in agreement with unpublished work of Hasan [2014] for galvanic corrosion of CS-Al in CO₂ environment. The decrease in the i_L is due to the increase in gas hold up in the solution, i.e. increase in the gas volume percent in the solution. Since the gas is not as corrosive as liquid therefore the corrosion rate decreases by increasing gas flow rate. Dry CO₂ gas is not itself corrosive at the temperatures encountered within oil and gas production systems but is so when dissolved in an aqueous phase through which it can promote an electrochemical reaction between steel and the contacting aqueous phase [Dugstad, 1992; Popoola et al, 2013].

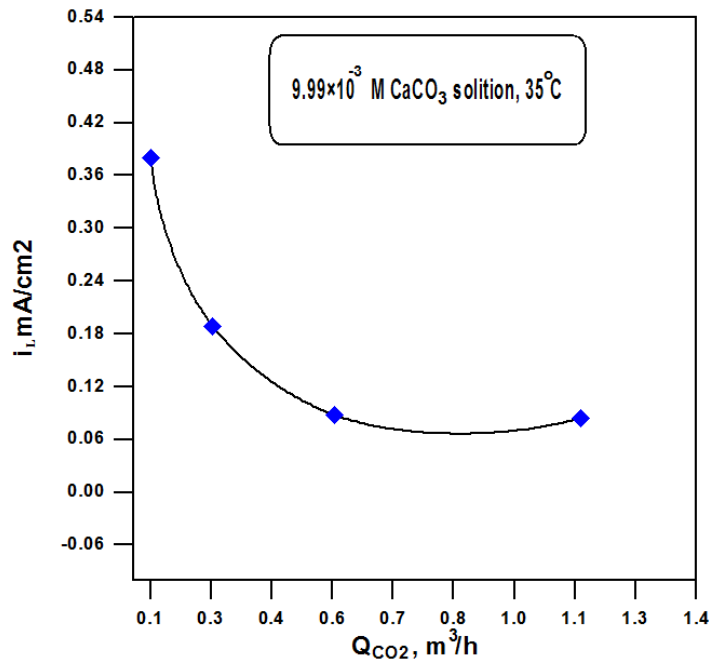


Figure 5-19 variation of flow rate of CO₂ on i_L in brine CaCO₃

Figure 5-20 shows the variation of limiting current density (i_L) with rotational velocity in 9.9×10^{-3} M CaCO₃ at 35 °C and different flow rate of CO₂. It is clear that the corrosion rate at low gas flow rate and constant velocity is high and decreases with increasing velocity. The decrease in the i_L is because that the increase in agitation velocity leads to increase the number of bubbles of CO₂ gas in the solution, and thus leads to increase the arrival of bubbles to the metal surface and more collision between bubbles and the metal specimen. Since the gas is not as corrosive as liquid therefore the corrosion rate decreases. The same effect of agitation velocity on the corrosion rate was noticed by the work of Hasan [2014] concerning galvanic corrosion in CO₂ saturated environment. The two phase gas –liquid dispersion systems is highly complicated with an unsteady nature, which is influenced by many factors, such as the velocities of gas and liquid, void fraction, temperature, properties of gas and liquid [George and Nestic, 2007; Zheng et al, 2008]. In dissolved CO₂

corrosion, the corrosion process is reaction kinetic control (activation control) resulting slow CO₂ hydration step as has been evidenced by previous works [George and Nestic, 2007, Hasan, 2014] that also found a decrease in corrosion rate with velocity in CO₂ corrosion systems. The decrease in corrosion rate with increased velocity especially at low flow rates of CO₂ indicates that the dissolved oxygen plays minor role because normally in oxygen saturated solutions the increased velocity leads to an increase in the corrosion rate by increasing O₂ transport to the metal surface. This minor role of O₂ in present system is expected because the concentration of O₂ is low as shown Table B-2.

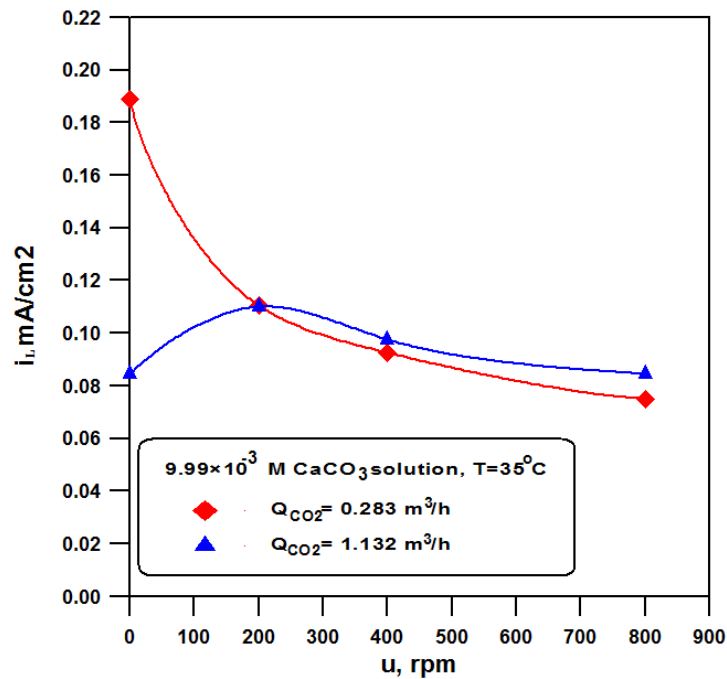


Figure 5-20 effect of velocity on i_L in brine CaCO₃- CO₂ solution.

Figure 5-21 illustrates the variation of i_L with time in 9.9×10^{-3} M CaCO₃ at flow rate of CO₂= 0.283 m³/h at different temperatures of 25, 35, and 45 °C under static conditions. This figure shows that i_L values decrease with time at all temperatures. The main reason for that is the resistance of the protective film

increases steadily with increasing time [Jang et.al, 2010]. The formation of (iron carbonate) FeCO_3 usually plays an important role in the process of corrosion since the FeCO_3 layer increases the mass transfer resistance of the corrosive species and reduces the exposed steel surface area to the corrosive environment. In fact the presence of the FeCO_3 layer largely reduces the CO_2 corrosion rate. The i_L decreases with time due to the continuous growth of the corrosion product layer (fouling layer) which decreases the arrival of oxidizer to the metal surface and the activity of the surface also decreases with time and hence the corrosion rate decreases. The works of Hausler and Stegmann [1988] and Dugstad [1992] revealed that the corrosion film influenced significantly on the corrosion rate of carbon steel, which may also, influenced the efficacy of the corrosion control practice by altering the chemical nature of the steel surface.

Temperature of the medium governs the solubilities of the corrosive species in the fluid, such as oxygen (O_2), carbon dioxide (CO_2), chlorides, and hydroxides. Temperature increases the rate of almost all the chemical reactions. When the rate determining step is the activation process, the temperature changes have the greatest effect. In open systems, the effect of temperature is complex in that the diffusivity of oxygen increases, but solubility decreases with temperature increase [Fotana, 1986; Scott, 1999; Revie and Uhlig 2008].

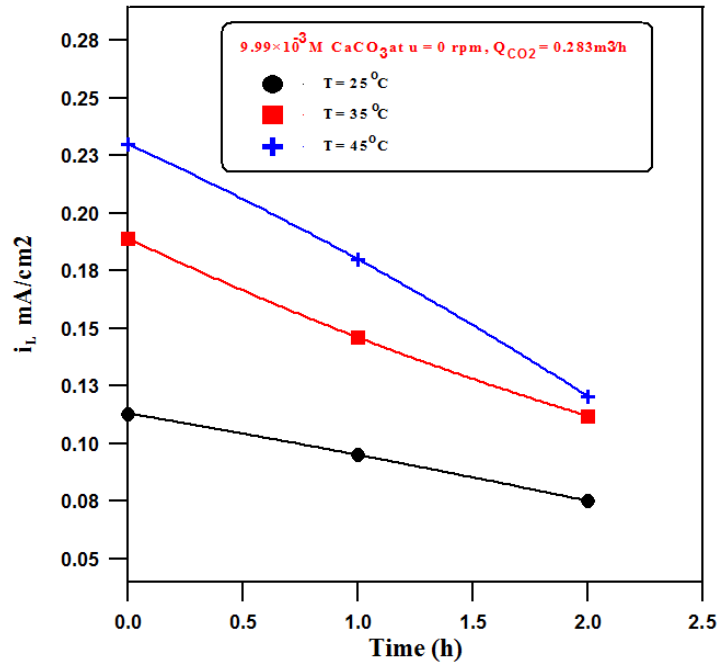


Figure 5-21 Variation of i_L with time at different temperatures in brine $\text{CaCO}_3\text{-CO}_2$

Figure 5-22 illustrates the variation of i_L with time in $9.9 \times 10^{-3} \text{ M CaCO}_3$ at $0.283 \text{ m}^3/\text{h}$ of CO_2 at different velocities and $35 \text{ }^\circ\text{C}$. This figure indicates that the i_L has clear decrease with time at static conditions. However, i_L increases clearly under dynamic conditions then the i_L start to decrease with further increase in time. At static corrosion product layer forms on the carbon steel surface leading to corrosion rate with time by increasing the electrical resistance (resistance polarization) which causes to decrease the arrival of oxidizer to the metal surface. For $u= 200 \text{ rpm}$ and $u= 800$ the i_L increases with velocity and then decreases. This trend can be interpreted as follows: at high velocity the initial formation of corrosion product layer, leads to an increase in the turbulence close to the metal wall and hence decrease the diffusion layer thickness which represents the main resistance to mass transfer therefore, the corrosion rate increases. With further increase of corrosion product layer thickness with time

the arrival of reactant to the metal surface decreases leading to a decrease in the CR, This phenomenon has also been noticed by some previous work concerning corrosion in natural water [Slaiman and Hasan, 2010].

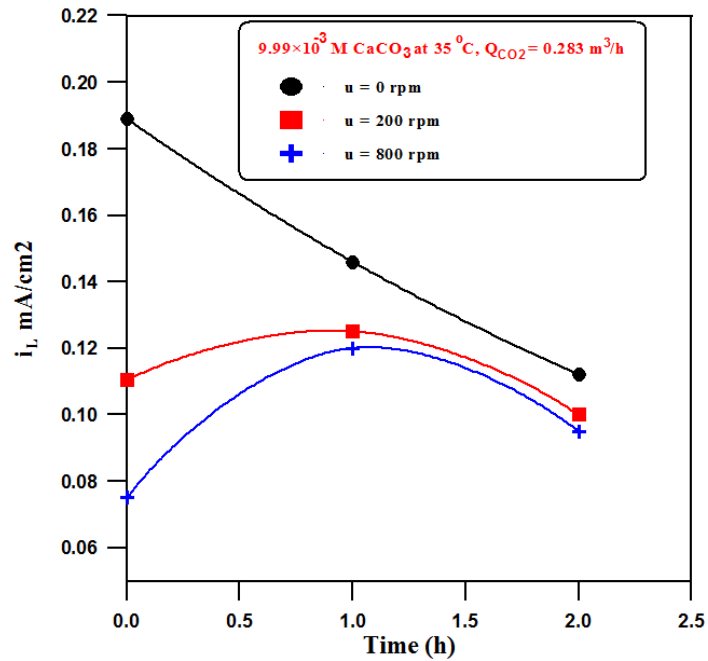


Figure 5-22 Variation of i_L with time at velocity in brine $\text{CaCO}_3\text{-CO}_2$

Evans and Haoar [1932] indicated the greater turbulence due to high velocities results in more uniform O_2 concentration near the surface. The effect of flow on CO_2 corrosion, when no protective films are present, is through increased mass transport of the corrosion species toward and away from the metal surface. When the mass transport rate of the species (e.g., hydrogen ion) is not high enough to support the electrochemical process at the metal surface, limiting reaction rates are reached. On the other hand, species accumulation, super saturation, and film precipitation can occur at the metal surface if the transport of the corrosion products (e.g., ferrous ions) away from the surface is not rapid enough. This is another mass-transfer effect of flow on CO_2 corrosion.

However, flow may also affect the formation and survival of corrosion product films by mechanical means via hydrodynamic stresses [George and Netic, 2007].

Figure 5-23 shows the variation of limiting current density (i_L) with temperature in 9.9×10^{-3} M CaCO_3 at different volumetric flow rate of CO_2 under static condition. It is clear that increasing the temperature leads to an increase in the (i_L). The increase in the i_L is due to the increase rate of chemical reaction with temperature. High corrosion rate at low gas flow rate $Q_{\text{CO}_2} = 0.283$ m^3/h is evident for three temperatures. Furthermore, the results show that the corrosion rate rises at higher temperatures. This is due to acceleration of anodic and cathodic reaction when the temperature increases. The increase of cathodic reaction in CO_2 corrosion is due to the carbonic acid contribution to hydrogen ions through possibly dissociation and reduction [George and Netic, 2007].

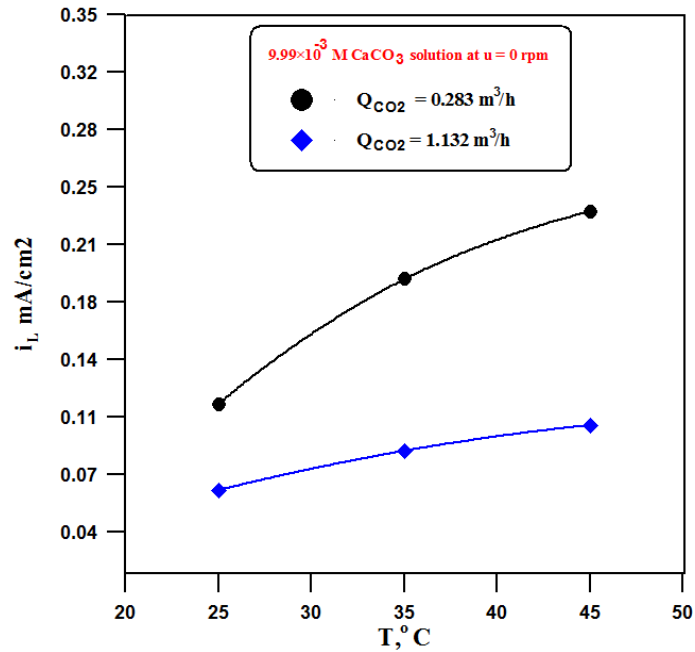


Figure 5-23 Effect of temperature on i_L in brine CaCO_3 - CO_2

5.6.2 Corrosion Potential

Figure 5-24 shows the effect of flow rate of CO_2 on the corrosion potential (E_{corr}) in 9.9×10^{-3} M CaCO_3 at 35°C . It is clear that corrosion potential shifts to more negative values with increasing flow rate of CO_2 and then increases slightly. The corrosion rate decreases with increased flow rate of CO_2 because the arrival more CO_2 bubbles to the metal surface shifting the corrosion potential to more negative thus decreasing the conductivity of solution leading to decrease the corrosion potential. Another reason is the concentration of oxygen is low because presence of CO_2 gas that decrease the concentration of oxygen in solution which in turn reduce the corrosion rate. It is well known that high concentration of O_2 leads to shift the corrosion potential more positive [Mahato et al, 1980; Revie and Uhlig, 2008; Hasan and Sadek, 2014].

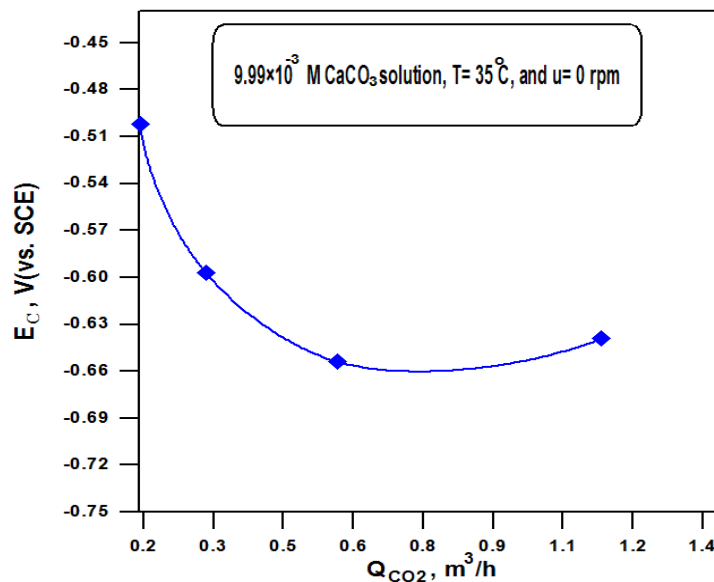


Figure 5- 24 variation of flow rate on corrosion potential in $\text{CaCO}_3 - \text{CO}_2$ solution.

Figure 5-25 illustrates the effect of velocity on the corrosion potential (E_{corr}) in 9.9×10^{-3} M CaCO_3 at different flow rate of CO_2 at 35°C . It is clear that the corrosion potential shifts to more positive values with increasing rotation

velocity and then decreases. The corrosion potential generally increases (becomes more positive) with increasing velocity. But at high velocity (400 and 800 rpm) the corrosion potential decreased (becomes more negative). This is due to the same reason mentioned previously that is the increase in the number of bubbles of CO₂ gas in the solution, and leading to more collision between bubbles and the metal specimen shifting the potential to more negative due to the increase in the resistance polarization.

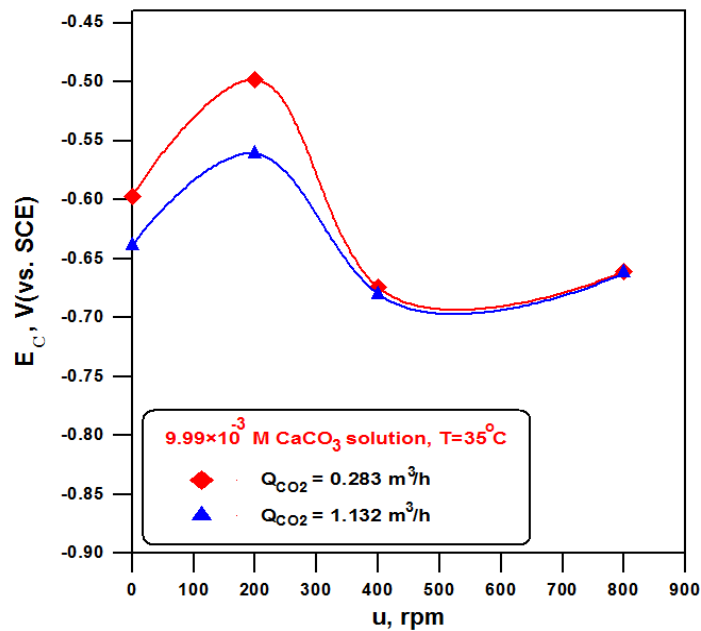


Figure 5-25 variation of velocity on corrosion potential in brine CaCO₃- CO₂ solution.

Figures 5-26 and 5-27 show the variation of corrosion potential with time for different values of temperatures and velocities in 9.9×10^{-3} M CaCO₃ at 0.283m³/h of CO₂. Fig.5-26 show variation of E_C with time at different temperatures of 25, 35, and 45 °C under static condition. It is clear that corrosion potential shifts to more negative with increase temperatures. Fig. 5-27 illustrates the variation of E_C with time at different velocities of 0, 200, and 800 rpm and constant temperature 35 °C. It is clear that corrosion potential shifts to more negative with increased velocity.

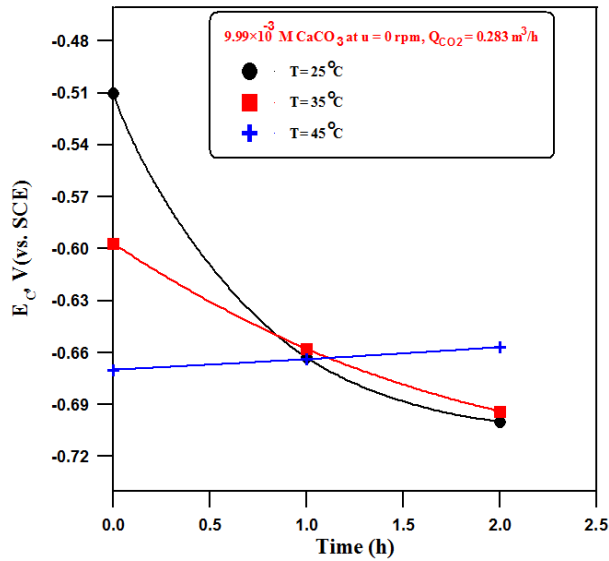


Figure 5-26 variation of time on E_c in CaCO_3 – CO_2 at different temperatures

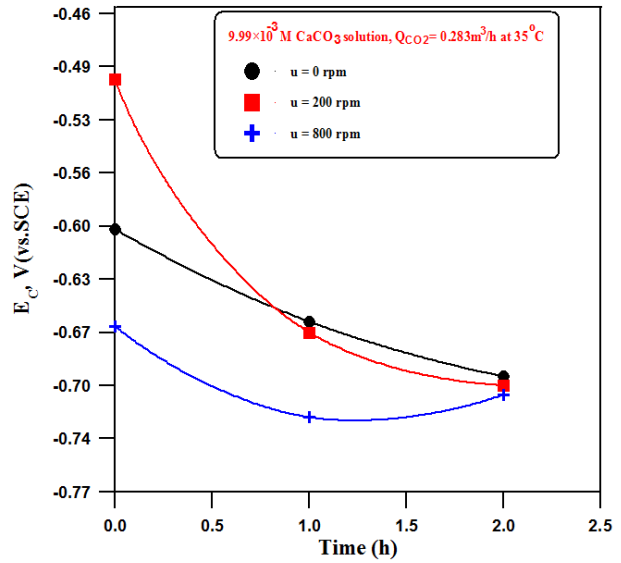


Figure 5-27 variation of time on E_c in CaCO_3 – CO_2 at different velocities

The decrease in corrosion potential is generally due to the increased electrical resistance between the solution and metal because of the formation of corrosion layer causing resistance polarization [Shrier, 2000; Revie and Uhlig, 2008]. Figure 5.28 shows the variation of corrosion potential (E_{CORR}) with temperatures in 9.9×10^{-3} M CaCO_3 at different flow rate of CO_2 under static condition. It can be observed that with the increase in the temperature, the corrosion potential (E_{CORR}) shifts to more negative values.

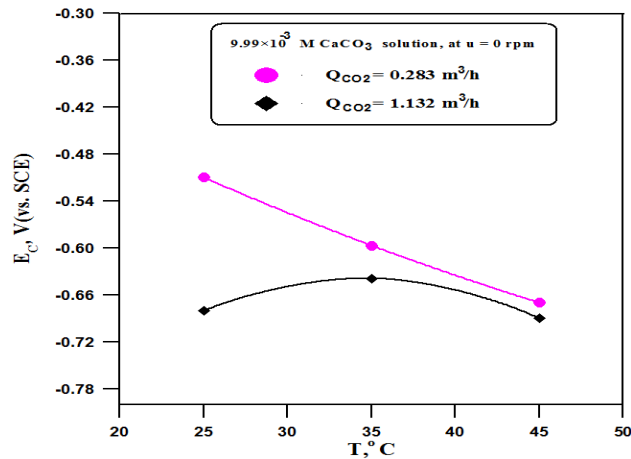


Figure 5-28 variation of temperature on corrosion potential in brine CaCO_3 - CO_2

Figure 5-29 shows photos the specimen of CS before and after exposure to cathodic polarization of CaCO_3 solution and flow rate of $\text{CO}_2 = 0.283 \text{ m}^3/\text{h}$ at $35 \text{ }^\circ\text{C}$. Photo (a) for the specimen before corrosion, Photo (b) shows the deposition of salt and corrosion product layer on the specimen. Photo (c) shows the corroded surface after cleaning.

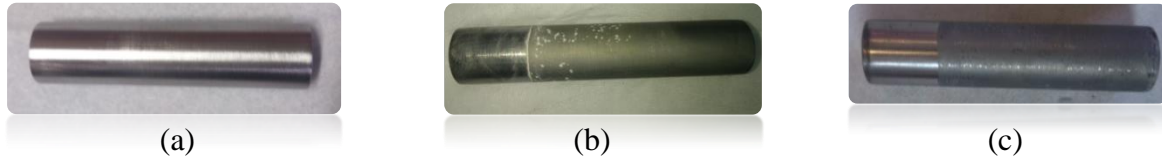


Figure 5-29 Carbon steel specimens (a) before (b) after corrosion $\text{CaCO}_3\text{-CO}_2$ (c) after cleaning corrosion product attack.

Figure 5-30 show photos of the specimen of CS before and after exposure to corrosion of CaCO_3 solution and flow rate of $\text{CO}_2 = 0.283 \text{ m}^3/\text{h}$ at 35 and $45 \text{ }^\circ\text{C}$. Photo b shows the deposition of corrosion product layer on the specimen after 2 h at 35°C . Photo c shows the deposition of $\text{CaCO}_3\text{-CO}_2$ and corrosion product layer on the specimen after 2 h at 45°C . Attack can be noticed on corroded specimen.

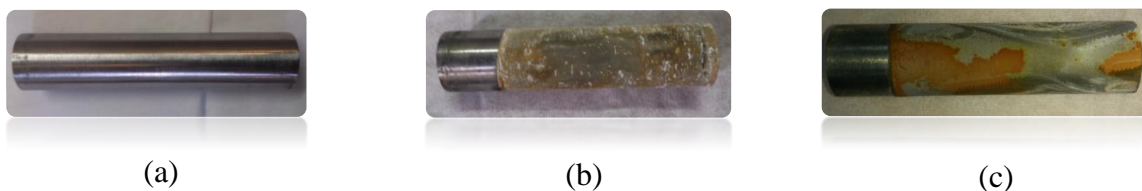


Figure 5-30 Carbon steel specimens (a) before (b) after corrosion $\text{CaCO}_3\text{-CO}_2$ after 2 h at 35°C (c) after corrosion $\text{CaCO}_3\text{-CO}_2$ after 2 h at 45°C .

5.7 Cathodic protection

The successful application of carbon steels in oil and gas pipelines and production tubular in carbon dioxide (CO_2) containing environments depends

mainly on either protect steel against corrosion by cathodic protection or the use of corrosion inhibitors [Hany et. al, 2012].

Zinc was used as a sacrificial anode to control the corrosion of CS in CO₂ containing solution under different operating conditions.

The best method for measuring the protection efficiency by cathodic protection is to determine the loss in weight of the structure, where monitoring the potential gives an indication on the cathodic protection but it does not give exactly the degree of protection.

5.7.1 Protection Potential

Figure 5-31 shows variation of protection potential with time in 9.9×10^{-3} M CaCO₃ solution, 0.283 m³/h of CO₂ at 35°C under static condition for three cases: carbon steel free corrosion potential, potential for carbon steel connected with Zinc, and free corrosion potential of zinc. The free corrosion potential of carbon steel decreases clearly with time. The free corrosion potential of zinc is more negative than that of carbon steel and exhibits some increase at the start and then decreases. The coupling protection potential of CS- Zn is evidently much lower than free corrosion potential of carbon steel. The shifts of corrosion potential of CS to more negative leads to decrease its corrosion rate. This is the principle of cathodic protection. The higher the shift of potential to more negative is the higher the decrease in its corrosion rate. In other words, connection Zn to CS leads to shift the potential to protective region. It is clear from Fig. 5-31 that the steady state potential value decreases from -0.653 to -0.888 which is a considerable change in the potential playing important role in decreasing carbon steel corrosion.

Einar [2003] stated that with a properly designed CP system with sacrificial anodes of a Zn- or Al-alloy, usually a potential in the range -900 to -1000 mV is obtained after short time of exposure of a steel structure. This potential range also gives the lowest current consumption because a layer of calcareous deposits (dominated by CaCO_3) is soon formed.

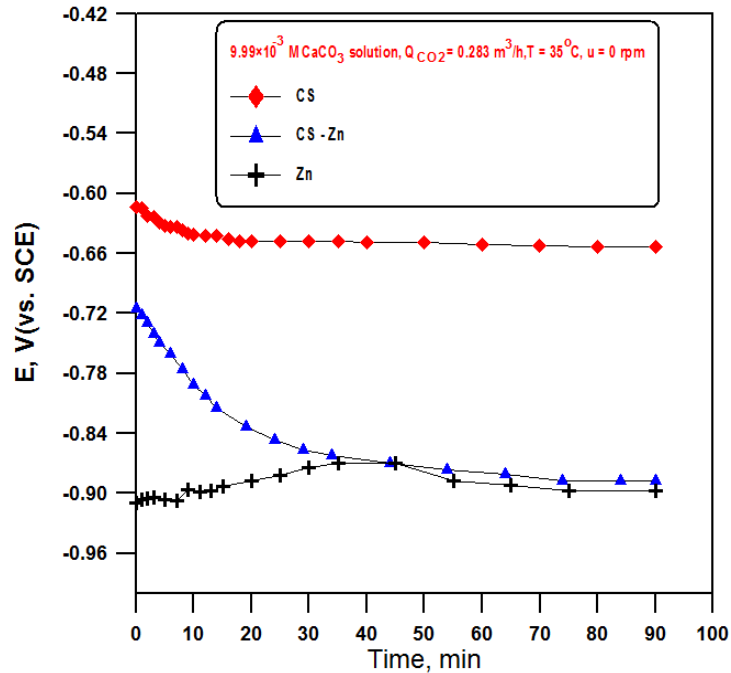


Figure 5-31 Potential vs. time for cathodic protection in CaCO_3 – CO_2 solution at $T=35^\circ\text{C}$ and $u=0$ rpm.

Figure 5-32 shows variation of potential with time in 9.9×10^{-3} M CaCO_3 solution, $0.283 \text{ m}^3/\text{h}$ of CO_2 at 25°C under static condition. Figure 5-32 shows the steady state potential value decreases from -0.655 to -0.861 . It is clear that the potential decreases to more negative with time. The coupling potential of CS and Zn is evidently much lower than free corrosion potential of carbon steel.

Figure 5-33 shows variation of potential with time, $0.283 \text{ m}^3/\text{h}$ of CO_2 at 45°C under static condition. It is clear that the potential decreases to more negative with time. Fig. 5-33 shows at steady state the potential value decreases

from -0.645 to -0.822. It is clear that the potential decreases to more negative with time. Comparing Figs. 5-31, 5-32, and 5-33 show that the decrease in potential is almost the same for three temperatures. The potential of zinc in aqueous media becomes increasingly more positive with a rise in temperature, due to film formation, which is attributed to a retardation of the anodic partial reaction (passivation) [Schwenk, 1997].

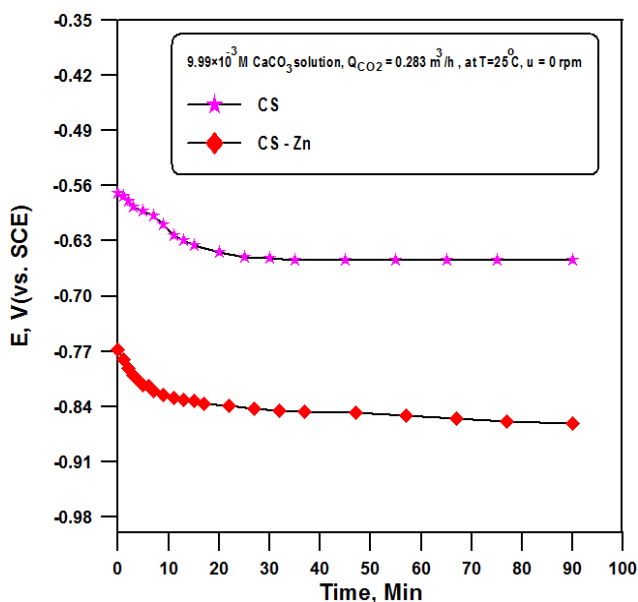


Figure 5-32 Potential vs. time for cathodic protection of $\text{CaCO}_3\text{-CO}_2$ at $T= 25^\circ\text{C}$ and $u= 0$ rpm.

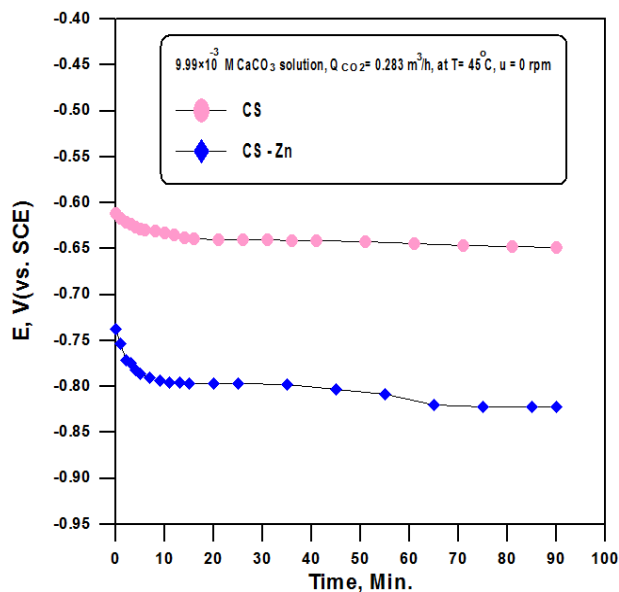


Figure 5-33 Potential vs. time for cathodic protection of $\text{CaCO}_3\text{-CO}_2$ at $T= 45^\circ\text{C}$ and $u= 0$ rpm.

Figures 5-34 through 5-36 show the variation of potential with time, 0.283 m^3/h of CO_2 at 35°C and 200, 400, 800 rpm respectively. The figures indicate that the potential decreases to more negative with time. Precisely the potential becomes rapidly more negative in the first 20 min, and then the curve reaches asymptotic value at -0.875 V, -0.857 V and -0.825 V vs SCE which represent the protection potential for 200 , 400 and 800 rpm respectively. Hence, the lower the rotation velocity is the better the protection. Also Fig. 5-36 reveals that the difference between the free corrosion potential of carbon steel and the coupling

(protection potential) of CS-Zn is low, therefore, the cathodic protection is lower in case of $u=800$.

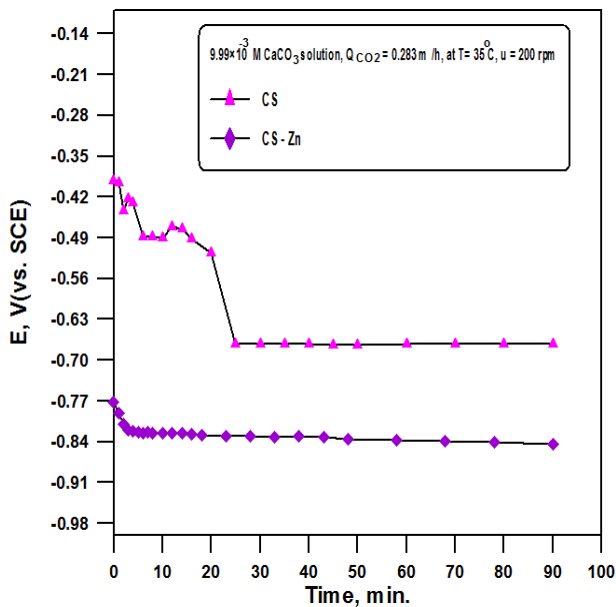


Figure 5-34 Potential vs. time for cathodic protection of $\text{CaCO}_3\text{-CO}_2$ at $T= 35^\circ\text{C}$ and $u= 200$ rpm.

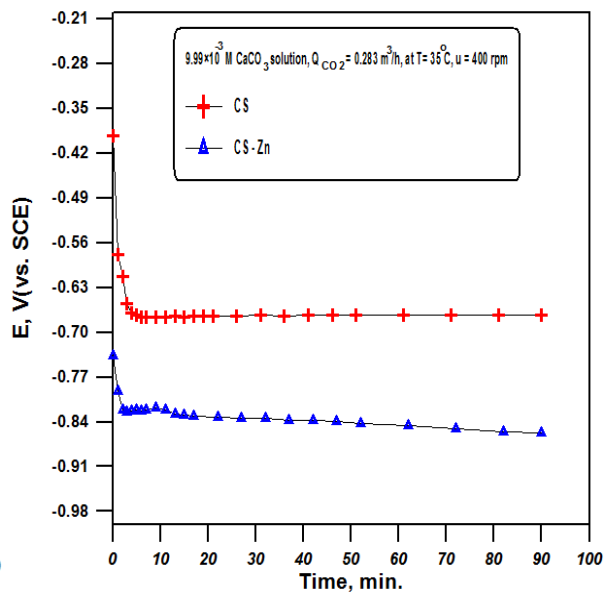


Figure 5-35 Potential vs. time for cathodic protection of $\text{CaCO}_3\text{-CO}_2$ at $T= 35^\circ\text{C}$ and $u= 400$ rpm.

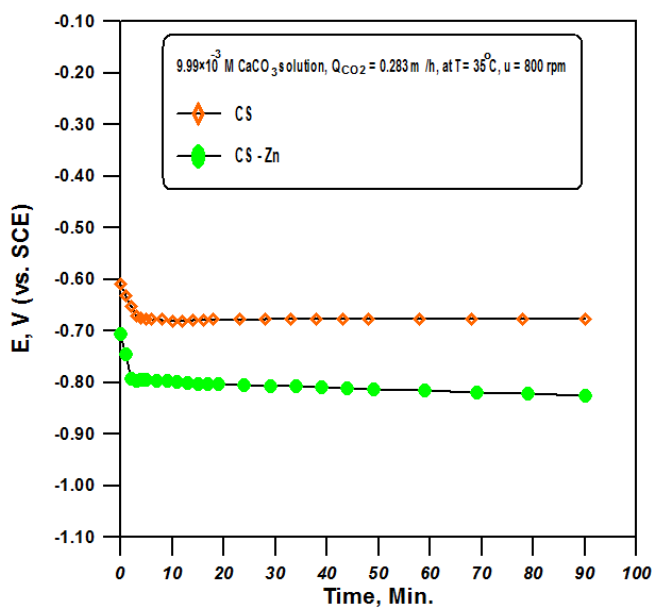


Figure 5-36 Potential vs. time for cathodic protection of $\text{CaCO}_3\text{-CO}_2$ at $T= 35^\circ\text{C}$ and $u= 800$ rpm.

Figures 5-37 and 5- 38 show the variation of potential with time in 9.9×10^{-3} M CaCO_3 solution, $0.566\text{m}^3/\text{h}$ and $1.132\text{m}^3/\text{h}$ of CO_2 at 35°C and 200 rpm. The figures indicate that the potential decreases to more negative with time. However, comparing the two figures show that the shift in protection at high flow rate of CO_2 ($1.132\text{m}^3/\text{h}$) is higher than low flow rate of CO_2 ($0.566\text{m}^3/\text{h}$). In other words, the higher the gas flow rate is the better the protection. The increase in the gas hold up leads to cause better protection Since the gas is not as corrosive as liquid therefore the corrosion rate decreases by an increasing gas flow rate.

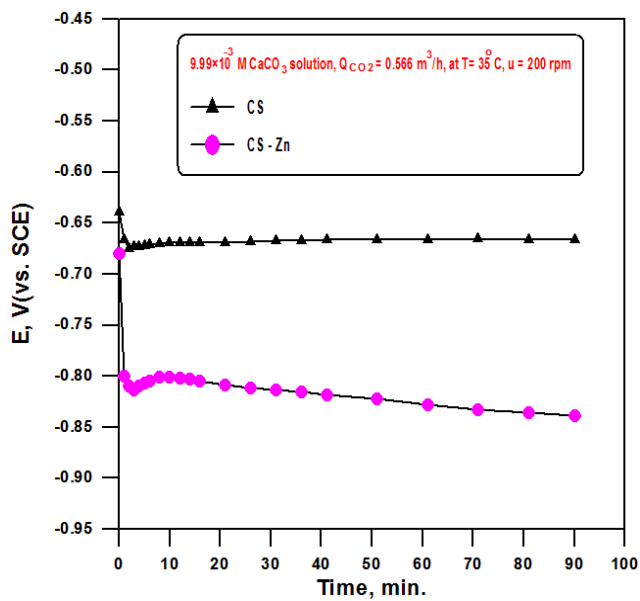


Figure 5-37 Potential vs. time for cathodic protection of CaCO_3 - CO_2 at $Q_{\text{CO}_2} = 0.566\text{m}^3/\text{h}$ and $u = 200\text{rpm}$.

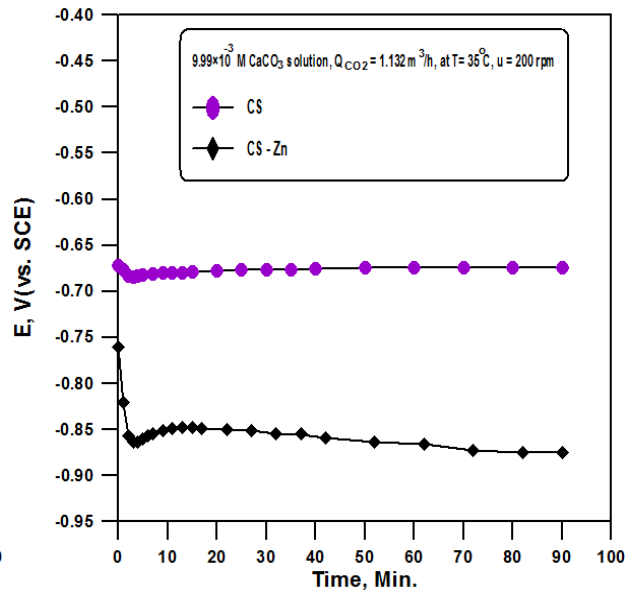


Figure 5-38 Potential vs. time for cathodic protection of CaCO_3 - CO_2 at $Q_{\text{CO}_2} = 1.132\text{m}^3/\text{h}$ and $u = 200\text{rpm}$.

5.7.2 Corrosion rates in presence of sacrificial anode

Figure 5-39 shows the effect of temperature on the corrosion rate of CS before and after coupling with Zn in 9.99×10^{-3} M CaCO_3 $0.283 \text{ m}^3/\text{h}$ of CO_2 under static condition. It is clear that the corrosion rate of carbon steel increases with increasing temperature and the protection by Zn cause considerable decrease in the corrosion rate of CS. The figure indicates a clear decrease in corrosion rate due to connection to Zn at three temperatures. From Fig.5-39 it can be seen that the corrosion rate at 25°C is higher than at 35°C and the corrosion rate at 45°C is higher than at 35°C and slightly lower than at 25°C . Also from this figure it can be seen that the protection is 93.62 % at 35°C higher than at 25°C which is 61.50 % and at 45°C which is 77.97 %. Figure 5-40 shows the effect of temperature on the corrosion rate of Zn coupled with CS at $u=0$ rpm and $Q_{\text{CO}_2}= 0.283 \text{ m}^3/\text{h}$. It is clear that the effect of solution temperature on the corrosion rate of Zn connected to carbon steel is to decrease with increasing temperature from 25 to 35°C and then is slightly increase further with increasing temperature to 45°C . So this result corresponds to the behavior of carbon steel. That is in agreement with previous findings of Konsowa and El-Shazly [2002] who studied the effect of flow and temperature on the rate of zinc consumption during cathodic protection of copper pipeline carrying saline water by measuring the loss in weight. They found that the rate of zinc consumption increases with increasing solution flow rate and temperature.

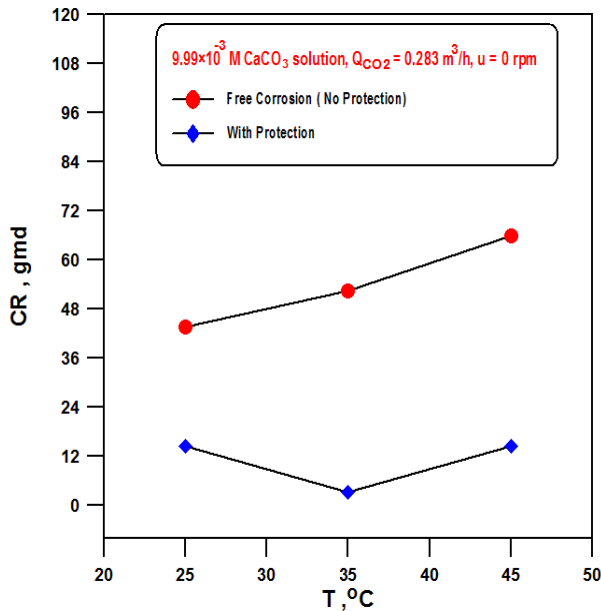


Figure 5-39 effect of temperature on CR of free corrosion of CS and protected

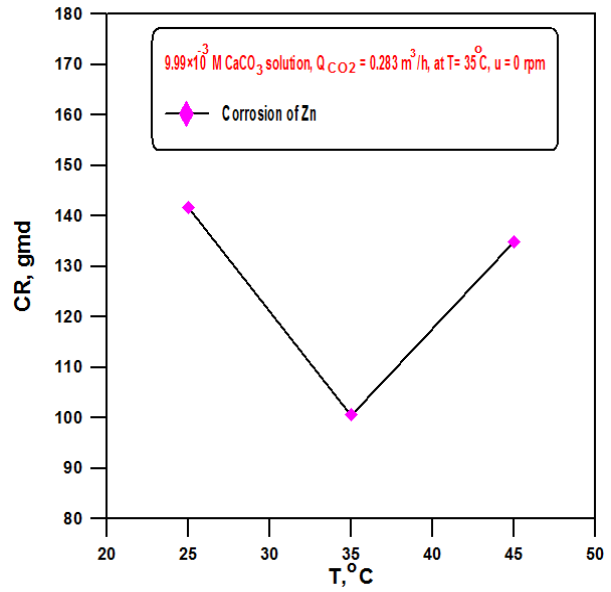


Figure 5-40 effect of temperature on CR of zinc coupled with CS

Figure 5-41 shows the effect of agitation velocity on the corrosion rate of CS before and after coupling with Zn at different velocities, $T = 35^{\circ}\text{C}$ and $Q_{\text{CO}_2} = 0.283 \text{ m}^3/\text{h}$. The decrease in corrosion rate of CS is clear by cathodic protection (coupling CS and Zn) at each agitation velocity. Also from Fig.6-41 it can be seen that the protection of 93.62 % at 0 rpm is higher than at 200 rpm which is 75.65 % and decrease at 400 rpm to 46.43% and then increase for furthermore velocity is 73.53% at 800 rpm. Figure 5-42 shows the effect of rotational velocity of the corrosion rate of Zn coupled with CS at different velocities, $T = 35^{\circ}\text{C}$ and $Q_{\text{CO}_2} = 0.283 \text{ m}^3/\text{h}$. It is clear that the corrosion rate of Zn decrease with the increase of velocity at 200 rpm and then increase slightly with further increase in velocity. The decrease in the corrosion rate of Zn is because that the increase in agitation velocity lead to increase the number of bubbles of CO_2 gas in the solution, and thus lead to increase the arrival of bubbles to the metal surface and more collision between bubbles and the metal specimen. Since the

gas is not as corrosive as liquid therefore the corrosion rate decreases [Dugstad, 1992, Popoola et al, 2013].

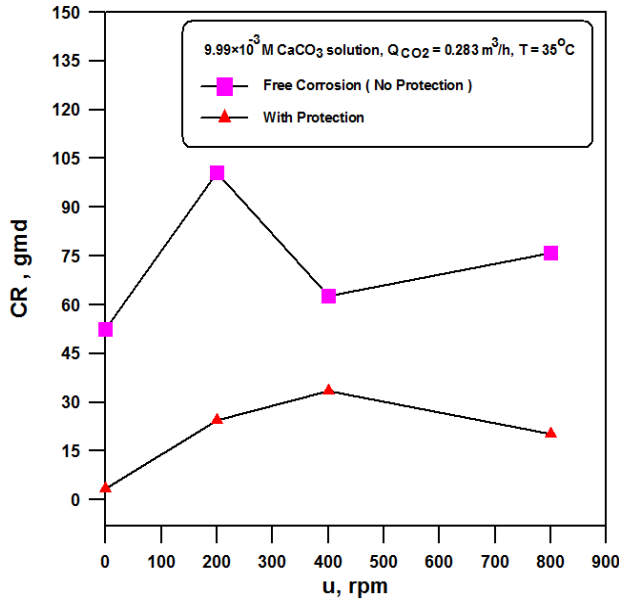


Figure 5-41 effect of velocity on CR of free corrosion of CS and protection with zinc

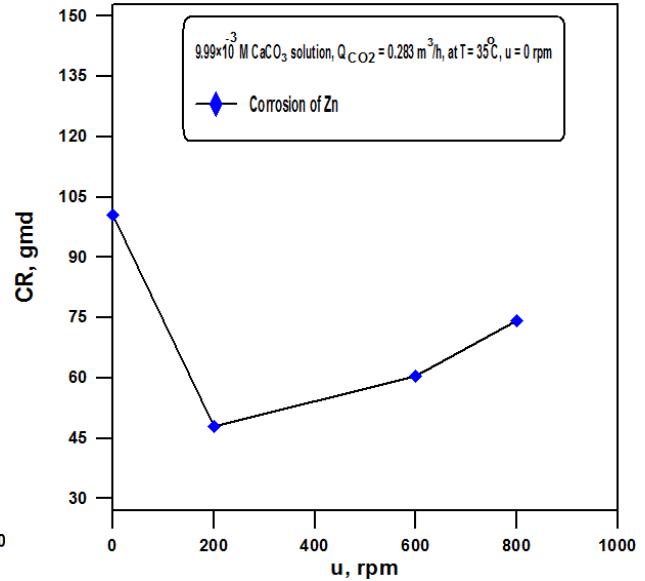


Figure 5-42 effect of velocity on CR of zinc coupled with CS

Figure 5-43 shows the effect of volumetric flow rate of CO_2 on the corrosion rate of CS free corrosion and on corrosion of CS coupled to Zn, $T=35^\circ\text{C}$ and $u=0$ rpm. It is clear that corrosion rate of carbon steel decreases with increasing flow rate of CO_2 and also the corrosion rate decreases by cathodic protection (coupling carbon steel and zinc) for different flow rate of CO_2 . The decrease in the corrosion rate is due to the increase in gas hold up in the solution, i.e. increase in the gas volume percent in the solution. Also from Fig.5-43 it can be seen that the protection is slightly increases with increasing as flow rate: 75.56, 85.71, and 86.05% at flow rate of CO_2 : 0.283, 0.566, and $1.132\text{m}^3/\text{h}$ respectively. Figure 5-44 shows the effect of volumetric flow rate of CO_2 on the corrosion rate of Zn coupled with CS at $T=35^\circ\text{C}$ and $u=0$ rpm. It is clear that

the corrosion rate of Zn increases with increased flow rate of CO₂ and then decreases for further increase in flow rate.

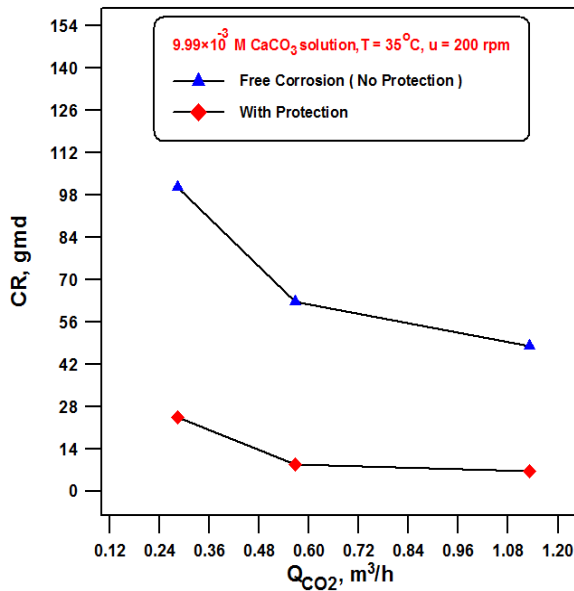


Figure 5-43 effect of flow rate on CR of free corrosion of CS and protected

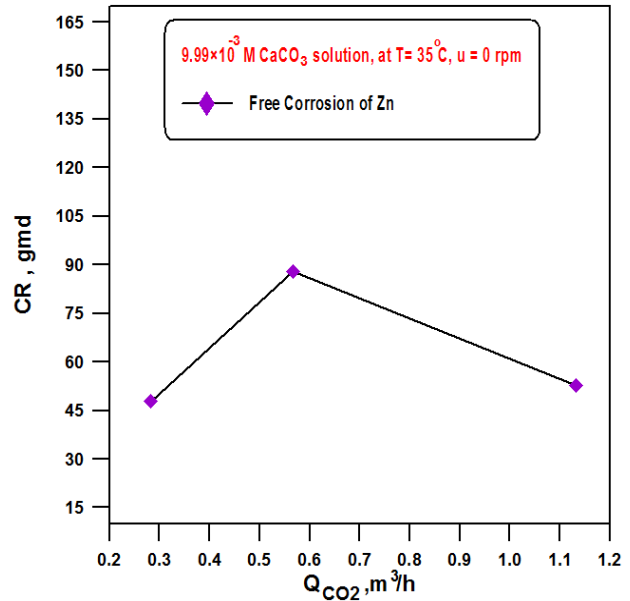


Figure 5-44 effect of flow rate on CR of zinc coupled with CS

Figure 5-45 shows photos of specimens of CS before and after exposure to corrosion in 9.99×10^{-3} M CaCO₃ solution and flow rate of CO₂ = 0.283 m³/h at 35 °C. Photo (a) before exposure and (b) after exposure to the solution. Photo (c) shows the specimen of CS and Zn after cathodic protection. Photo the CS of indicates that the CS is not corroded as it is protected by Zn. In addition, the Zn specimen is clearly attacked because it sacrifices by coupling it with CS.

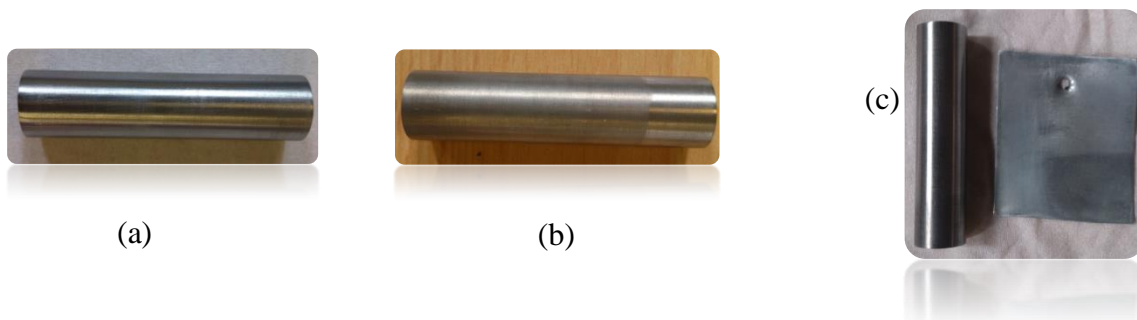


Figure 5-45 Carbon steel specimens (a) before (b) after corrosion in CaCO₃-CO₂ (c) specimen of CS and Zn after cathodic protection

Chapter Four

Results

4.1 Introduction

This chapter presents the experimental results for the whole investigated ranges of salt and gasoil-acid concentrations, rotational velocities, temperature, time, carbon dioxide concentration, and cathodic protection by sacrificial anode method.

4.2 Corrosion rate in CaCO₃ solution

Weight loss experiments were carried out to determine corrosion rates of carbon steel in single phase CaCO₃ solution and two phase mixture of CaCO₃ solution/ Gasoil over a range of velocities and at constant temperature of 35°C. Corrosion rates have been expressed in various ways in the literature.

The results of weight loss experiments in the present work were expressed in different expressions calculated readily from the weight loss of specimens. First expression is “gmd” which means gram lost per square meter per day was estimated using Eq. (3.1). This expression takes account the influence of area and time.

The second expression used for expressing corrosion rate is mm/y which means milli meter per year is given by [Shreir, 2000]:

$$\text{mm/y} = \frac{\text{gmd}}{2.74 \times \rho_{\text{metal}}} \quad (4.1)$$

Where ρ is the density of specimen in g/cm³ (for steel and iron $\rho = 7.87$ g/cm³) [Uligh, 1976].

The third expression used is the corrosion current calculated from weight loss by faradays law:

$$i_c = z F N \quad (4.2)$$

where i_c is the corrosion current density in (A/m^2), F is Faradays constant (96487 coulomb/equivelant), z is the number of electron freed by corrosion reaction ($z_{Fe}=2$), and N is the molar flux of Fe reacted due to corrosion in $gmol/m^2.s$.

Mass transfer coefficient can be estimated from data of weight loss measurements using:

$$k = \frac{i_L}{z F C_b} \quad (4.3)$$

where k is the mass transfer coefficient, and C_b is the bulk concentration of oxygen in solution, $z_{O_2}=4$ for oxygen reduction, and i_L is the limiting current density for oxygen reduction on Fe according to the combining of Eqs. (2.1) and (2.4) to gives:



Hence, in salt water the reduction current of oxygen reduction (i_L) will be equal to the corrosion current of Fe, i.e. $i_L = i_c$, where i_c is estimated via Eq.(4.2) from weight loss measurements. It is worthy to note that the molar flux of oxygen is half that of iron, i.e., $N_{O_2} = 0.5 N_{Fe}$. Knowing i_L or i_c , the mass transfer coefficient can be estimated by Eq. (4.3).

In the first part of the experimental work, weight loss method was employed to measure the corrosion rate of carbon steel at ($T = 35^\circ C$) to study the effect of rotation in different solutions.

Table 4-1 the corrosion rate of carbon steel in $2.5 \times 10^{-3} M CaCO_3$ under $35^\circ C$ for different rotational velocities for 3.5 h of immersion time.

Table 4-1 Corrosion rate of carbon steel in 2.5×10^{-3} M CaCO_3 at 35°C for different velocities.

u, rpm	CR, Gmd	CR, mm/y	$N_{\text{Fe}}, \times 10^6$ mol/m².s	$N_{\text{O}_2}, \times 10^6$ mol/m².s	$i_{\text{L}}=i_{\text{corr.}}$ A/m²	k, $\times 10^6$ m/s
0	12.924	0.5993	2.677	1.339	0.517	6.970
200	17.710	0.8213	3.668	1.834	0.708	9.547
400	19.625	0.6883	4.065	2.032	0.785	10.593
800	20.582	0.9544	4.263	2.132	0.823	11.106
1200	19.146	0.8878	3.966	1.983	0.765	10.322

Tables 4-2, 4-3, and 4-4 show the corrosion rate of carbon steel in 2.5×10^{-3} M CaCO_3 mixed with 1, 2, and 5% by volume gas oil at 35°C and different velocities.

Table 4-2 Corrosion rate of carbon steel in 2.5×10^{-3} M CaCO_3 + 1% (v/v) Gas oil at 35°C

u, rpm	CR, gmd	CR, mm/y
200	2.872	0.1338
300	3.351	0.1561
400	2.633	0.1227

Table 4-3 Corrosion rate of carbon steel in 2.5×10^{-3} M CaCO_3 + 2% (v/v) Gas oil at 35°C

u, rpm	CR, gmd	CR, mm/y
200	3.111	0.1449
300	2.633	0.1227
400	1.675	0.0780

Table 4-4 Corrosion rate of carbon steel in 2.5×10^{-3} M CaCO_3 +5% (v/v) Gas oil at 35°C

u, rpm	CR, gmd	CR, mm/y
200	3.351	0.1561
300	3.829	0.1784
400	3.111	0.1449

4.3 Corrosion rate of two phase mixture in presence of acids

Tables 4-5, 4- 6, and 4- 7 show the corrosion rate of carbon steel in 2.5×10^{-3} M CaCO_3 mixed with 2, 5, 10% Gas oil and 2 % by volume hydrochloric acid at 35°C and different velocity for 2 h of immersion time.

Table 4-5 Corrosion rate of carbon steel in 2.5×10^{-3} M CaCO_3 +2%(v/v) Gasoil + 2% (v/v) HCl at 35°C.

u, rpm	CR, gmd	CR, mm/y
200	38.772	1.8065
300	56.961	2.6540
400	68.449	3.1893

Table 4-6 Corrosion rate of carbon steel in 2.5×10^{-3} M CaCO_3 +5 % (v/v) Gasoil + 2% (v/v) HCl at 35°C.

u, rpm	CR, gmd	CR, mm/y
200	62.226	2.8994
300	71.321	3.3231
400	124.452	5.7987

Table 4-7 Corrosion rate of carbon steel in 2.5×10^{-3} M CaCO_3 + 10 % (v/v) Gas oil + 2% (v/v) HCl at 35°C.

u, rpm	CR, gmd	CR, mm/y
200	68.449	3.1893
300	93.339	4.3490
400	140.348	6.5394

Tables 4-8, and 4-9 show the corrosion rate of carbon steel in 2.5×10^{-3} M CaCO_3 mixed with 5% Gas oil and 2 % by volume hydrochloric acid at different temperatures 25, 45 °C and different velocity.

Table 4-8 Corrosion rate of carbon steel in 2.5×10^{-3} M CaCO_3 + 5%(v/v) Gas oil + 2% (v/v) HCl at 25°C.

u, rpm	CR, gmd	CR, mm/y
200	52.174	2.4309
300	70.363	3.2784
400	104.827	4.8843

Table 4-9 Corrosion rate of carbon steel in 2.5×10^{-3} M CaCO_3 + 5%(v/v) Gas oil + 2% (v/v) HCl at 45°C .

u, rpm	CR, gmd	CR, mm/y
200	97.647	4.5497
300	103.391	4.8174
400	131.632	6.1333

Tables 4-10, and 4-11 show the corrosion rate of carbon steel in 2.5×10^{-3} M CaCO_3 mixed with 5, 10% Gas oil and 2 % by volume sulfuric acid at 35°C and different velocity for 2 h of immersions time.

Table 4-10 Corrosion rate of carbon steel in 2.5×10^{-3} M CaCO_3 + 5 % (v/v) Gas oil + 2% (v/v) H_2SO_4 at 35°C .

u, rpm	CR, gmd	CR, mm/y
200	113.921	5.3080
300	154.608	7.2038
400	200.080	9.3225

Table 4-11 Corrosion rate of carbon steel in 2.5×10^{-3} M CaCO_3 + 10 % (v/v) Gas oil + 2% (v/v) H_2SO_4 at 35°C .

u, rpm	CR, gmd	CR, mm/y
200	145.034	6.7577
300	164.308	7.6558
400	230.505	10.7401

Table 4-12 Corrosion rate of carbon steel in 2.5×10^{-3} M CaCO_3 + 5% Gasoil + 2% H_2SO_4 at different temperatures and velocity 300 rpm.

T, $^\circ\text{C}$	CR, gmd	CR, mm/y
25	150.778	7.0253
35	154.608	7.2038
45	445.634	20.7639

4.4 Corrosion rate in two phase system (CaCO₃ solution-CO₂gas)

The corrosion rate in this system was determined by electrochemical polarization method. A typical polarization curve for carbon steel in water-salt solution is presented in Fig. 4-1. The figure shows the regions that are to be considered. The curve marked (abcd) is the cathodic region, (de) is the anodic region, (ba) is the hydrogen evaluation region, (cb) is the limiting current density region, and d is corrosion potential region. The most important characteristic of the cathodic region in air saturated environment is the limiting current density of oxygen reduction (i_L). The limiting current density is determined from the plateau defined in terms of initial and final potentials, i.e., E_1 and E_2 in Fig. 4-1. i_L refers to the start of the limiting value of oxygen reduction, while i_2 refers to the start stage of enhanced hydrogen evolution reaction [Gabe and Makanjola, 1986]. The corrosion potentials (E_c) were also determined from the polarization curves when the applied current becomes zero, i.e., open circuit potential (or free corrosion potential). The cathodic polarization curves were determined experimentally by plotting cathode potential versus the logarithm of current density.

The limiting current density i_L was obtained from polarization curves for all the investigated ranges of velocity, salt concentration, temperature, CO₂ flow rate and time. The limiting current plateau is not well defined, thus the method given by Gabe and Makanjola [Gabe and Makanjola, 1986] was adopted to find the limiting current density values, i.e.:

$$i_L = \frac{i_1 + i_2}{2} \quad (4.6)$$

Where i_1 and i_2 are the currents associated with E_1 and E_2 respectively Fig.4-1. The polarization curves obtained for the whole investigated ranges of velocity, temperature, salt concentration, CO₂ flow rate and time are presented in Appendix B. There is an obvious limiting diffusive current density.

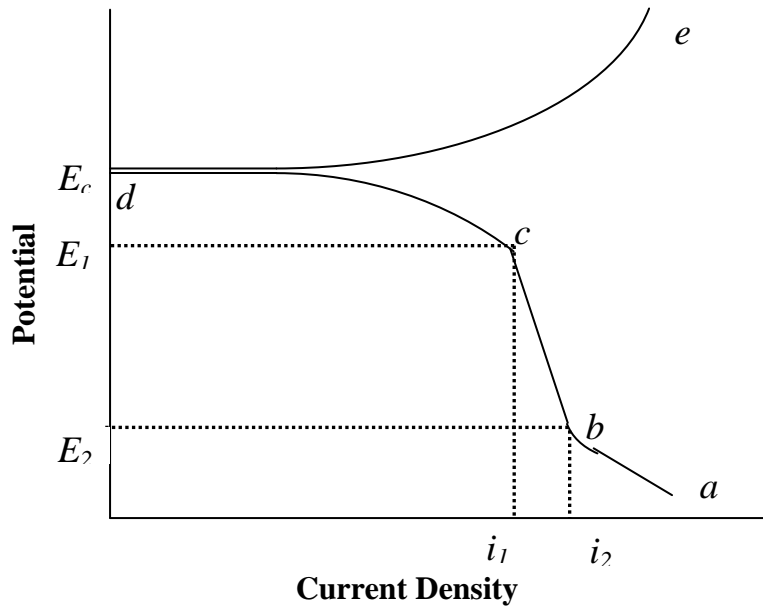


Figure 4-1 Typical Polarization Curve

The limiting current density values are presented in Tables 4-13 through 4-20. The values of corrosion rate are also expressed in different ways (gmd and mm/y) calculated from i_L via Eqs. (4.1) and (4.2). The tables show that the variables, i.e., velocity, salt concentration, temperature and time affect i_L (or corrosion rate).

Table 4-13 Corrosion rate and corrosion potential of carbon steel in 2.5×10^{-3} M CaCO₃ at different velocity and T=35°C.

u, rpm	Re	$i_L=i_{corr}$, mA/cm ²	CR, gmd	CR, mm/y	$N_{O_2} \times 10^6$ mol/m ² .s	$N_{Fe} \times 10^6$ mol/m ² .s	$k \times 10^6$ m/s	E_{corr} , V
0	static	0.027	6.745	0.314	0.699	1.398	3.636	-0.157
200	45794	0.049	12.246	0.571	1.269	2.538	6.602	-0.130
400	91587	0.0425	10.626	0.495	1.101	2.202	5.728	-0.120
800	183174	0.1275	31.879	1.485	3.33	6.607	17.325	-0.133
1200	271386	0.111	27.753	1.293	2.876	5.752	14.963	-0.158

Table 4-14 Corrosion rate and corrosion potential of carbon steel in 9.9×10^{-3} M CaCO₃ at different velocities and T=35 °C.

u, rpm	Re	$i_L=i_{corr}$, mA/cm ²	CR, gmd	CR, mm/y	$N_{O_2} \times 10^6$ mol/m ² .s	$N_{Fe} \times 10^6$ mol/m ² .s	$k \times 10^6$ m/s	E_{corr} , V
0	static	0.085	21.253	0.99	2.202	4.404	13.509	-0.176
200	45794	0.1005	25.128	1.171	2.603	5.207	15.969	-0.160
400	91587	0.11	27.504	1.282	2.850	5.701	17.485	-0.155
800	183174	0.15	37.505	1.747	3.886	7.773	23.841	-0.170
1200	271386	0.1075	26.879	1.252	2.785	5.57	17.086	-0.165

Table 4-15 Corrosion rate and corrosion potential of carbon steel in different salt concentrations at 35 °C and velocity of 0 rpm.

Salt CaCO ₃ , M	$i_L=i_{corr}$, mA/cm ²	CR, gmd	CR, mm/y	$N_{O_2} \times 10^6$ mol/m ² .s	$N_{Fe} \times 10^6$ mol/m ² .s	$k \times 10^6$ m/s	E_{corr} , V
2.5×10^{-3}	0.027	6.745	0.314	0.699	1.398	3.636	-0.157
4.99×10^{-3}	0.0575	14.377	0.669	1.489	2.979	7.747	-0.151
9.99×10^{-3}	0.0715	17.877	0.833	1.852	3.705	11.361	-0.176

Table 4-16 Corrosion rate and corrosion potential of carbon steel in 9.99×10^{-3} M CaCO_3 at different temperatures and velocity of 0 rpm.

T, °C	$i_L=i_{\text{corr}}$, mA/cm ²	CR, gmd	CR, mm/y	$N_{\text{O}_2}, \times 10^6$ mol/m ² .s	$N_{\text{Fe}}, \times 10^6$ mol/m ² .s	$k, \times 10^6$ m/s	E_{corr} , V
35	0.0715	17.877	0.833	1.852	3.705	11.361	-0.176
45	0.09	22.503	1.049	2.331	4.663	15.803	-0.195
55	0.125	31.254	1.456	3.238	6.477	33.210	-0.122

Table 4-17 Corrosion rate and corrosion potential of carbon steel in 9.99×10^{-3} M CaCO_3 at different temperatures and velocity of 400 rpm.

T, °C	$i_L=i_{\text{corr}}$, mA/cm ²	CR, gmd	CR, mm/y	$N_{\text{O}_2}, \times 10^6$ mol/m ² .s	$N_{\text{Fe}}, \times 10^6$ mol/m ² .s	$k, \times 10^6$ m/s	E_{corr} , V
35	0.11	27.504	1.282	2.850	5.701	17.484	-0.155
45	0.115	28.754	1.339	2.979	5.959	20.196	-0.175
55	0.165	41.254	1.922	4.275	8.55	43.846	-0.110

Table 4-18 Corrosion rate and corrosion potential of carbon steel in 9.99×10^{-3} M CaCO_3 at 35 °C for different exposure times at velocity of 0 rpm.

Time, h	$i_L=i_{\text{corr}}$, mA/cm ²	CR, gmd	CR, mm/y	$N_{\text{O}_2}, \times 10^6$ mol/m ² .s	$N_{\text{Fe}}, \times 10^6$ mol/m ² .s	$k, \times 10^6$ m/s	E_{corr} , V
0	0.071	17.752	0.827	1.839	3.679	11.268	-0.142
1	0.0575	14.377	0.669	1.489	2.979	9.135	-0.193
2	0.05	12.502	0.583	1.295	2.591	7.945	-0.236

Table 4-19 Corrosion rate and corrosion potential of carbon steel in 9.99×10^{-3} M CaCO_3 at 35 °C for different exposure times at velocity of 400 rpm.

Time, h	$i_L = i_{\text{corr}}$, mA/cm ²	CR, gmd	CR, mm/y	$N_{\text{O}_2}, \times 10^6$ mol/m ² .s	$N_{\text{Fe}}, \times 10^6$ mol/m ² .s	$k, \times 10^6$ m/s	E_{corr} , V
0	0.1	25.003	1.165	2.591	5.182	15.895	-0.130
1	0.0815	20.371	0.949	2.111	4.222	12.953	-0.162
2	0.061	15.252	0.711	1.580	3.161	9.693	-0.222

Table 4-20 Corrosion rate and corrosion potential of carbon steel in 9.99×10^{-3} M CaCO_3 at 35 °C for different exposure times at velocity of 1200 rpm.

Time, h	$i_L = i_{\text{corr}}$, mA/cm ²	CR, gmd	CR, mm/y	$N_{\text{O}_2}, \times 10^6$ mol/m ² .s	$N_{\text{Fe}}, \times 10^6$ mol/m ² .s	$k, \times 10^6$ m/s	E_{corr} , V
0	0.14	35.005	1.631	3.627	7.254	22.251	-0.18
1	0.11	27.504	1.282	2.85	5.700	17.428	-0.192
2	0.0975	24.378	1.136	2.526	5.052	15.497	-0.244

The limiting current density values are presented in Tables 4-21 through 4-30. The tables show the effect of operating variables, i.e., flow rate, velocity, temperature and time on i_L (or corrosion rate) in brine- CO_2 gas system.

Table 4-21 Corrosion rate and corrosion potential of carbon steel in 9.99×10^{-3} M CaCO_3 with different flow rates of CO_2 at $T = 35$ °C, and $u = 0$ rpm

Q_{CO_2} , m ³ /h	i_L , mA/cm ²	CR, gmd	CR, mm/y	$N_{\text{H}_2\text{CO}_3}, \times 10^6$ mol/m ² .s	$N_{\text{Fe}}, \times 10^6$ mol/m ² .s	E_{corr} , V
0.142	0.38	95.013	4.4270	39.384	1.97	-0.502
0.283	0.189	47.256	2.202	19.588	9.79	-0.597
0.566	0.0875	21.878	1.019	9.069	4.53	-0.654
1.132	0.0845	21.128	0.984	8.757	4.38	-0.639

Table 4-22 Corrosion rate and corrosion potential of carbon steel in 9.99×10^{-3} M CaCO_3 with flow rate of $\text{CO}_2 = 0.283 \text{ m}^3/\text{h}$ at different velocities and $T = 35^\circ\text{C}$.

u, rpm	i_L, mA/cm^2	CR, gmd	CR, mm/y	$N_{\text{H}_2\text{CO}_3}, \times 10^6$ $\text{mol}/\text{m}^2 \cdot \text{s}$	$N_{\text{Fe}}, \times 10^6$ $\text{mol}/\text{m}^2 \cdot \text{s}$	E_{corr}, V
0	0.189	47.256	2.202	19.588	9.79	-0.597
200	0.1105	27.629	1.287	11.452	5.726	-0.498
400	0.0925	23.128	1.078	9.587	4.793	-0.674
800	0.075	18.753	0.874	7.773	3.886	-0.661

Table 4-23 Corrosion rate and corrosion potential of carbon steel in 9.99×10^{-3} M CaCO_3 with flow rate of $\text{CO}_2 = 1.132 \text{ m}^3/\text{h}$ at different velocities and $T = 35^\circ\text{C}$.

u, rpm	$i_L = i_{\text{corr}}$, mA/cm^2	CR, gmd	CR, mm/y	$N_{\text{H}_2\text{CO}_3}, \times 10^6$ $\text{mol}/\text{m}^2 \cdot \text{s}$	$N_{\text{Fe}}, \times 10^6$ $\text{mol}/\text{m}^2 \cdot \text{s}$	E_{corr}, V
0	0.0845	21.128	0.984	8.757	4.38	-0.639
200	0.110	27.504	1.282	11.400	5.700	-0.561
400	0.0975	24.378	1.136	10.105	5.053	-0.680
800	0.0845	21.128	0.984	8.758	4.379	-0.662

Table 4-24 Corrosion rate and corrosion potential of carbon steel in 9.99×10^{-3} M CaCO_3 with flow rate of $\text{CO}_2 = 0.283 \text{ m}^3/\text{h}$ for immersion different exposure times at $T = 25^\circ\text{C}$, and $u = 0$ rpm.

Time, h	i_L, mA/cm^2	CR, gmd	CR, mm/y	$N_{\text{H}_2\text{CO}_3}, \times 10^6$ $\text{mol}/\text{m}^2 \cdot \text{s}$	$N_{\text{Fe}}, \times 10^6$ $\text{mol}/\text{m}^2 \cdot \text{s}$	E_{corr}, V
0	0.113	28.254	1.316	11.711	5.856	-0.510
1	0.095	23.753	1.107	9.8460	4.923	-0.663
2	0.075	18.752	0.874	7.773	3.887	-0.700

Table 4-25 Corrosion rate and corrosion potential of carbon steel in 9.99×10^{-3} M CaCO_3 with flow rate of $\text{CO}_2 = 0.283 \text{ m}^3/\text{h}$ for immersion different exposure times at $T = 35^\circ\text{C}$, and $u = 0$ rpm.

Time, h	I_L , mA/cm^2	CR, gmd	CR, mm/y	$N_{\text{H}_2\text{CO}_3} \times 10^6$, $\text{mol}/\text{m}^2 \cdot \text{s}$	$N_{\text{Fe}} \times 10^6$, $\text{mol}/\text{m}^2 \cdot \text{s}$	E_{corr} , V
0	0.189	47.256	2.202	19.588	9.794	-0.597
1	0.146	36.628	1.701	15.513	7.565	-0.658
2	0.112	28.003	1.305	11.611	5.804	-0.694

Table 4-26 Corrosion rate and corrosion potential of carbon steel in 9.99×10^{-3} M CaCO_3 with flow rate of $\text{CO}_2 = 0.283 \text{ m}^3/\text{h}$ for immersion different exposure times at $T = 45^\circ\text{C}$, and $u = 0$ rpm.

Time, h	I_L , mA/cm^2	CR, gmd	CR, mm/y	$N_{\text{H}_2\text{CO}_3} \times 10^6$, $\text{mol}/\text{m}^2 \cdot \text{s}$	$N_{\text{Fe}} \times 10^6$, $\text{mol}/\text{m}^2 \cdot \text{s}$	E_{corr} , V
0	0.23	57.508	2.679	23.837	11.919	-0.67
1	0.18	45.006	2.097	18.655	9.328	-0.664
2	0.1205	30.129	1.404	12.489	6.244	-0.657

Table 4-27 Corrosion rate and corrosion potential of carbon steel in 9.99×10^{-3} M CaCO_3 with flow rate of $\text{CO}_2 = 0.283 \text{ m}^3/\text{h}$ for immersion different exposure times at $T = 35^\circ\text{C}$, and $u = 200$ rpm.

Time, h	I_L , mA/cm^2	CR, gmd	CR, mm/y	$N_{\text{H}_2\text{CO}_3} \times 10^6$, $\text{mol}/\text{m}^2 \cdot \text{s}$	$N_{\text{Fe}} \times 10^6$, $\text{mol}/\text{m}^2 \cdot \text{s}$	E_{corr} , V
0	0.1105	27.628	1.287	11.451	5.726	-0.498
1	0.125	31.254	1.456	12.955	6.478	-0.665
2	0.1	25.004	1.165	10.362	5.182	-0.700

Table 4-28 Corrosion rate and corrosion potential of carbon steel in 9.99×10^{-3} M CaCO_3 with flow rate of $\text{CO}_2 = 0.283 \text{ m}^3/\text{h}$ for immersion different exposure times at $T = 35^\circ\text{C}$, and $u = 800$ rpm.

Time, h	I_L , mA/cm^2	CR, gmd	CR, mm/y	$N_{\text{H}_2\text{CO}_3}, \times 10^6$ mol/ $\text{m}^2 \cdot \text{s}$	$N_{\text{Fe}}, \times 10^6$ mol/ $\text{m}^2 \cdot \text{s}$	E_{corr} , V
0	0.075	18.505	0.874	7.773	3.887	-0.661
1	0.12	30.004	1.398	12.444	6.218	-0.721
2	0.095	23.753	1.107	9.846	4.923	-0.706

Table 4-29 Corrosion rate and corrosion potential of carbon steel in 9.99×10^{-3} M CaCO_3 with flow rate of $\text{CO}_2 = 0.283 \text{ m}^3/\text{h}$ for different temperatures, and $u = 0$ rpm.

T, $^\circ\text{C}$	I_L , mA/cm^2	CR, gmd	CR, mm/y	$N_{\text{H}_2\text{CO}_3}, \times 10^6$ mol/ $\text{m}^2 \cdot \text{s}$	$N_{\text{Fe}}, \times 10^6$ mol/ $\text{m}^2 \cdot \text{s}$	E_{corr} , V
25	0.113	28.254	1.316	11.711	5.856	-0.510
35	0.189	47.256	2.202	19.588	9.794	-0.597
45	0.23	57.508	2.679	23.837	11.919	-0.67

Table 4-30 Corrosion rate and corrosion potential of carbon steel in 9.99×10^{-3} M CaCO_3 with flow rate of $\text{CO}_2 = 1.132 \text{ m}^3/\text{h}$ for different temperatures, and $u = 0$ rpm.

T, $^\circ\text{C}$	I_L , mA/cm^2	CR, gmd	CR, mm/y	$N_{\text{H}_2\text{CO}_3}, \times 10^6$ mol/ $\text{m}^2 \cdot \text{s}$	$N_{\text{Fe}}, \times 10^6$ mol/ $\text{m}^2 \cdot \text{s}$	E_{corr} , V
25	0.0605	15.127	0.705	6.270	3.135	-0.680
35	0.0845	21.128	0.984	8.757	4.38	-0.639
45	0.1	25.003	0.885	10.364	5.182	-0.669

4.6 Cathodic Protection Results

4.6.1 Corrosion Rate Results with sacrificial anode.

A series of experiments were carried out to control the corrosion of CS in two phase system of CaCO_3 solution with CO_2 gas pumping through the solution

at different operating conditions by cathodic protection using Zn as sacrificial anodes. The loss in weight was measured and the results are presented in tables 4-31 through 4-33 showing the corrosion rate of carbon steel with and without protection by zinc. Also the corrosion rate of zinc when connecting it to CS was determined.

Table 4.31 corrosion rate of carbon steel, zinc and protection efficiency in 9.99×10^{-3} M CaCO_3 at different temperatures for immersion time of 1.5 h, $u=0$ rpm and $Q_{\text{CO}_2}=0.283$ m³/h.

T, °C	CR of CS, gmd (no protection)	CR of CS, gmd (protected)	CR of Zn, gmd (connected to CS)	% protection
25	43.558	16.753	141.71	61.50
35	52.493	3.351	100.57	93.62
45	65.896	14.519	134.85	77.97

Table 4-32 corrosion rate of carbon steel, zinc and protection efficiency in 9.99×10^{-3} M CaCO_3 at different velocity for immersion time of 1.5 h, $T=35$ °C and $Q_{\text{CO}_2}=0.283$ m³/h.

u, rpm	CR of CS, gmd (no protection)	CR of CS, gmd (protected)	CR of Zn, gmd (connected to CS)	% protection
0	52.493	3.351	100.57	93.62
200	100.519	24.571	48	75.56
400	62.545	33.506	60.57	46.43
800	75.948	20.104	74.29	73.53

Table 4-33 corrosion rate of carbon steel, zinc and protection efficiency in 9.99×10^{-3} M CaCO_3 at different flow rates for immersion time of 1.5 h, $T=35$ °C, and $u= 200$ rpm.

Q_{CO_2} , m^3/h	CR of CS, gmd (no protection)	CR of CS, gmd (protected)	CR of Zn, gmd (connected to CS)	% protection
0.283	100.519	24.571	48	75.56
0.566	62.545	8.935	88	85.71
1.132	48.026	6.701	52.57	86.05

4.6.2 Protection Potential

The relationship between protection potential and time for various conditions of velocity, temperature, and CO_2 flow rate with sacrificial anode. The protection potentials with respect to saturated calomel electrode (SCE). The data for cathodic polarization protection experiments results are shown in tables in Appendix D.

Measured experimental value of pH, conductivity, and oxygen solubility were tabled in Appendix B.

Chapter One

Introduction

Corrosion is a destructive attack of a metal by a chemical or electrochemical reaction with its environment [Revie and Uhlig, 2008]. Also it can be defined as destruction or deterioration of a material because of reaction with its environment [Fontana and Greene, 1978].

In spite of much advancement in the field of corrosion science and technology, the phenomenon of corrosion remains a major concern to industries around the world. Though the serious consequences of corrosion can be controlled to a great extent by selection of highly corrosion resistant materials, the cost factor associated with the same, favors the use of cheap metallic materials along with efficient corrosion prevention methods in many industrial applications [Nathan, 1973].

The importance of corrosion studies is three folds:

The first area of significance is economic including the objective of reducing material losses resulting from the corrosion of piping, tanks, metal components of machines, ships, bridges, marine structures, and so on. The second area is improved safety of operating equipment which, through corrosion, may fail with catastrophic consequences. Examples are pressure vessels, boilers, metallic containers for toxic materials, turbine blades and rotors, bridges, airplane components, and automotive steering mechanisms. Third is conservation, applied primarily to metal resources - the world's supply of these is limited, and the wastage of them includes corresponding losses of energy and

water reserves associated with the production and fabrication of metal structures [Revie and Uhlig, 1985].

Carbon steel, the most widely used engineering material, accounts for approximately 85% of the annual steel production worldwide. Despite its relatively limited corrosion resistance, carbon steel is used in large tonnages in marine applications, chemical processing, petroleum production and refining, construction and metal processing equipment.

Corrosion problems occur in the petroleum industry in at least three general areas: (1) production, (2) transportation and storage, and (3) refinery operations.

During crude oil production from wells, a voluminous amount of water containing different salts accompanies the oil. The presence of saline water (brine) cause severe corrosion damage of the equipment, pipelines, tanks, etc. Despite many primary treatments to remove the saline water, considerable amounts reach to the refining process and even reached to the storage tanks causing considerable corrosion attack of tanks, equipments, pipelines, etc. The corrosion attack increases with increasing flow velocity and the interaction between two phases of the water-petroleum mixtures.

Acidization of oil and gas wells is the most widely used work over and stimulation practice in oil industry [Migahed and Nassar, 2007]. Acidification is increasing well productivity. Different acids are used in conventional acidization treatment. The most common are hydrochloric acid HCl, hydrofluoric acid HF, acetic acid CH_3COOH , formic acid HCOOH , sulfamic acid $\text{H}_2\text{NSO}_3\text{H}$, and chloro acetic acid ClCH_2COOH . Choice of the acid for a given situation depends on the underground reservoir characteristics and specific intention of the

treatment. Among various acids, HCl is widely used for stimulating carbonate-based reservoirs like lime stone and dolomite [Tayaperumal et. al, 2000].

Oil well stimulation, usually done with hot solutions of hydrochloric acid, may induce severe corrosion attack on production tubing, downhole tools and casing, oil well stimulation is the general term describing a variety of operations performed on a well to improve its productivity [Rajeev et.al, 2012].

Oxygen, which plays such an important role in corrosion, is not normally present in producing formations. It is only at the drilling stage that oxygen contaminated fluids are first introduced. Drilling muds, left untreated, will corrode not only well casing, but also drilling equipment, pipelines and mud handling equipment. Water and carbon dioxide, produced or injected for secondary recovery, can cause severe corrosion of oil well steels. Acids, used to remove scale, readily attack metal [Lopez et.al 2003].

Carbon dioxide CO₂ and H₂S gases in combination with water are the main cause of corrosion in oil and gas production. In addition, it is normal practice to re-inject production water downhole to maintain the reservoir pressure and stability as well as perform water flooding (using seawater or fresh water sources) to drive oil out of the formation. As field ages, the ratio of watery oil in the produced fluids increases and can reach levels of 95% or higher. This rise in water content implies an increase of the corrosion problems. Internal corrosion caused by the produced fluids is the most costly of the corrosion problems in the oil and gas industry since internal mitigation methods cannot be easily maintained and inspected. Therefore, as a field ages, corrosion control becomes more expensive. Approximately 60% of oilfield failures are related to CO₂ corrosion mainly due to inadequate predictive capability and the poor resistance of carbon and low alloy steels to this type of corrosive attack, CO₂ can

produce not only general corrosion but also localized corrosion, which is a much more serious problem [Lopez et. al, 2003].

The most common methods to prevent corrosion are:

Cathodic protection, anodic protection, protective coating such as paint, selection of suitable materials, addition of inhibitors, successful design [Fontana and Greene, 1978]. Selection of the method depends on many factors such as cost, availability, contamination of environment with corroding metal etc. Sacrificial anodes system in cathodic protection generates protective current which depends upon the inherent potential difference between the anodes and the structure to be protected. Thus, if the structure is made of iron or steel, any metal that is more active in the electromotive force series can theoretically be used as an anode material [Shrier, 2000].

Aim of the work

The aim of this work is to study the corrosion behavior of carbon steel in oil-brine solution as well as the effect of acids (HCl and H₂SO₄) presence in the solution. In addition, it is aimed to investigate the corrosion behavior under two phase flow of brine- CO₂ mixture using flat blade mixer (Rushton type mixer) with study the influence of different operating conditions such as agitation velocity, temperature, concentration of petroleum fraction, salt, and acid on the corrosion rate and corrosion potential. Understanding the corrosion behavior under various conditions will help to suggest appropriate method to control the corrosion for such complicated system.

Chapter Six

Conclusions and Recommendations

6.1 Conclusions

From the results obtained the following points are concluded:

1. The corrosion rate in single phase brine CaCO_3 solution increases about two times with increasing rotational velocity from 0 to 1200 rpm.
2. The corrosion rate in two phase brine-gas oil mixture increases with the increase in rotational velocity up to 300 rpm. Further increase in velocity of agitation causes more dispersion of gasoil leading to a decrease in the corrosion rate. Also in brine-gasoil mixture, the corrosion rate increases with increased volume percent of gasoil.
3. In brine - gasoil system in presence of acids, the corrosion rate is higher than that in single phase CaCO_3 solution and increases with increasing agitation velocity and temperature. The limiting current density (corrosion rate) increases with the increase in rotational velocity, salt concentration, and temperature. The corrosion rate decreases with time due to the formation of corrosion products layer.
4. In CO_2 corrosion of carbon steel, the corrosion potential is shifted to more negative value with increasing rotational velocity, concentration of brine, and time. However, it shifts to more positive values with increasing temperature.
5. In two phase CaCO_3 - CO_2 gas mixture, increasing flow rate of gas, rotational (mixing) velocity, and time leads to a decrease in the corrosion rate (i_L) while temperature increases the corrosion rate.

6. In the cathodic protection by sacrificial anodes, the potential shifts the positive direction when the temperature, agitation velocity (mixing) and flow rate of CO₂ gas is increased.

7- Corrosion protection efficiency by zinc as sacrificial anode, depends on different operating parameters and under some conditions reaches to 93.62 %.

8- The protection potential of CS by Zn decreases with time in first few minutes reaching to constant value depending on temperature, agitation velocity, and time.

6.2 Recommendations

1- Measuring the effect of presence of acetic acid (HAc) on CO₂ corrosion under different operation conditions because practically HAc forms.

2- Performing experiment for wider ranges of temperature and velocity

3- Use of chemical inhibitors such as synthetic organic compounds or natural inhibitors to control corrosion.

4- Studing corrosion behavior of other important metals such as copper and Aluminum.

5- Studying CO₂ corrosion in pipe flow system.

Chapter Three

Experimental Work

3.1 Introduction

Experimental work was carried out to determine the corrosion rate of carbon steel under two phase flow conditions of mixtures consist of brine solution with gas oil and with CO₂ pumped through the solution. Flat blade agitated mixer was used with rotational speed up 1200 rpm. Experimental tests were carried out at temperatures of 25, 35, and 45 °C, with gasoil of 1 to 10 % by volume and CaCO₃ concentration range of 2.5×10^{-3} to 9.99×10^{-3} M. Using weight loss method and electrochemical polarization technique. The effect of presence of some acides such as 2% HCl and 2% H₂SO₄ in the mixture was also investigated. The experimental work included five parts:

1. Weight loss measurements under static conditions to determine the average corrosion rates of carbon steel in solutions containing: 2.5×10^{-3} M in the presence and absence of gasoil under different operating conditions.
2. Weight loss measurements under static conditions to determine the average corrosion rates in presence of HCl and H₂SO₄ in two phase mixture.
3. Electrochemical polarization measurements with CaCO₃ solution to measure the instantaneous corrosion rate using limiting current density technique under different conditions of agitation velocity, CaCO₃ concentrations, temperature, and time.
4. Electrochemical polarization measurements on CaCO₃ solution-CO₂ gas mixture to measure the instantaneous corrosion rate using limiting current

density technique under different conditions of agitation velocity, temperature, time, and flow rate of CO₂.

- Corrosion prevention by cathodic protection using sacrificial anode method. This was done by connecting zinc as sacrificial anode with carbon steel and the weight loss of each specimen was determined under different conditions.

3.2 Material Analysis

Chemical composition of carbon steel and zinc were analyzed using x-ray diffraction in the State Company for Inspection and Engineering Rehabilitation and the technical affairs department / Ministry of Sciences and Technology. The chemical composition is shown in tables 3-1 and 3-2:

Table 3-1: Chemical composition of carbon steel used

sample	C%	Si%	Mn%	P%	S%	Cr%	Mo%	Ni%	Al%	Co%	Cu%	V%	Fe%
(wt.%)	0.454	0.218	0.685	0.011	0.027	0.067	0.012	0.093	0.005	0.009	0.29	0.000	balance

Table 3-2: Chemical composition of zinc used

Pb	Sn	Al	Zn
00.0	0.00	0.00	99.01

3.3 The Solutions

Different solutions were used in the experiments:

- The first was CaCO₃ solution (brine) of concentrations 2.5×10^{-3} M CaCO₃. The required concentration of CaCO₃ was obtained by dissolving annular CaCO₃ in distilled water to obtain the required molarities.
- The second solution consisted of brine-gas oil mixture with different volume percent gas oil: 1, 2, and 5% vol.
- The third solution consisted of brine, acid, gas oil mixture with different volume percent of gas oil: 2, 5, and 10% vol. with 2% HCl. Also using 2%

H₂SO₄ acid concentration with brine solution and different volume percent gas oil: 5, and 10% vol.

4. The fourth solution consisted of different CaCO₃ concentrations of 9.99×10^{-4} , 2.5×10^{-3} , 4.99×10^{-3} , and 9.99×10^{-3} M CaCO₃.
5. The fifth solution consisted of brine- CO₂ mixture with different flow rate of CO₂ gas.

Salt used was calcium carbonate (CaCO₃) produced by “Scharlau Company-Spain” having assay of 99% and a molecular weight of 100.09 g / gmole. The hydrochloric acid that used was produced by “Scharlau Company- Spain” having assay of 36% and a molecular weight of 36.64 g / gmole and density of 1.185 g/cm³ and sulfuric acid that used was produced by “Gainland Chemical Company” of assay of 98%, and a molecular weight of 98.07 g/gmole and density of 1.83 g/cm³.

3.4 Materials

Ethanol was used to clean the specimens. It was produced by “Scharlau Company- Spain” and having assay of 99.9 %. For the corrosion experiments in CaCO₃ there was clear corrosion product layer. A 50 gm thioharnstoff corrosion inhibitor (H₂NCSNH₂) that produced by MERCK company with assay of 99.8 % was added to the cleaning solution with 10 % HCl. Blank testes showed no appreciable weight loss caused by cleaning solution. Carbon steel rod specimen was prepared to fit the specimen holder with a surface area of 14.3256 cm² having a dimension of 35 mm long (L), 12 mm outside diameter (d_o) that were measured by using electronic digital caliper and it serves as a cathode (Fig.3-1).

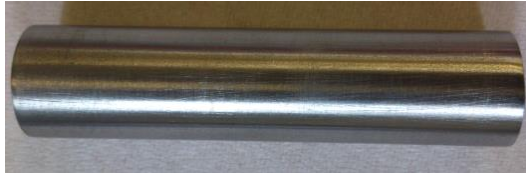


Figure 3-1: Carbon steel specimen

3.5 Experimental Apparatus

1. Baffled mixing tank shown in Fig. 4-10 and described in details in section 4.6 later.
2. Carbon steel specimen was fixed by plastic tube as a holder. The exposed length of specimen to the solution is 35 mm and the diameter is 12 mm.
3. Stirrer: type of ss10 manufactured by Stuart (UK) which is a rotating motor used to obtain the required rotational velocity that range from 0 to 2000 rpm.
4. Heater and Controller made of stainless steel type Techne TE-8J, was used to obtain the required temperature in the bath. The heater was combined with thermostat to control the temperature within accuracy of $\pm 0.5^{\circ}\text{C}$.
5. Thermometer: of range -10 to 200°C is used to measure the solutions temperature.
6. Desiccator: made of Pyrex to keep the specimen from moisture using highly active silica gel.
7. Balance: electronic high accuracy digital balance type Sartorius with maximum weight of 210 gram and accuracy of 0.1 mg was used to weigh the specimens before and after the experiment.
8. Power supply: power supply of range up to 50 V (DC) was used to provide a constant applied voltage of 5 V between the electrodes.
9. Voltmeter: to measure the potential in V.

10. Ammeter: to measure the current in mA.
11. Resistance box type PE 06 RN manufacture by POPULAR company range from 0 to 10^6 Ohm is used to control the current flow.
12. Reference Electrode: was saturated calomel electrode (SCE) used to measure the carbon steel specimen (working electrode) potentials. The luggin capillary of the reference electrode was placed about 2 mm from the working electrode.
13. Counter (auxiliary) electrode: made of graphite and served as anode. The surface area of the counter electrode was made larger than that of the working electrode ($A_a/A_c = 17.99$) to ensure that the limiting current density occurs on the cathode rather than anode.
14. pH – meter: A digital pH meter manufactured by Hanna Instruments Company. Microprocessor pH meter having a range of pH from -2.00 to 16.00 with accuracy of ± 0.01 . Also it contains temperature probe to read the temperature for range of 0 to 100 °C with accuracy of ± 0.5 °C. The pH meter was calibrated using 4.001 and 7.001 pH buffer solutions.
15. Conductivity meter: Auto- ranging microprocessor type HI 2300 manufactured by Hanna instruments and used to measure the conductivity of the solution at different temperatures and salt concentrations, with conductivity range 0.00 to 500.00 mS, temperature range -9.9 to 120 °C, and accuracy of $\pm 1\%$, ± 0.4 °C for conductivity and temperature respectively.
16. Dissolved oxygen meter: This was used to measure the concentration of oxygen in the solution (C_b) in ppm. Manufactured by Hanna instruments type HI 2400 with accuracy of $\pm 1.5 \%$ for range 0.00 to 45.00 ppm. It

measures the solubility of oxygen for a range of temperature 0.0 to 50.0 °C with accuracy of ± 0.5 °C.

17. Rotameter: rotameter for measuring flow rate of gas at range (5-60 ft³/h).

3.6 Agitation System

The agitation system consisted of cylindrical Perspex vessel of wall thickness 4 mm, vessel diameter $D_t=30$ cm and $H=30$ cm height, filled with test solution. Five equally spaced vertical baffles made of perspex each of width equal to $J=2.5$ cm. A perspex 4-blade disc impeller of diameter equal to $D_a=10$ cm, blade length $L=2.5$ cm, blade width $W=2$ cm, as shown in Figs. 3-2 and 3-3, was used and located $E=10$ cm from the tank bottom. Before each test, the vessel was washed with tap water using liquid detergent, rinsed with tap water, and concentrated (HCl) to remove corrosion products and deposits, then washed with tap water, followed by distilled water.



Figure 3-2 Circular Disk Turbine (four- blades).

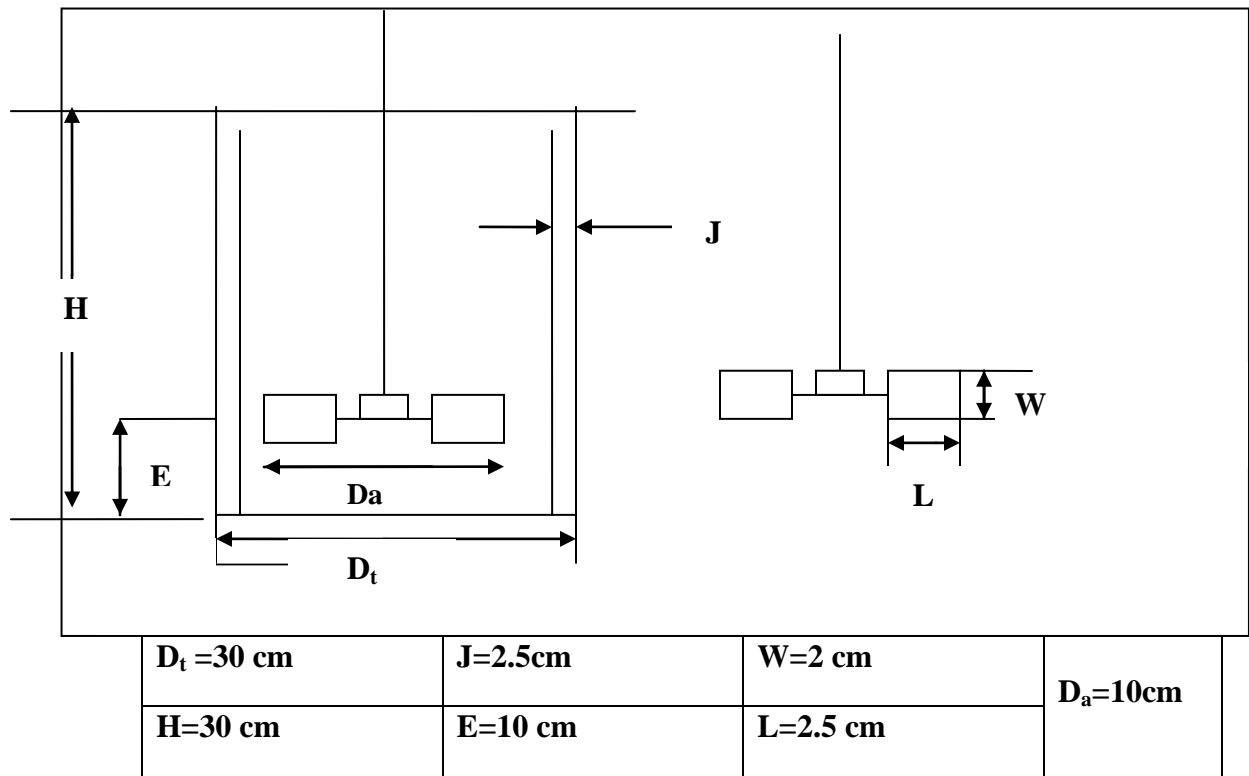


Figure 3-3 Dimensions of Tank and Disk Turbine.

Figures 3-4 to 3-5 show the Rig picture and schematic of the experimental apparatus respectively.



Figure 3- 4 Experimental rig picture.

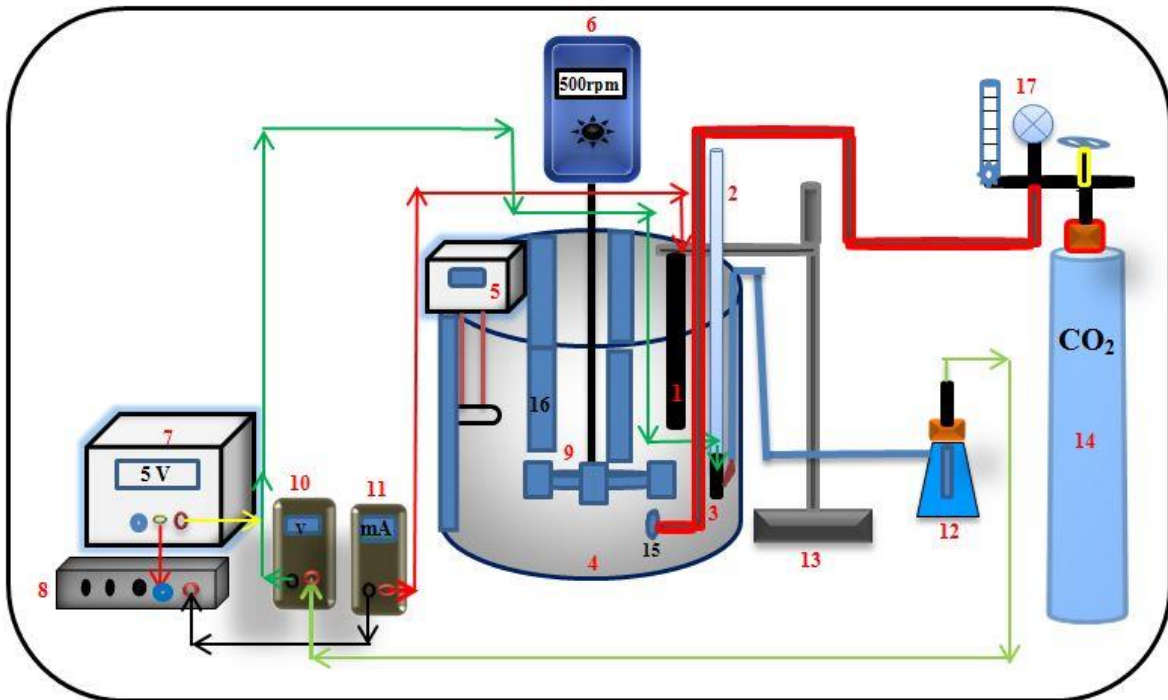


Figure 3- 5 Schematic illustrates the experimental apparatus.

- 1- Graphite electrode (anode), 2- holder of specimen, 3- working electrode (specimen), 4- Agitation tank , 5- Heater and controller, 6- stirrer, 7- power supply, 8- resistance box, 9- impeller, 10- voltmeter, 11-ammeter, 12- calomel electrode (reference electrode), 13- stand 14- CO₂ gas bottle, 15- gas distributor, 16.baffles, 17- rotameter.

3.7 Experimental Procedures

3.7.1 Weight Loss Experiments

Before each experiment, the carbon steel specimen (working electrode) was polished with 120, 180, 220, 400 and 2000 grade silicon carbide papers, washed with brushing by plastic brush with running tap water, immersed in ethanol for 30 second dried with clean tissue, and then dried by using electrical oven to temperature of about 105 °C for 5 minutes [Mahato et.al, 1980, Hasan

and Sadek, 2014]. The specimen then was stored in vacuum desiccator over high activity silica gel until use. Then the specimen was weighted (w_1) by using digital balance.

The test solution was prepared at the required conditions of components concentrations, temperature, and rotational velocity. After that the specimen was exposed to corrosion environment for 3.5 h in brine solutions and in brine solution-gasoil mixture and 2 h for brine solution- gasoil- acid mixture. At the end of experiment, the specimen was washed by tap water with brushing to remove the corrosion products that formed on the outside surface and then immersed in 10% hydrochloric acid containing chemical inhibitor (thioharnstoff) for 30 second [Fontana, 1986; Slaiman et al., 2010]. Blank tests showed no appreciable weight loss caused by cleaning with inhibited acidic solution. After that, the specimen was washed by tap water, distilled water, dried with clean tissue, rinsed in ethanol and dried by using electrical oven to a temperature about 105 °C for 5 minute. Then the specimen was kept in the desiccator to cool and weighted (w_2). So that, the corrosion rate in gmd can be determined using:

$$CR = \frac{\Delta W}{A \times t} \quad (3.1)$$

where, CR is the corrosion rate in gmd, ΔW is the loss in weight in gram, A is the specimen area in m^2 , and t is the time in day. Each run was carried out twice with third one when the reproducibility is in doubt.

3.7.2 Preparation of test solution

Corrosion tests were carried out with 2.5×10^{-3} M $CaCO_3$ solution prepared from annular calcium carbonate added to distilled water. 12 liters of solution was

used for each test run. The electrical conductivity of the solution was measured using digital electrical conductivity meter also the pH of solution was measured before each test and monitored during the test run.

3.7.3 Polarization Experiments

A 12 liter of 2.5×10^{-3} M CaCO_3 solution was used in polarization experiments. The test section components (working electrode, counter electrode, reference electrode) were mounted in their positions. The solution was let to reach the desired temperature and the electrical circuit was switched on where maximum current pass through the cell because the resistance is very low. The specimen was cathodically polarized from a potential of nearly -1.4 V (vs. SCE) to the corrosion potential (where $i_{\text{app}} = 0$) at a sweep rate of $5 - 10$ mV by changing the applied current using rheostat, that is, 5 mV when the change of current with potential is high (near corrosion potential) and 10 mV when the change of current with potential is low, i.e. in the limiting current density region. The current was recorded for step changes in potential. Two minutes were allowed for steady state to be reached after each potential increment [Pickett and Ong, 1974; Slaiman and Hasan, 2010]. For two phase system experiments with CO_2 -gas bubbling, the CO_2 was pumped at specific condition of flow rate, temperature and agitation velocity. CO_2 was pumped for 30 minutes before each run and the bubbling was kept until the end of the run. The oxygen concentration was measured at such conditions and monitored along the run using dissolved oxygen meter.

The method given by Gabe and Makanjoula [1986] for determining the limiting current is used in this work as explained in section 4.5. The obtained values of i_L represent values for clean surface ($t = 0$), i.e. no corrosion products

were formed, since during the polarization experiment no free corrosion occurred (except at low currents near the corrosion potential) because the specimen was cathodically protected. To investigate the influence of time on the instantaneous corrosion rate, the electrical circuit was switched off and the specimen was allowed to corrode freely at a particular velocity and temperature. A free corrosion of the specimen continues for 1 h during this interval the corrosion proceeds and the corrosion product forms on the surface of the specimen. At the end of 1 h, the electrical circuit was again switched on and the specimen was polarized to -1.4 V (vs. SCE) and polarization experiment was repeated to obtain the complete polarization curve and new i_L . This value of i_L represents the value at $t = 1$ h. At the end of the second polarization measurement, the electrical circuit was switched off while the specimen was kept corroding in the solution for another 1 h. During this second interval, the specimen will undergo a free corrosion forming additional corrosion products. The specimen was then polarized to -1.4 V (vs. SCE) by switching on the electrical circuit again to repeat the polarization experiment and to obtain new i_L at $t = 2$ h. The solubility of oxygen at different velocities, temperatures, and salt concentration was measured in ppm at each 15 min using oxygen meter. Each run was carried out twice with third one when the reproducibility is in doubt. The average reproducibility of the results is with $\pm 10\%$.

3.7.4 Cathodic Protection Tests

Sacrificial anode cathodic protection was adopted to prevent the corrosion of carbon steel specimen in CaCO_3 - CO_2 gas mixture under various conditions. In these experiments, the carbon steel was connected to zinc sheet analysis shown in Fig.3.6 (of analysis shown in Table 3.2). The carbon steel specimen

was placed in the solution by holding it by plastic tube (Fig. 3.5). The zinc sheet (of dimensions 40 mm × 35 mm × 0.3 mm) was placed in the solution at a distance 40 mm from carbon steel. The zinc specimen was placed in the solution by fixing it on the wool plate using fine screw. One face of zinc was exposed to the solution while other face was completely insulated using tape. The same procedure for weight loss measurements described in section 3.7.1 was used for carbon steel and zinc to determine the corrosion rate and protection efficiency except for the case of zinc sheet the cleaning by acid has not been used neither before nor after the run because the zinc is very weak against acids. The percent protection was estimated using the following equation:

$$\% \text{ Protection} = \frac{CR_{\text{before}} - CR_{\text{after}}}{CR_{\text{before}}} \times 100 \quad (3.2)$$

where CR_{before} is the corrosion rate of carbon steel before connecting it with zinc sheet and CR_{after} is the corrosion rate of carbon steel after connecting it with zinc sheet.



3- 6 Carbon steel and Zinc specimens.

Chapter Two

Corrosion in Petroleum Industry

2.1 Corrosion Theory

The corrosion occurs because of the natural tendency for most metals to return to their nature state; e.g iron in the presences of moist air will revert to its noble state iron oxide [Melchers, 2005].This process results in the loss of properties of the material, causing economic losses, affecting safety, and raising environmental concerns [Hussein, 2009].

Corrosion of metals in electrolytic environments is an electrochemical process, with which respective oxidation and reduction reactions are linked. In the case of corrosion of carbon steel in a moist atmosphere, in natural waters and soil, oxidation of iron (dissolution) occurs as in equation [Darowicki et.al, 2001].



Since metals have a high electric conductivity, their corrosion is usually of an electrochemical nature. Of all types of destruction of structural materials, corrosion of metals draws the greatest amount of attention. Hence, where no particular reference is made to material, it is to be normally understood that a metal is being attacked [Fontana and Greene, 1978].

2.2 Corrosion Cell

2.2.1 Corrosion Cell Parts

Corrosion is the deterioration of a material through reaction with its environment. In the case of a metal, this deterioration occurs mainly through an

electrochemical process. The electrochemical process consists of four distinct parts: anode, cathode, electrolyte, and metallic path. These four parts constitute what is called the corrosion cell. Electrochemical corrosion occurs when all four parts of the corrosion cell are present. To understand these four parts of the electrochemical corrosion cell Fig.2-1 illustrates the four essential elements of a corrosion cell.

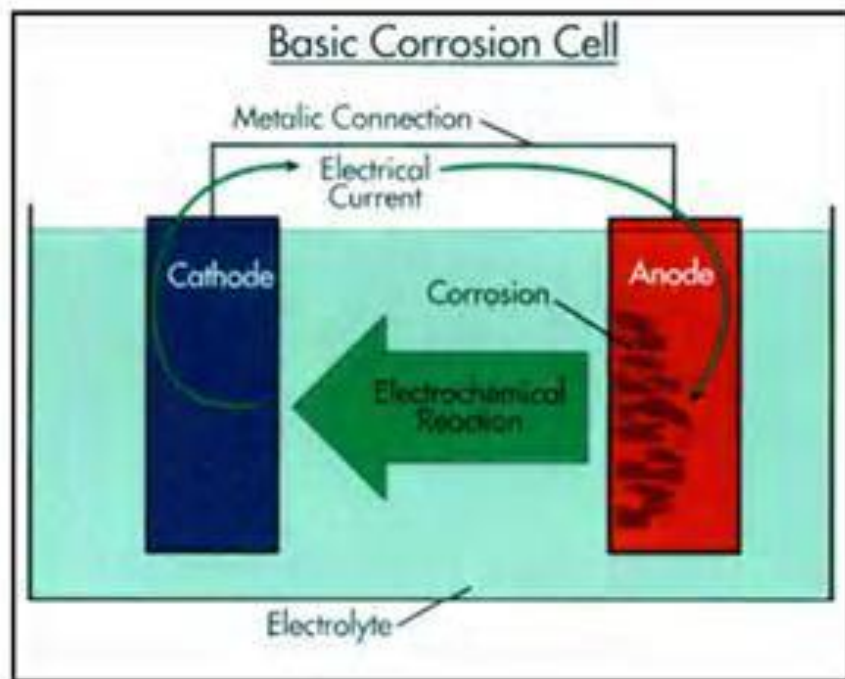
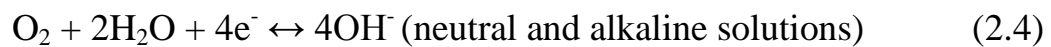


Figure 2-1: Corrosion Cell [Peabody, 1974]

Several cathodic reactions are possible depending on what reducible species are present in the solution. Typical reactions are the reduction of dissolved oxygen gas or the reduction of hydrogen ions:



However, if oxygen is present, two other reactions may occur:



Most corrosion of steel can be considered as an electrochemical process which occurs in stages. Initial attack occurs at anodic areas on the surface, where ferrous ions go into solution. Electrons are released from the anode and move through the metallic structure to the adjacent cathodic sites on the surface where they combine with oxygen and water to form hydroxyl ions. These react with the ferrous ions from the anode to produce ferrous hydroxide which itself is further oxidized in air to produce hydrated ferric oxide, red rust the sum of these reactions is described by the following equation [Robert et. al., 2003]:



Iron and steel + oxygen + water = rust

2.2.2 Types of Cells

There are three main types of cells that take part in corrosion reactions [Revie and Uhlig, 2008]:

1. Dissimilar Electrode Cells
2. Concentration Cells
3. Differential Temperature Cells

2.3 Classification of corrosion

Corrosion has been classified in many different ways. One method divides corrosion into low-temperature and high temperature corrosion. The other separates corrosion into direct chemical and electrochemical corrosion. The preferred classification here is:

- (1) Wet corrosion
- (2) Dry corrosion

2.3.1 Wet corrosion

Wet corrosion occurs when a liquid is present. This usually involves aqueous solutions or electrolytes and accounts for the greatest amount of corrosion by far. A common example is corrosion of steel in water or acid liquid [Fontana and Greene, 1978]. In wet corrosion the oxidation of the metal and reduction of a species in solution (electron acceptor or oxidizing agent) occur at different areas on the metal surface with consequent electron transfer through the metal from the anode (metal oxidized) to the cathode (electron acceptor reduced) the thermodynamically stable phases formed at the metal/solution interface may be solid compounds or hydrated ions (cations or anions) which may be transported away from the interface by processes such as migration, diffusion and convection [Heitz, 1974; Shreir et. al., 2000].

2.3.2 Dry corrosion

Dry corrosion occurs in the absence of a liquid phase or above the dew point of the environment. Vapors and gases are usually the coronets. Dry corrosion is most often associated with high temperatures. An example is attack on steel by furnace gases. The presence of even small amounts of moisture could change the corrosion completely. For example, dry chlorine is practically non corrosive to ordinary steel but moist chlorine, or chlorine dissolved in water, is extremely corrosive and attacks most of the common metals and alloys [West,1976]. These are generally metal/gas or metal/vapor reactions involving non-metals such as oxygen, halogens, hydrogen sulphide, sulphur vapor, etc. and oxidation, scaling and tarnishing are the more important forms. A characteristic of these reactions is that the initial oxidation of the metal, reduction of the non-

metal, and formation of compound must occur at one and the same place at the metal/non-metal interface [Heitz, 1974; Shreir et. al., 2000].

2.4 Factors Effecting Corrosion Rate

2.4.1 Diffusion

In the majority of cases, the corrosion rates of metals are controlled by the diffusion of reactants to and from the metal surface, this factor is controller on type of polarization, hence freshly exposed bare steel surfaces will corrode at a greater rate than those covered with a compact layer of rust.

2.4.2 Solution pH

The pH value is used to represent the acidity of a solution. First, consider the exposure of iron to aerated water at room temperature (aerated water will contain dissolved oxygen). The corrosion rate for iron as a function of pH is illustrated in Fig. 2- 2. The range of pH = 4 to pH =10 in this pH range, the corrosion rate is governed largely by the rate at which oxygen reacts with absorbed atomic hydrogen, thereby depolarizing the surface and allowing the reduction reaction to continue. For pH values below 4.0, ferrous oxide (FeO) is soluble. Thus, the oxide dissolves as it is formed rather than depositing on the metal surface to form a film. In the absence of the protective oxide film, the metal surface is in direct contact with the acid solution, and the corrosion reaction proceeds at a greater rate than it does at higher pH values. It is also observed that hydrogen is produced in acid solutions below a pH of 4, indicating that the corrosion rate no longer depends entirely on depolarization by oxygen, but on a combination of the two factors [hydrogen evolution and oxygen reduction reaction (depolarization)]. For pH values above about pH 10, the corrosion rate is observed to fall as pH is increased. This is believed to be due to

an increase in the rate of the reaction of oxygen with $\text{Fe}(\text{OH})_2$ (Hydrated FeO) in the oxide layer to form the more protective Fe_2O_3 [Gedeon, 2000].

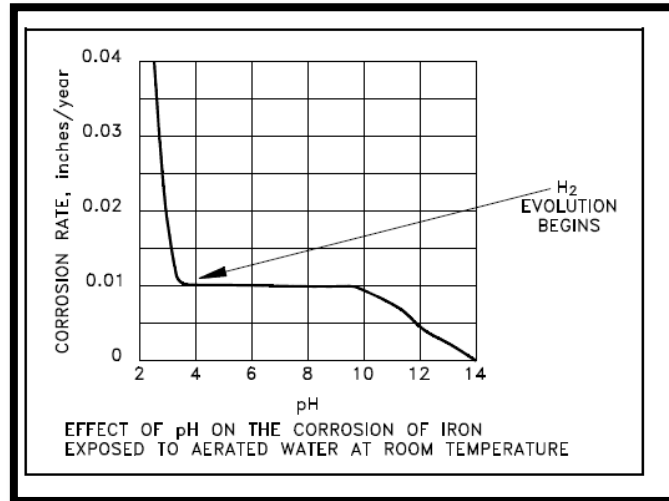


Figure 2-2 Effect of pH on corrosion rate of iron[Gedeon, 2000]

2.4.3 Effect of Temperature

Temperature increases the rate of almost all chemical reactions. When the rate determining step is the activation process, the temperature change has the greatest effect. In general, if diffusion rates are doubled for a certain increase in temperature, activation process may be increased by 10-100 times, depending on the magnitude of the activation energy [Henry and Scott, 1999].

Temperature gives such a great effect on the rate of corrosion on metal, in case of corrosion in a neutral solution, the increase of temperature has a favorable effect on the overpotential of oxygen depolarization and the rate of oxygen diffusion, but it leads to a decrease of oxygen solubility. In case of corrosion in an acid medium, the corrosion rate increases with temperature increase because the hydrogen evolution overpotential decreases [Amin et. al., 2011]. When corrosion is controlled by the diffusion of oxygen, the corrosion

rate at given oxygen concentration approximately doubles for every 30°C rise in temperature [Eid, 1989]. In a closed system, oxygen cannot escape and the corrosion rate continues to increase with temperature until all the oxygen is consumed. When corrosion is attended by hydrogen evolution, the rate of increase will increase more than double for every 30°C rise in temperature show in Fig.2-3 [Wan, 2011].

The corrosion of mild steel in aerated water at varying temperatures is influenced in general by the manner in which temperature affects i - the specific reaction rates of the various corrosion reactions ii- oxygen solubility in the water iii - rate of transfer of dissolved oxygen through the liquid film and the product layer and iv- the nature of corrosion product [Mahato et.al, 1968a].The studies of Rajappa et.al[1998], Sun et.al[2003], and George and Nescic [2004] indicated that the corrosion rate increase with the temperature increase.

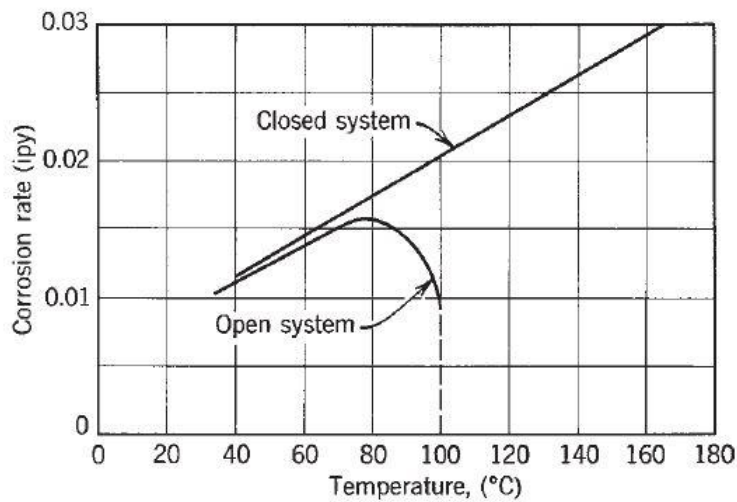


Figure 2-3 Effect of temperature on corrosion of iron in water containing dissolved oxygen [Wan, 2011].

2.4.4 Effect of Velocity

Fluid velocity is one of the most important parameters to be considered during corrosion of metals, due to the flow effects on both anodic and cathodic reactions [Shrier et.al, 2000; Musa et. al., 2011]. Corrosion process can be influenced, in different ways, by the relative movement between the metal and the corroding environment. This relative movement can increase the heat and mass transfer of reactants towards and from the surface of the corroding metal, with a consequent increase in the corrosion rate. Also, if solid particles are present, removal of protective films, erosion and wear on the metallic surface can occur. The corrosion of the metallic structure under turbulent flow is complex, but this problem has been studied [Rodriguez et. al., 2009; Genesca et. al.,2010; Mora-Mendoza et. al., 2002; Papavinasam et. al., 2003; Poulson, 1993], mainly where, the flow are very important in the behavior of the phenomenon processes.

The manner in which velocity affects the limiting diffusion current is a marked function of the physical geometry of the system. In addition the diffusion process is affected differently by velocity when the flow conditions are laminar as compared to a situation where turbulence exists. For most conditions the limiting diffusion current can be expressed by the equation:

$$i_L = K \times u^n \quad (2.6)$$

where (K) is a constant, (u) is the velocity of the environment relative to the surface and (n) is a constant for a particular system. Values of n vary from 0.2 to 1. Fig. 2-4 shows the effect of velocity on the limiting current density [Uhlig, 1976 and Stern, 1957]. The corrosion rate would be directly proportional to the limiting diffusion current until the intersection of anodic and cathodic

polarization curves occur at a current less than the limiting diffusion current. At higher velocities the corrosion rate will be relatively independent of velocity until cavitations or erosion changes the physical conditions of the system. Figure 2-5 shows the typical observations when agitation or solution velocity is increased. For corrosion processes which are controlled by activation polarization, agitation and velocity have no effect on the corrosion rate as illustrated in curve B. If corrosion process is under cathodic control, then agitation or velocity increases the corrosion rate as shown in curve A, section 1. This effect generally occurs when an oxidizer present in very small amounts as in the case of dissolved oxygen in acids or water. If the process is under diffusion control and the metal is readily passivated, then the behavior corresponding to curve A, section 1 and 2, will be observed [Fontana and Green, 1987].

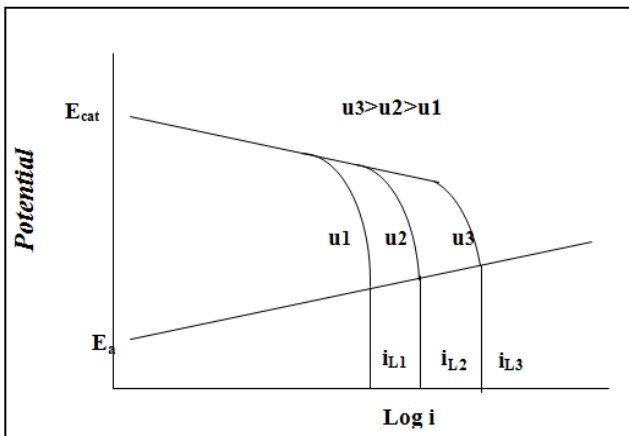


Figure 2-4 Effect of Velocity on i_L
[Uhlig, 1976 and Stern, 1957].

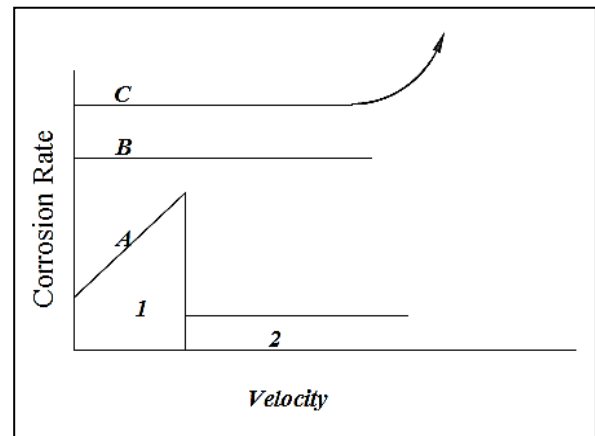


Figure 2-5 Effect of Velocity on the CR
[Fontana and Green, 1987].

Some metals owe their corrosion resistance in certain medium to the formation of massive bulk protective films on their surface. When materials such as these are exposed to extremely high corrosive velocities, mechanical damage or removal of these films can occur, resulting in accelerated attack as shown in

curve C. This is called erosion corrosion [Fontana and Green, 1987]. It is well known that, in the presence of oxygen in acid solutions, two cathodic reactions take place which are hydrogen evolution reaction (HER) and oxygen reduction reaction. The first reaction, i.e., HER, is an activation controlled process [Fontana and Green, 1987; Revie and Uhlig, 2008]. It was stated earlier, that oxygen transfer to the cathodic area is often rate controlling, i.e., a mass transfer controlled process. Therefore, the effect of flow on the limiting current density (i_L) of the oxygen reduction reaction in acid solutions is to increase i_L as the flow increases [Revie and Uhlig, 2008; Alwash et.al, 1987].

2.5 Oxygen Reductions and Transport

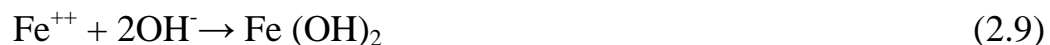
Most aqueous solutions (ranging from bulk natural water and chemical solutions to thin condensed films of moisture) will be in contact with the atmosphere and will contain dissolved oxygen, which can act as a cathode reactant. The solubility of oxygen in water decreases significantly with the increase in temperature and slightly with concentration of dissolved salts. On the other hand, the concentration of H_3O^+ in acid solution, which is given by the pH, is high, and since this ion has a high rate of diffusion; its rate of reduction is normally controlled by the activation energy for electron transfer. Furthermore, the vigorous evolution of hydrogen that occurs during corrosion facilitates transport, so that the diffusion is not a significant factor in controlling the rate of the reaction except at very high current densities. As pH in acid solution increases the hydrogen evolution reaction becomes kinetically more difficult and requires a high overpotential. Oxygen reduction is more significant than hydrogen evolution in near-neutral solutions, and that in the case of former, transport of oxygen to the metal surface will be more significant than activation-

controlled electron transfer. A further important factor is that in near-neutral solutions solid corrosion product will be thermodynamically stable and will affect the corrosion rate either by passivating the metal or by forming barrier that hinders transport of oxygen to the metal surface [Shreir, 1976].

2.6 Differential oxygen concentration

Corrosion can often take place in pipelines and equipment in which aqueous liquids are being transported (flow differential oxidation corrosion). This usually occurs at positions where there is difference in velocity between different portions of the liquid, i.e. at bends, nozzles, constriction, and etc. when liquid containing oxygen flows rapidly past a given section of pipe the oxygen can be supplied far more quickly to the surface than it can in parts where the liquid is comparatively stagnant. In consequence the stagnant part of the pipe become the anode and corrodes [Banerjee, 1985].

The section of the pipe in which water moves rapidly becomes the cathode. This form of corrosion can be avoided only by insuring that the water is properly deoxygenated. Differential oxidation corrosion, of particular importance to the oil industry or other industries where organic liquids are being stored in steel vessel where corrosion takes place at the bottom of tanks if traces of moisture have settled. The bottom of the tank then becomes the anode and the reaction-taking place:



The area of the vessel in contact with the oil or other organic liquids becomes the cathode. Since this area is very large and is kept from corroding by

the oil film on top, it acts as a most effective cathode. In general the amount of dissolved oxygen in oil is sufficiently large to cause a rapid cathode reaction:



As oil often contain NaCl and other salts, reaction can very rapid. The same kind of corrosion is often found in oil pipelines and other equipment containing organic liquids if the design includes an elbow where water can collect. The rate of corrosion that takes place at the bottom of oil filled vessel is usually rapid because anodic area is small and cathodic area is large [Banerjee, 1985].

2.7 Limiting Current Density

The limiting current is defined as the maximum current that can be generated by a given electrochemical reaction, at a given reactant concentration, hydrodynamic conditions. This definition implies that the limiting rate is determined by the composition and transport properties of electrolytic solution and by the hydrodynamic conditions at the electrode surface. Mass transport coefficients (k) for certain redox couples calculated from the limiting current values are frequently used in order to characterize the mass transport conditions of electrochemical cells and reactors. The limiting current condition arises when the electro active species in the diffusion boundary layer reacts immediately on contact with the electrode the charged species sinks through the ionic channels of an ion exchange membrane as soon as it contacts its surface. Under these conditions, the current is limited by the rate at which the electro active species reaches the surface. In an electrochemical process, the definition of the limiting current is when the change of current with potential is minimum or zero, i.e., $d(I)/d(E) = 0$. During the reduction of metal ions, the limiting current is achieved

when the concentration of an electro active species at the electrode surface is negligible. The limiting current region can be affected by factors such as the secondary reaction, electrolyte composition (including pH), increase of the electrode area due to metal deposition, changes in the concentration of the electro active species and uneven current and/or potential distribution [Ponce-de-Leo'n et. al., 2007]. At the limiting current the rate of transport of reactant to the interface is lower than the rate at which it can be potentially consumed by the charge transfer reaction; as a result, at the interface the concentration of this species approaches zero [Selman, 1981]. The flux of reacting species is given by:

$$N_A = \frac{i_L}{Z \times F \times (1-t^+)} \quad (2.11)$$

Where: N_A = molar flux mole/ $m^2.s$, Z = Number of electrons transferred, F = Faraday No. (96487 Columb/equivalent). When concentration of the reacting species relative to the total ionic concentration of the electrolyte is small, $t^+ \ll 1$, Eq. (2.12) becomes;

$$N_A = \frac{i_L}{Z \times F} \quad (2.12)$$

From the measured current, a mass transfer coefficient, K , defined by;

$$N_A = K \times (C_b - C_s) \quad (2.13)$$

May be calculated, since at the limiting current we set $C_s = 0$, hence:

$$K = \frac{i_L}{Z \times F \times \Delta C} \quad (2.14)$$

2.8 Polarization

When the metal is not in equilibrium with a solution of its ions, the electrode potential differs from the equilibrium potential by an amount known as

the polarization. Other terms having equivalent meaning are over voltage and over potential. The symbol commonly used is (η). Polarization is an extremely important parameter because it allows useful statements to be made about the rates of corrosion process. In practical situations, polarization is sometimes defined as the potential change away from some other arbitrary potential and in mixed potential experiments; this is the free corrosion potential [Tretheway and Chamberlain, 1996]. If the electrochemical system (electrode and electrolyte) is at equilibrium, then the net rate of reaction is zero. In comparison, reaction rates are governed by chemical kinetics, while corrosion rates are primarily governed by electrochemical kinetics. Thus, electrode reactions are assumed to induce deviations from equilibrium due to the passage of an electrical current through an electrochemical cell causing a change in the working electrode potential [Perez, 2004]. Cathodic polarization η_c means that electrons are supplied to the surface and they build up a negative potential in the metal. Therefore η_c is negative by definition. Anodic polarization η_a is the opposite process [Fontana, 1986]. The potential at which the reaction is occurring changes, when a reaction is forced a way from equilibrium i.e., when one direction of the reaction is favored over the other, the amount by which the potential changes is the over voltage which is defined as:

$$\eta = E_i - E_{eq} \quad (2.15)$$

The current applied to cause the departure from equilibrium is the net rate of reaction, thus:

$$i_{app} = \sum \vec{i} - \sum \overleftarrow{i} \quad (2.16)$$

where: \vec{i} , \overleftarrow{i} and i_{app} are the anodic, cathodic current density respectively.

An anodic current density ($i_{app} > 0$) causes a positive anodic over potential and a

cathodic current density ($i_{app} < 0$) causes a negative over potential. The polarization is said to be either anodic, when the anodic processes on the electrode are accelerated by changing the specimen potential in the positive (noble) direction, or cathodic, when the cathodic processes are accelerated by moving the potential in the negative (active) direction [Roberge, 1999].

2.9 Polarization Types

There are three distinct types of polarization and these are additive, as expressed in equation [Roberge, 1999]:

$$\eta^T = \eta^A + \eta^C + \eta^R \quad (2.17)$$

2.9.1 Activation polarization

This polarization refers to an electrochemical process, which is controlled by the reaction sequence at the metal-electrolyte interface [Fontana, 1986]. Or stated in another way the reaction at the electrode requires activation energy in order to go. Activation polarization is usually the controlling factor during corrosion in strong acids. This is easily illustrated by considering hydrogen evolution reaction on zinc during corrosion in acid solution. Activation polarization is a function of the nature and concentration of the species being reduced, surface roughness, composition and temperature. In addition it is sensitive to traces of reducible impurities in the system [Tretheway, 1996]. The activation-over potential, and hence the activation energy varies exponentially with the rate of charge transfer per unit area of electrode surface, as defined by Tafel equation [Shreir, 2000]:

$$\eta = a \pm b \log i \quad (2.18)$$

where:

i , is current density,

a & b , are Tafel constants, and

\pm is anodic or cathodic over potential respectively.

2.9.2 Concentration polarization

It refers to electrochemical reaction, which is controlled by a mass transfer process, such that a drop in the concentration of the electrochemically active species on the electrode surface may result in causing a change in potential. The relationship between the reaction rate and concentration polarization is [West, 1976]:

$$i = i_{lm} \left[1 - \exp\left(-\frac{zF}{RT} \eta_c\right) \right] \quad (2.19)$$

where, i_{lm} is the maximum rate of a possible reaction for a given system, under which all the transferred species to the electrode react very soon.

η_c = concentration polarization

The maximum rate is known as the limiting current and can be defined mathematically by the following equation [Fontana, 1986]:

$$i_{lm} = \frac{D z F C_b}{\delta_m} \quad (2.20)$$

The value of the concentration polarization depends on the concentration, temperature and diffusion boundary layer thickness. For a particular electrode in any system, the diffusion layer thickness is dependent on the velocity of the solution past the electrode surface. As the velocity increases, the thickness of this layers decreases and the limiting current increases [Steigerwald, 1968].

2.9.3 Combined Polarization

Both activation and concentration polarization usually occur at an electrode. At low reaction rates, activation polarization usually controls, while at higher reaction rates, concentration polarization becomes controlling [Fontana, 1986; Revie and Uhlig, 2008]. The total polarization of an electrode is the contribution of activation polarization and concentration polarization:

$$\eta_t = \eta_A + \eta_C \quad (2.21)$$

where η_T is total overvoltage. During reduction process such as hydrogen evolution or oxygen reduction, concentration polarization is important as the reduction rate approaches the limiting diffusion current density. The overall cathodic over potential for activation process is given by [Fontana and Green, 1986]:

$$\eta_{red} = -b_c \log \left(\frac{i_c}{i_o} \right) + \frac{2.303 RT}{ZF} \log \left(1 - \frac{i}{i_L} \right) \quad (2.22)$$

2.9.4 Resistance Polarization

Since in corrosion the resistance of the metallic path for charge transfer is negligible, resistance overpotential η_R is determined by factors associated with the solution or with the metal surface. Thus resistance overpotential may be defined as:

$$\eta^R = I (R_{sol.} + R_F) \quad (2.23)$$

Where R_{sol} is the electrical resistance of the solution, which depends on the electrical resistivity (Ωcm) of the solution and the geometry of the corroding system, and R_F is the resistance produced by films or coatings formed on or applied to the surface of the sites. Thus, in addition to the resistivity of the

solution, any insulating film deposited either at the cathodic or anodic sites that restricts or completely blocks contact between the metal and the solution will increase the resistance overpotential, although the resistivity of the solution is unaffected [Shreir et.al, 2000].

2.10 Cathodic protection

The science of cathodic protection began in 1824 when Sir Humphrey Davy used iron anodes to protect the copper sheeting on the bottom of the British Navy's sailing ships. Since its development, cathodic protection has been used in several areas including marine and underground structures, storage tanks, and pipelines. Cathodic protection is an electrical method of mitigating corrosion on structures that are exposed to electrolytes such as soils and waters. It has had widespread application on underground pipelines, and ever increasing use as the most effective corrosion control method for numerous other underground and underwater structures such as lead cable, water storage tanks, lock gates and dams, steel pilings, underground storage tank, well casings, ship hulls and interiors. It is a scientific method which combats corrosion by use of the same laws which cause the corrosion process [James, 2013].

The principle of cathodic protection is in connecting an external anode to the metal to be protected and the passing of an electrical DC current so that all areas of the metal surface become cathodic and therefore do not corrode. The external anode may be a sacrificial anode, where the current is a result of the potential difference between the two metals, or it may be an impressed current anode, where the current is impressed from an external DC power source. In electro-chemical terms, the electrical potential between the metal and the electrolyte solution with which it is in contact is made more negative, by the

supply of negative charged electrons, to a value at which the corroding (anodic) reactions are stifled and only cathodic reactions can take place [Melchers, 2005].

There are two types of Cathodic Protection Systems:

1. Sacrificial or galvanic cathodic protection system which used of metals which are more reactive than the metal to be protected from corrosion.
2. Impressed current cathodic protection system which used of adirect current power source and auxiliary anodes.

2.11 Sacrificial Anode Method

Sacrificial anode types provide cathodic current by galvanic corrosion. The current is generated by metallicly connecting the structure to be protected to a metal/alloy that is electrochemically more active than the material to be protected (Both the structure and the anode must be in contact with the electrolyte). Current is discharged from the expendable anode, to the electrolyte, and onto the structure to be protected, as shown in Fig. 2-6[Schwenk et.al, 1997].

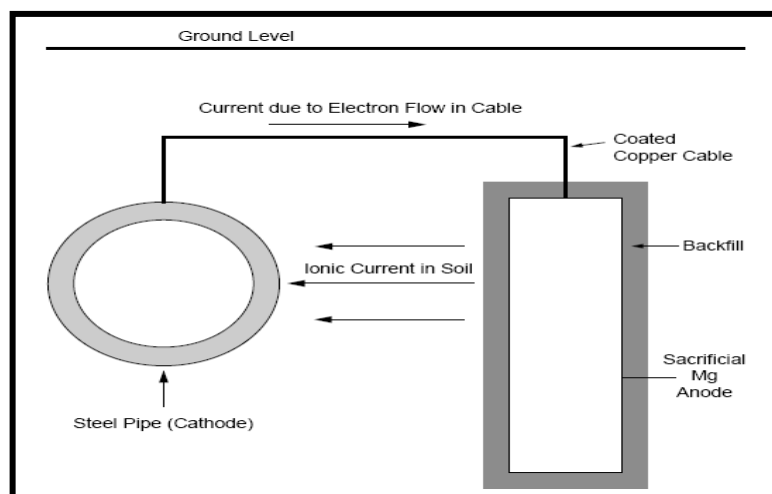


Figure 2-6 Principle of cathodic protection with sacrificial anodes [Schwenk et.al, 1997].

The basic components of a single, sacrificial anode type cathodic protection installation are the structure to be protected, the anode (with or without a special backfill), and an insulated lead wire connecting the structure to the anode [Shreir et.al, 1994].

Typical applications include buried tanks, underground pipelines, buried communication and power cables, water and gas distribution systems, internal protection of heat exchangers and hot water tanks, ships, and marine structures [Roberge, 1999].

2.12 Sacrificial Material

The materials used for sacrificial anodes are either relatively pure active metals such as zinc or magnesium, or alloys magnesium or aluminum that have been specifically developed for use as sacrificial anodes. In applications where the anodes are buried, a specific chemical backfill material surrounds the anode in order to insure that the anode will produce the desired output [Unified Facilities Criteria, 2004]. The anode material must provide a certain driving voltage to generate sufficient current to adequately protect a structure. The driving voltage is defined as the difference between the operating voltage of the anode and the potential of the polarized structure it is protecting [Roberge, 1999]. When the anode alloy is placed in the electrolyte for the protection of a structure, a certain amount of the current is generated due to the self-corrosion of the anode [James, 2013].

Zinc is widely used to protect steel against corrosion by cathodic protection, where the submerged steel structure is connected to a mass of zinc which dissolves sacrificially to protect the steel structure [Shreir, 1994].

Zinc Anode Advantages [Shreir, 1994]:

1. Very high efficiency = >90%
2. Low driving potential– This is an advantage in low resistivity environments such as sea water, brackish waters and soils with resistivities less than 2000 Ohm-cm.
3. Lowest cost in terms of dollars per pound of anode metal and lower in cost vs. magnesium anodes in underground applications where soil resistivities are less than 2000 ohm-cm.
4. Available for use both underground and under water (both salt and fresh waters).
5. Available in many size and shapes for many applications
6. All of the design formulae and principals of design used with magnesium anodes apply equally with zinc.

Zinc Anode Limitations [Shreir, 1994]:

1. Must not be used in applications where temperatures exceed 120^o Fahrenheit because inter-granular corrosion attack of the zinc will cause very premature failure of the material.
2. Susceptible to potential reversal if installed as bare anode material instead of installing with select gypsum-bentonite-sodium sulfate backfill in underground applications. Generally, this material should never be used underground except when installed with this select backfill.
3. Typically higher cost per ampere-year of cathodic protection provide than Aluminum Anodes in Seawater Applications.
4. Due to low driving potential, should not be used (except under very special circumstances) in soil resistivities greater than 2000 ohm-cm.

2.13 Corrosion in Petroleum Industry

2.13.1 Introduction

The petroleum industry contains a wide variety of corrosive environments, the oilfields are situated in tropical areas where high humidity salt bearing winds and air borne sand take the toll of structure and equipment. Moreover costly pipeline convey the crude oil often itself activity corrosive toward iron and steel to long distance either to refineries or to coastal installations. The internal corrosion experienced in typical oil and gas wells is normally associated with hydrogen sulphide, carbon dioxide and organic acids present in the oil, brine or gas. Internal corrosion is normally referred to as being sour (from "sour oil wells") or sweet ("sweet oil wells") according to the higher or lower sulphur content (mainly H_2S) of the oil [Boreman et.al 2000]. Corrosion problems may occur in numerous systems within the petroleum industry. Acidization of oil and gas wells is probably the most widely used work over and stimulation practice in oil industry as shown fig.2-7 [Migahed and Nassar, 2007].

Corrosion which takes place in an oil pipeline is basically similar that occurs in a producing oil well or any water-containing system. The water associated with pipelines always contains ions from dissolved gases (e.g. CO_3^{2-} obtained by dissolved CO_2) and salts (e.g. NaCl), thus functioning as a charge-conductive electrolyte. Gases dissolved in water or brine in a pipeline is the major cause of corrosion. Gases that are commonly found in pipelines are carbon dioxide (CO_2), hydrogen sulfide (H_2S), and oxygen (O_2) [Brondel et.al, 1994].

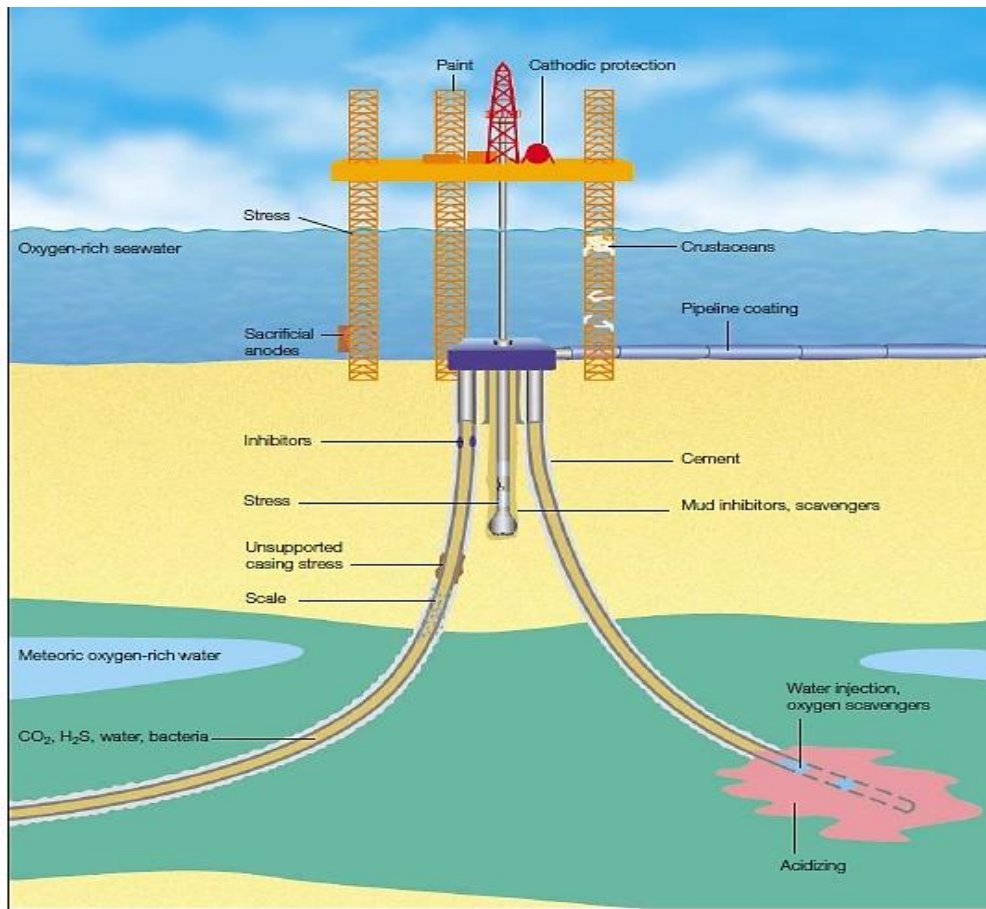


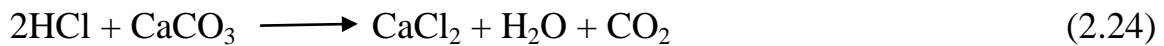
Figure 2-7 Corrosion in every aspect of oil industry, Oil well stimulation [Migahed and Nassar, 2007].

2.13.2 Acidization of oil well

Oil well stimulation, usually done with hot solutions of hydrochloric acid, may induce severe corrosion attack on production tubing, downhole tools and casing. Oil well stimulation is the general term describing a variety of operations performed on a well to improve its productivity. Opening up new channels in the rock for the oil and gas to flow through is called stimulation. Three stimulation treatments are commonly used: explosives to break up the rock, injection of acid to partially dissolve the rock, and hydraulic fracturing to split the rock and prop it open with proppants. Stimulation operations can be focused solely on the well bore or on the reservoir; it can be conducted on old wells and new wells alike;

and it can be designed for remedial purposes or for enhanced production. Its main two types of operations are matrix acidization and hydraulic fracturing [Williams and Nierode 1972].

Fracture acidizing is an alternative to hydraulic fracturing and propping in carbonate reservoirs. In fracture acidizing, the reservoir is hydraulically fractured and then the fracture faces are etched with acid to provide linear flow channels to the well bore. In limestone or carbonate formations, the acid dissolves portions of the rock in the formation, opening up existing spaces to allow for the flow of petroleum. Fracturing consists of injecting a fluid into the well, the pressure of which 'cracks' or opens up fractures already present in the formation. In addition to the fluid being injected, 'propping agents' are also used. These propping agents can consist of sand, glass beads, epoxy, or silica sand, and serve to prop open the newly widened fissures in the formation. Hydraulic fracturing involves the injection of water into the formation, while CO₂ fracturing uses gaseous carbon dioxide. Fracturing, acidizing, and lifting equipment may all be used on the same well to increase permeability, widening the pores of the formation, The acid reaction may be represented by the following equations [Williams and Nierode 1972].



Investigations into the field of corrosion under multiphase flow are typically considered huge amount of experimental parameters which may affect synergistic damage mechanism, including: flow conditions, composition of the structural material, chemical composition of the flowing system and temperature. Multiphase flows exhibit the additional challenge of requiring further phase

composition parameters with the respective physical and modeling descriptors. Furthermore, experiments in realistic conditions are extremely hard to manage. An overall lack of productivity is therefore characteristic for this kind of studies [Benedetto et. al, 2003].

However, corrosion environment of oil pipeline is more complex in real situation, and it is hard to imitate the corrosion of oil pipeline in the transportation of crude oil by the simulate experiment. Therefore, it is necessary to study the corrosion of oil pipeline by mixture of oil and water in oil field and the effect of presence of some corrosive compounds such as CO₂ [Lopez et.al, 2003].

2.13.3 Carbon Dioxide (Sweet) Corrosion

Corrosion of mild steel carbon dioxide is a major problem in the oil and gas industry, and it occurs at all stages of production from downhole to surface equipment and processing facilities [Fu et. al, 1996]. An important consideration in oil and gas industry is multiphase transport from remote wells for much more economical transport of oil and gas combined. The multiphase transport pipelines are mostly made of carbon steel and low-alloy steel, which are able to meet many of the mechanical, structural, fabrication requirements and may offer considerable capital savings over the more expensive alloys [Zheng et al, 2008].

Carbon dioxide corrosion, usually called sweet corrosion, is one of the most serious forms of corrosion in the oil and gas production, storage and transportation industry. In addition to its natural presence in deep natural gas reservoirs, the presence of CO₂ in oil is also due to its injection into the reservoir to force the oil to flow out more easily for enhanced oil recovery [Jiang et.al 2006]. Carbon steels are the most commonly used pipeline materials in

petroleum production. However, carbon steels are very prone to corrosion in environments containing CO₂ [Simison et.al, 2003]. In oil industry, CO₂ corrosion results from the water saturated with CO₂ containing chloride associated with the crude/gas production. In the last two decades the CO₂ corrosion has gained a very serious concern with the use of enhanced oil recovery techniques based on CO₂ injection reservoirs and sweet gas production from deeper wells [Takabe and Ueda, 2001].

Electrochemical corrosion of steel in carbon dioxide (CO₂) containing aqueous media is a major problem that occurs in industrial infrastructures such as carbon capture, transmission and sequestration facilities, as well as in oil and gas wells and pipelines [Wanga et.al 2011].

It is well-known that CO₂ containing solution is significantly more corrosive than normal weak acid solution at a given pH [Schmitt et. al 1984]. More corrosion of steel is caused by an aqueous CO₂ containing solution than by hydrochloric acid [Whitman et.al 1924]. The presence of carbon dioxide in a brine solution can also promote formation of a layer on the metal surface. This scale is mainly formed by calcium carbonate (CaCO₃) and iron carbonate (FeCO₃). The formation of a layer on the metal surface will depend on the brine concentration, pH, temperature and other parameters. This layer can be either protective or not, depending on the homogeneity, porosity, tenacity, thickness, adherence and the nature of the corrosion layer [Mora et.al, 2002].

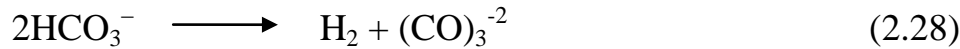
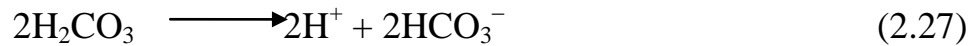
2.13.4 Mechanisms CO₂ Corrosion

The water phase dissolves CO₂, which causes its own cathodic reactions. The water phase contains also considerable amounts of dissolved salts, and thus its conductivity is high. In the oil/gas system the partial pressure of CO₂ equals

the mole fraction of CO₂ in the gas multiplied by the total pressure. The total pressure is often of the order of 100 bar, while the CO₂ partial pressure may be, e.g. about 1 bar, although it varies considerably from one site to another. A precipitated water phase in such a system dissolves CO₂ up to a concentration proportional to the partial pressure of CO₂ in the gas phase. The solubility depends also on the temperature. When CO₂ dissolves in water it gives carbonic acid [Einar, 2003]:



In an oxygen-free environment, three cathodic reactions and one anodic reaction control the subsequent corrosion process [Zhang and Cheng, 2009]:



When carbon steel corrodes in water containing CO₂, the anodic reaction is:



When the concentrations of Fe²⁺ and CO₃²⁻ ions exceed the solubility limit, solid iron carbonate precipitates on the steel surface [Sun et.al, 2004]:



Leading to the formation of iron carbonate scale. Therefore, the overall electrochemical reaction of CO₂ corrosion can be written as:



The formation of iron carbonate scale is one of the most important factors governing the rate of corrosion. When the rate of scale precipitation at the steel surface equals or exceeds the rate of corrosion, a dense, protective scale forms. If the opposite occurs, a porous and unprotective scale forms, which can sometimes be very thick [Sun et.al, 2004]. During the process of CO₂ corrosion, the

corrosion products such as FeCO_3 and $\text{Fe}(\text{HCO}_3)_2$ build up over time, partially passivating the corroding steel surface due to their limited solubility [De Waard and Milliams, 1975]. The solubility of FeCO_3 is low and decreases with increasing temperature. FeCO_3 is therefore deposited when the temperature exceeds a limit that depends on the CO_2 partial pressure (often 60–80°C). At higher temperatures it is decomposed to FeCO_3 and H_2CO_3 [Einar, 2003]. Figure 2-8 shows the principles of all available mechanistic models. The liquid phase consists of water and additives. CO_2 (g) dissolves in the liquid phase; it hydrates, dissociates to HCO_3^- and CO_3^{2-} and makes the liquid acidic. CO_2 (aq) diffuses to the pipe surface and reacts cathodically at the surface by using electrons and producing HCO_3^- and H_2 (aq) [Crolet and Bonis, 1985].

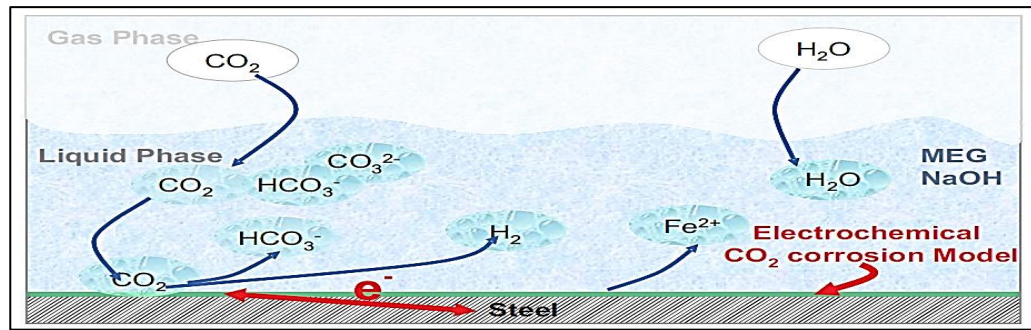
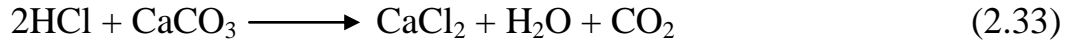


Figure 2-8: CO_2 dissolves in the condensed aqueous liquid phase diffuses to the surface and dissolves iron by an electrochemical mechanism [Crolet and Bonis, 1985].

2.14 Corrosion of iron by Acids in petroleum industry

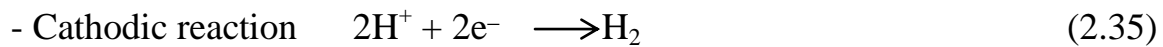
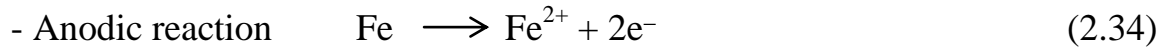
Solutions of hydrochloride acid and sulphuric acid have wide industrial applications, the most important fields being acid pickling, acid descaling in petroleum and chemical processes, industrial cleaning and oil-well acidizing [Banas et.al, 1992]. Acid is used to remove damage near the wellbore in all types of wells. In carbonate formations, acid may be used to create linear flow systems by acid fracturing. Hydrochloric acid used in field is normally 15% by weight

HCl; however, acid concentration may vary between 5% to about 35%. Hydrochloric acid will dissolve limestone, dolomite, and other carbonates. The chemical equation for the reaction between HCl acid and limestone is as follows:



The concern for corrosion by sulfuric acid has increased in the oil and gas industry because of the recent policy concerning the transformation of H₂S and SO₂ produced during oil extraction and refining into concentrated sulfuric acid.

When carbon steel contacts dilute sulfuric acid, an immediate attack on the metal takes place with the formation of hydrogen gas and ferrous ions, as shown in reactions [International Energy Agency, 2009]:



The rate of corrosion of carbon steels in dilute acids depends strongly on steel chemical compositions, especially the carbon content. Accordingly, the oxidation reaction of iron ($\text{Fe} = \text{Fe}^{2+} + 2\text{e}^-$) occurs on the ferrite phase, and the cathodic reduction reaction of hydrogen ($2\text{H}^+ + 2\text{e}^- = \text{H}_2$) occurs on the cementite phase. When carbon steel contacts concentrated sulfuric acid, the former is in fact reduced to form H₂ and the iron oxidizes with the formation of ferrous sulfate (FeSO₄), as shown in reaction:



The FeSO₄ adheres to the steel surface and forms a protective layer. This layer prevents the metal against further attack by concentrated sulfuric acid [Dean and Grab, 1985].

2.15 Mixing and Agitation

The mixing of immiscible liquid phases is among the most important chemical engineering operations. Quantitative information on the mixing process is rather lacking. Most available information is applicable only to specialized equipment or to a particular liquid system. In mixing two immiscible fluids in a stirred system, energy is transferred to the fluid by the stirrer and the energy serves to suspend the dispersed phase to create turbulence in the fluid. If the intensity of the turbulence is uniform throughout the tank, the suspended droplets would be subdivided until they were of size that was no longer affected by the turbulence. In the usual case, the intensity of the turbulence is not uniform throughout the tank and regions of varying intensity exist. In region of lower intensity, colliding droplets may coalesce, the larger droplets thus formed on passing to regions of higher intensity will again be sheared and broken up. The end state of this sequence of dispersion is a dynamic equilibrium where distribution of droplet size is established throughout the tank. Agitation systems give good similarity for emulsion type that occurs in the equipment under actual production in oil and gas deposit. Metal surface comes in contact with emulsion of oil in water or water in oil types. The first type is normally encountered in tanks and reservoirs with high water content. Also in oil refineries, these two types of emulsion are encountered. Because of considerable experimental difficulties involved, corrosion of metals in emulsion systems has been recently studied and the mechanism of this process remains unclear for a long time. Crude oil must undergo refining before it can be used as product. Once oil is pumped from the ground, it travels through pipelines to tank batteries. A typical tank battery contains a separator to separate oil, gas, and water [Jaske and

Beavers, 1998]. Corrosion rates in oil and gas pipeline applications can be predicted based on diffusion (or mass transfer) controlled corrosion models need to predict corrosion rates not only in single-phase flow conditions but, more importantly, in multiphase flow conditions. It is well known that the flow variations along pipelines, such as flow regime, wall wetting, and liquid flow velocity, have significant effects on the corrosion process in multiphase flow conditions [Wang and Nesic, 2003].

2.15.1 Standard Turbine Design

The designer of an agitated vessel has large number of choices to make as to type and location of the impeller. The proportions of the vessel, the number and properties of the baffles, and so forth each of these decisions affect the circulation rate of the liquid, the velocity patterns, and the power consumed. As starting point for design in ordinary agitation problems, a turbine agitator of the type as shown in Fig. 2-9 is commonly used. Typical proportions are in Table 3-1 [Mc Cabe et.al, 1993]:

Table 2-1 Design Equations of Agitator (Vessel)

$\frac{D_a}{D_t} = \frac{1}{3}$,	$\frac{H}{D_t} = 1$,	$\frac{J}{D_t} = \frac{1}{12}$
$\frac{E}{D_t} = \frac{1}{3}$,	$\frac{W}{D_a} = \frac{1}{5}$,	$\frac{L}{D_a} = \frac{1}{4}$

where:

Da: diameter of impeller. **Dt:** diameter of tank (cylinder).

E: distance from center of impeller to bottom of tank (cylinder). **H:** height of

tank (cylinder). **J:** width of baffles. **L:** length of impeller. **W:** width of impeller.

The number of baffles is usually four, the number of the impeller blades ranges from (4-16) but it is generally (6-8). Special situation may, of course, dictate different proportions from these listed above: it may be advantageous, for example, to place the agitator higher or lower of the tank, or a much deeper tank may be needed to achieve the desired process result. The listed standard proportions, nonetheless, are widely accepted and are the basis of many published correlation of agitator performance [Mc Cabe et.al, 1993].

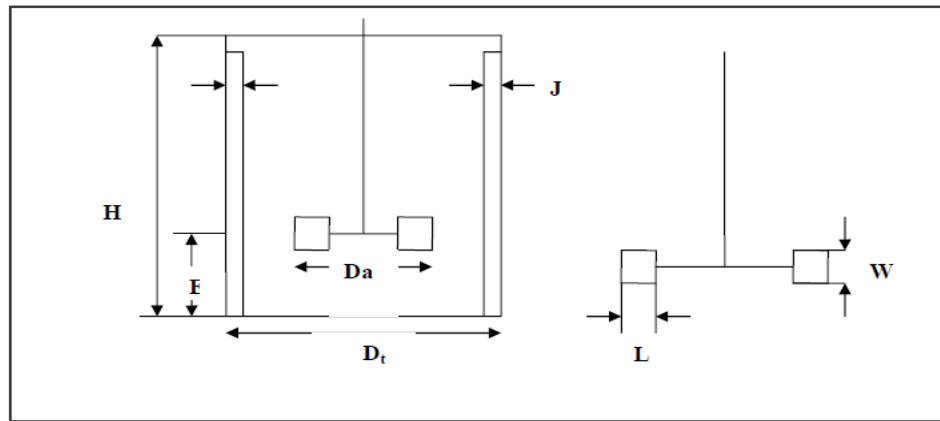


Figure 2-9 Measurements of Turbine [Mc Cabe et.al, 1993].

2.15.2 Mixing of Liquids

The key to effective mixing for liquids is to create multiple flow patterns in the fluid being mixed. This motion is imparted to a fluid "pocket" as it contacts the blade on the rotating agitator. The momentum of this pocket will keep it in motion until it either contacts the wall of the vessel, or runs into another moving pocket. The nature of the liquids and suspensions themselves affect fluid flow and mixing properties as well. These properties of concern are the fluid densities, viscosity, temperatures, pressures, and volatility. These properties have been grouped in a dimensionless formula called the Reynolds Impeller Number defined here [Oldshue, 1983]:

$$\text{Re} = \frac{\rho \times D_a^2 \times N_I}{\mu} \quad (2.37)$$

where: D_a = impeller diameter (m), N_I = rotational speed of the impeller (rps),
 ρ = fluid density (kg/m^3), μ = fluid viscosity (kg/m.s.)

2.15.3 Gas-liquid mixing

Numerous processing operations involving chemical reactions, such as aerobic fermentation, wastewater treatment, oxidation of hydrocarbons, and so on, require good contacting between a gas and a liquid. The purpose of mixing here is to produce a high interfacial area by dispersing the gas phase in the form of bubbles into the liquid. Generally, gas-liquid mixtures or dispersions are unstable and separate rapidly if agitation is stopped, provided that foam is not formed. In some cases stable foam is needed, and this can be formed by injecting gas into a liquid which is rapidly agitated, often in the presence of a surface-active agent [Coulson et.al, 1999]. Dispersion of the gas passes through several stages depending on the gas feed rate to the underside of the impeller and the horsepower to the impeller, varying from inadequate dispersion at low flow to total gas bubble dispersion throughout the vessel. The open, without disk, radial flow type impeller is the preferred dispersing unit because it requires lower horsepower than the axial flow impeller. The impeller determines the bubble size and interfacial area [Ludwig, 1999].

2.16 Literature Review

In addition to the studies stated previously, there are some studies in literature considered the effect of various factors on the corrosion of carbon steel and its control in brines solutions within petroleum processes and the possible methods to control the corrosion:

Hasan and Sadek, [2012] studied corrosion of carbon steel in sodium sulphate solution (Na_2SO_4) under flow conditions by using rotating cylinder electrode (RCE). The corrosion rate was determined by using both weight loss method and electrochemical polarization technique (limiting current density). The effect of time (or corrosion product formation) and the effect of oxygen concentration through air bubbling in the solution were also investigated. The results showed that increasing the rotational velocity lead to an increase in the corrosion rate. Also the corrosion rate had unstable trend with salt concentrations and temperature.

Ciubotariu et.al, [2010] studied the electrochemical corrosion behavior of carbon steel in sodium chloride, sodium sulphate and sulphuric acid 0.5M concentration. Corrosion data was taken for different times of immersion at room temperature under static condition. It was found that the corrosion rate is higher in 0.5M H_2SO_4 , and concluded that the polarization resistance decreases with time in H_2SO_4 because of the possibility of general corrosion with the dissolution of corrosion products while in 0.5M Na_2SO_4 and 0.5M NaCl solutions it increases with time.

Slaiman et.al, [2008] studied the corrosion of carbon steel in single-phase of 0.1N NaCl solution and two immiscible phases (kerosene–water) using turbulently agitated system. The experiments were carried out at 40°C for ranges of Re and different kerosene volume percents. It was found that increasing Re increased the corrosion rate and the presence of water enhanced the corrosion rate by increasing the solution electrical conductivity. For two-phase solution containing 8% vol and 16% vol of water, the corrosion rate was higher than single phase (100% vol water). The main parameters that play the major role in determining the corrosion rate in two phases were concentration of oxygen,

solution electrical conductivity, and the interfacial area between the two phases (dispersed and continuous).

Nor et.al, [2011] studied the corrosion of carbon steel in high CO₂ environment corrosion using a high-pressure, high-temperature, rotating cylinder electrode (RCE) autoclave and a pipe flow loop system. Corrosion rates were measured via weight loss and by electrochemical methods at various pH from 3 to 5, temperatures range of 25 to 50°C, near critical and supercritical CO₂ partial pressures and at equivalent fluid velocities from 0 to 1.5 m/s. The authors found that reducing the flow effect at high pressure due to increase the concentration of carbonic acid whose reduction is limited by hydration of dissolved CO₂. The flow velocity was not clearly observed at pH 3 even at low pressure. since the anodic reaction was under charge transfer control flow has no effect.

Martin and Mokhtar, [2009] studied the mechanism and kinetics of CO₂ corrosion in the presence of a low concentration of acetic acid in turbulent flow conditions at fixed pH and various temperatures. They observed that corrosion rate increases with increasing temperature. Furthermore, an increase in the corrosion rate due to an increase in the rotational velocity was recorded in that study until 2000 rpm. Beyond this, not much effect of rotational velocity was observed. Flow effect is related to the transport of species towards and away from metal surfaces.

Dharma et.al, [2003] studied corrosion of carbon steel in the presence of CO₂, H₂S and elemental sulfur the selected water-soluble organic inhibitors were found to be effective for controlling corrosion of carbon steel in the presence of CO₂, H₂S and S.

Ikeda et.al, [1984] found that there is a qualitative change in the corrosion kinetics at temperatures around 60°C. Below 60°C, the corrosion rate increases

with increased temperature, accompanied with the formation of the non-protective corrosion product film of iron carbide Fe_3C . However, from 60°C to 90°C , the corrosion rate reaches its maximum with increasing temperature, accompanied with the formation of the protective product film iron carbonate FeCO_3 . The corrosion rate decreases with increased temperature above 90°C due to the formation of protective iron oxide Fe_2O_3 , which becomes the main component of the product layer.

De Waard et al. [1979] proposed the first electrochemical mechanism for CO_2 corrosion of steel, considering the reduction of carbonic acid as the main cathodic reaction. Later on, Gray et al. [1980] provided a more detailed approach to the de Waard model, taking into account the reduction of hydrogen ions, carbonic acid, and water as the main cathodic reactions, and the dissolution of iron as the anodic reaction. Nesic et al.[1996] produced a mechanistic model for CO_2 corrosion based on the individual electrochemical reactions for a $\text{H}_2\text{O}-\text{CO}_2$ system. There after Pots [1995] proposed a mechanistic model to predict the corrosion rate in a CO_2 system with multiphase flow conditions. The model was based on the assumption that the transport of species happened concurrently. The model also considered mass transfer, chemical reaction, and charge transfer processes.

References

- ❖ Alwash S.H., V. Ashworth, M. Shirkhazadeh, and G.E Thompson, “an Investigation of the Reduction of Oxygen at a Rotating Disk Electrode with Heat Transfer Facilities”, *Corrosion Science*, vol. 27, pp. 1301-1311, 1987.
- ❖ Amin M. A., M. A. Ahmed, H. A. Arida, T. Arslan, M. Saracoglu, and F. Kandemirli, “Monitoring corrosion and corrosion control of iron in HCl by nonionic surfactants of the TRITON-X series Part II Temperature Effect, Activation Energies and Thermodynamics of Adsorption”, *Corrosion Science*, vol. 53, pp. 540–548, 2011.
- ❖ Bahar S. S., M. Sc. Thesis, Chem. Eng. Dept., Al-nahrian University, Bahgdad, 2002.
- ❖ Banas J., B. Mazurkiewicz and B. Stypula, *Electrochimica Acta*, 37, 1992.
- ❖ Banerjee S.N.,” an introduction to science of corrosion and it is inhibitor”, Oxonian press pvt., 1985.
- ❖ Bird R.B., W.E. Stewart, and E.N. Lightfoot, “Transport Phenomena”, second edition, John Wiley & Sons, New York, 2002.
- ❖ Boreman D.J., B.O. Wimmer, and K.G. Leewis, “Repair Technologies for Gas Transmission Pipelines,”*Pipeline and Gas Journal*, March 2000.
- ❖ Benedetto B., Marco E. Ricotti , Marco Boniardi, Claudio Melea, “Evaluation of erosion–corrosion in multiphase flow via CFD and experimental analysis”, *Wear* 255, 2003.
- ❖ Brodkey, R. S. and H. C. Hershey, “Transport Phenomena”, second edition, McGraw Hill, New York, 1998.
- ❖ Brondel D., R. Edwards, A. Hayman, D. Hill, S. Mehta, T. Semerad, *Corrosion in the Oil industry*, 1994.
- ❖ Ciubotariu A. C., L. Benea, and P. L. Bonora, “Corrosion studies of carbon steel X60 by electrochemical methods” *Journal of Optoelectronics and Advanced Materials*, No. 5, vol. 12, p. 1170 – 1175, 2010.
- ❖ Coulson J, M. and J. F. Richardson , J. R. Backhurst and J. H. Marker, “CHEMICAL ENGINEERING“ Sixth edition , Volume 1, 1999.
- ❖ Crolet, J. L.; Bonis, M. R. A “tentative method for predicting the corrosivity of wells in new CO₂ fields”. In: Burke, P. A.; Asphahani, A. I.; Wright, B. S. *Advances in CO₂ corrosion* vol. 2, 23, 1985.
- ❖ Darowicki K., Bohdanowicz W., Walaszkowski J., "Pro-Ecological Aspects of Application of Cathodic Protection" *Polish Journal of Environmental Studies* Vol. 10, No. 5, P. 325-330. 2001.

- ❖ De Waard, C., and Lotz, U., "Prediction of CO₂ Corrosion of Carbon Steel."CORROSION/93, paper no.69. Houston, NACE, 1979.
- ❖ Dean S.W., G.D. Grab, Corrosion of carbon steel by concentrated sulfuric acid, Materials Performance 24 (6), 21–25, 1985.
- ❖ Dharma Abayarathna, Ali R. Naraghi, and Nihal U. Obeyesekere, “Inhibition of Corrosion of Carbon Steel in The Presence of CO₂, H₂S and S”, Corrosion, March, 2003.
- ❖ Dugstad A. The importance of FeCO₃ supersaturation on the CO₂ corrosion of carbon steels, corrosion " paper 14. NACE, Houston 1992.
- ❖ Eid N.M.A. “Localized corrosion at welds in structural steel under desalination plant conditions Part II: Effect of heat treatment, test temperature and test media”, Corrosion Science, vol. 73, pp. 407-415, 1989.
- ❖ Einar B., "Corrosion and Protection" Engineering Materials and Processes, Springer, 2003.
- ❖ El-Batsh H.M., M.A. Doheim, A.F. Hassan, “On the application of mixture model for two-phase flow induced corrosion in a complex pipeline configuration” Applied Mathematical Modelling, 2012.
- ❖ Evans, U. R. and T. P. Haoar, “Electrochemical Mechanism of Atmospheric Rusting,” Proc. R. Soc. Lond. Ser., 1932.
- ❖ Fontana and Greene, "Corrosion Engineering", 2nd edition, McGraw – Hill, N.Y. P 2, 1978.
- ❖ Fontana M.G., “Corrosion engineering,” third edition, McGraw-Hill Book Company, New York, 1986.
- ❖ Foroulis Z. A. "The Influence of Velocity and Dissolved Oxygen on the Initial Corrosion Behavior of Iron in High Purity Water", Corrosion, Vol. 35, pp. 340-344, 1979.
- ❖ Fu S.L., J.G. Garcia, A.M. Griffin, Corrosion 96, paper no. 21, NACE International, 1996.
- ❖ Gabe D.R., and P.A. Mankanjoula, Electrochemical Eng., AIChE Symposium Series, No. 98, P.309, 1986.
- ❖ Gedeon G, “Corrosion Overview”, corrosion, vol. 4 pp. 37- 43, 2000.
- ❖ Genesca J. , R. Olalde, A. Garnica, N. Balderas, J. Mendoza, and R. Duran-Romero, “Electrochemical Evaluation of Corrosion Inhibitors in CO₂ Containing Brines”, Corrosion, NACE, vol. 00162, pp.23, 2010.
- ❖ George K. and S. Nestic, “Electrochemical Investigation and Modeling of Carbon Dioxide Corrosion of Carbon Steel in the Presence of Acetic Acid”, Corrosion 2004 NACE, vol. 04379, pp.25, 2004.

- ❖ George K. S., and S. Nestic, “Investigation of Carbon Dioxide Corrosion of Mild Steel in the Presence of Acetic Acid – Part 1: Basic Mechanisms”, Corrosion, 2007.
- ❖ Gray, L., Anderson, B., Danysh, M., and Tremaine, R., "Mechanism of Carbon Steel Corrosion in Brines Containing Dissolved Carbon Dioxide at pH 4."CORROSION /89, paper no.464. Houston, TX:NACE, 1989.
- ❖ Hany M. A., Vagif M. A., Leylufer I. A. and Teyyub A. I.” Corrosion Protection of Steel Pipelines Against CO₂ Corrosion-A Review” 1Mamedaliev Institute of Petrochemical Processes, National Academy of Sciences of Azerbaijan, 2012.
- ❖ Hasan B. O., S. A. Sadek,” Corrosion of Carbon Steel in Sodium Sulphate Salt Solution under Flow Conditions” M. Sc. Thesis, Chemical Engineering Department, Al-Nahrain University, December, 2012.
- ❖ Hasan B. O., S. A. Sadiq “The Effect of Temperature and Hydrodynamics on Carbon Steel Corrosion and Its inhibition in Oxygenated Acid- Salt Solution”, Journal of Industrial and Engineering Chemistry (JIEC), 2014.
- ❖ Hasan, B. O., “Galvanic corrosion of Al-CS in two phase flow of Gas-Liquid dispersion (CO₂-brine), unpublished Data, Chemical Eng. Dept, Alnahrain University, 2014.
- ❖ Hasan, B.O., "Heat, Mass and Momentum Analogies to Estimate Corrosion Rates under Turbulent Flow Conditions", Ph. D. Thesis. Chem. Eng. Dep., Al-Nahrain University, Baghdad, 2003.
- ❖ Hausler, R.H., and Stegmann, D.W. “CO₂ Corrosion and its Prevention by Chemical Inhibition in Oil and Gas Production”. Proceedings of CORROSION/88, NACE International, Houston, Taxes, paper No. 863, 1988.
- ❖ Heitz E., “Corrosion of Metals in Organic Solvents”, Advances in Corrosion Science and Technology, Vol. 4, 1974.
- ❖ Henry, S. D. and W. M. Scott, “Corrosion in the Petrochemical Industry”, ASM International, First Edition USA, 1999.
- ❖ Holland F. A. "Fluid flow for chemical Eng." 2nd edition, Holland and R. Bragg, 1995.
- ❖ Hussein A. M., M. Sc. Thesis, Chem. Eng. Dept, Nahrain University” Corrosion under two – phase flow kerosene / water simulated by turbulently agitated systems”, June, 2006.
- ❖ Ikeda, M. Ueda, S. Mukai, CO₂ Behavior of Carbon and Cr Steels, Advances in CO₂ Corrosion, NACE, 1984.

- ❖ International Energy Agency, Key World Energy Statistics, Paris, 6p, 2009.
- ❖ James B. B., P.E. "Corrosion and Cathodic Protection Theory", Principal Corrosion Engineer Bushman & Associates, Inc Medina, Ohio, 2013.
- ❖ Jang Y.W., N.D. Nam, M.J. Kim, J.G. Kim, Effect of tin on the corrosion behavior of low-alloy steel in an acid chloride solution, Corros. Sci. 52, 14–20, 2010.
- ❖ Jaske, C. E. and J. A. Beavers, "Predicting the Failures and Remaining Life of gas Pipelines Subject to Stress Corrosion Cracking," in Proceedings of 1998 International Gas Research Conference, pp. 281–290, 1998.
- ❖ Jiang X., Y.G. Zheng, D.R. Qu, W. Ke, Effect of calcium ions on pitting corrosion and inhibition performance in CO₂ corrosion of N80 steel, Corrosion, 2006.
- ❖ Kermani M.B., L.M. Smith, CO₂ Corrosion Control in Oil and Gas Production, the Institute of Materials, London, 1997.
- ❖ Kermani, M.B., and Morshed, A. "Carbon dioxide corrosion in oil and gas production" – A compendium. Corrosion, 59, pp. 659-683, 2003.
- ❖ Khadom A. A., A. S. Yaro, A. H. Kadum, A.S. AlTaie and A. Y. Musa "The Effect of Temperature and Acid Concentration on Corrosion of Low Carbon Steel in Hydrochloric Acid Media", American Journal of Applied Sciences, No. 7, vol. 6, pp. 1403-1409, 2009.
- ❖ Lopez, D.A., Perez, T., Simison, S.N., The influence of microstructure and chemical composition of carbon and low alloy steels in CO₂ corrosion- A state of art appraisal, Material & Design, 24, 2003.
- ❖ Ludwig, Ernest E., "Applied Process Design for Chemical and Petrochemical Plants" Third Edition, Volume 1, 1999.
- ❖ Mahato B. K., C. Y. Cha and W. Shemlit, "Unsteady State Mass Transfer Coefficients Controlling Steel Pipe Corrosion under Isothermal Flow Conditions", Corrosion Science, vol.20, pp.421–441, 1980.
- ❖ Mahato B. K., F. R. Stewrd and L. W. Shimlit, "Steel Pipe Corrosion under Flow Condition - II Mass Transfer Correlations with Temperature Effects", Corrosion Science J., vol.8, pp.737–749, 1968a.
- ❖ Mahato B. K., S. K. Voora and L. W. Shemilt, "Steel Pipe Corrosion under Flow Condition - an Isothermal Correlation for a Mass Transfer Model" Corrosion science, vol. 8, pp. 173–193, 1968b.
- ❖ Martin Choirul Fatah and Mokhtar Che Ismail, "Effect of Low Concentration Acetic Acid on CO₂ Corrosion in Turbulent Flow

- Conditions" Department of Mechanical Engineering University Teknologi Petronas , December 2009.
- ❖ Maxwell S: “Assessment of Sulfide Corrosion Risks in Offshore Systems by Biological Monitoring”, SPE Production Engineering, Vol. (1), No. (5), P. (363-368), September, 1986.
 - ❖ McCabe W. L., Smith L., Harriott P.,”Unit Operations Of Chemical Eng.”, McGraw –Hill international 6th edition, 1993.
 - ❖ Melchers, R. E., "The Effect of Corrosion on the structure reliability of Steel Offshore Structures", Corrosion Science, Vol. 47, No.10, Pp.2391-2410, 2005.
 - ❖ Migahed M.A., I.F. Nassar “Corrosion inhibition of Tubing steel during acidization of oil and gas wells” Egyptian Petroleum Research Institute, Nasr City, Cairo, 7 November, 2007.
 - ❖ Mora-Mendoza J. L., J. G. Chacon-Nava, G. Zavala-Olivares, M. A Gonzalez-Nunez, and S. Turgoose, “Influence of Turbulent Flow on the Localized Corrosion Process of Mild Steel with Inhibited Aqueous Carbon Dioxide Systems”, Corrosion, vol.58, pp.608-619, 2002.
 - ❖ Musa A. Y., A. A. H. Kadhum, A. B. Mohamad, M. S. Takriff, S. K. Kamarudin, and A. R. Daud, “Determination of Mild Steel Corrosion Rate under Turbulent Flow in Highly Acidic Solution”, journal of applied science, No. 13, vol. 11, pp.2464-2466, 2011.
 - ❖ Nathan C., “Corrosion Inhibitors”, National Association of Corrosion Engineers, Houston, 1973.
 - ❖ Nelson, W. L., “Petroleum Refinery Engineering,” 4th ed., McGraw-Hill, New York, 1958.
 - ❖ Niyazi A. and U. Serpen, “Acidizing in Geothermal Wells and HCl Corrosion” Dokuz Eylul University-Izmir-Turkey, Bali, Indonesia, 25-29, April 2010.
 - ❖ Nor A. M., M.F. Suhor, M.F. Mohamed, M. Singer and S. Nestic, “Corrosion of Carbon Steel in High CO₂ Environment: Flow Effect” NACE International, corrosion 2011, vol. 11242, pp. 18, 2011.
 - ❖ Ohio, Jones L., “Corrosion and Water Technology for Petroleum Producers”. ASM Handbook Volume 13 Corrosion. Materials, USA: ASM International, 1992. For an easier read: Tulsa, Oklahoma, USA: OGCI Publications, 1988.
 - ❖ Oldshue J.Y.,”Fluid Mixing Technology, Chemical Eng.”, 1st. Ed., New york , McGraw –Hill Newyork, 1983.

- ❖ Panvel I., Training manual on production operations for non- production engineers, Institute of oil & gas production Technology, ONGC Ltd, 2006.
- ❖ Papavinasam S., R.W. Revie, M. Attard, A. Demoz, and K. Michaelian, “Comparison of Laboratory Methodologies to Evaluate Corrosion Inhibitors for Oil and Gas Pipelines”, Corrosion, vol.59, pp.897-912, 2003.
- ❖ Perez N. “Electrochemistry and Corrosion Science” Kluwer Academic Publishers, USA, 2004.
- ❖ Perry, R. H. and C. H. Chilton, “Chemical Engineering Hand-Book,” 6th ed., McGraw-Hill, USA, 1997.
- ❖ Pickett D. J., K. L. ong “The influence of Hydrogen and Mass Transfer Entrance Effects on The operation Of parallels Electro. Cell” Vol.19,1974.
- ❖ Ponce-de-Leo’n C., C. T. J. Low, G. Kear, and F. C. Walsh, “Strategies for the Determination of the Convective-Diffusion Limiting Current from Steady State Linear Sweep Voltammetry”, J. Appl. Electrochem. , vol. 37, pp. 1261–1270, 2007.
- ❖ Popoola, L. T. , Alhaji S. G., Ganiyu K. L., Babagana G., Adebori S. B., Corrosion problems during oil and gas production and its mitigation International Journal of Industrial Chemistry, 2013.
- ❖ Postlethwaite J., S. Nestic , S. Olsen, An Electrochemical Model for Prediction of Corrosion of Mild Steel in Aqueous Carbon Dioxide Solution, Paper No. 67, NACE International, 1996.
- ❖ Pots, B. F. M., "Mechanism Models for the Prediction of CO₂ Corrosion Rates under Multi-Phase Flow Conditions. “Corrosion/95, paper no.137. Houston, TX: NACE, 1995.
- ❖ Poulson B., “Advances in Understanding Hydrodynamic Effect on Corrosion”, Corrosion Science, No.1- 4, vol.35, pp.655-665, 1993.
- ❖ Rajappa S., R. Zhang, and M. Gopal, “Corrosion in Multiphase Systems Center”, Corrosion 98 NACE, vol.26, pp.2-26, 1998.
- ❖ Revie R.W. and H. H. Uhlig, “Corrosion and Corrosion Control an Introduction to Corrosion Science and Engineering” fourth edition, John Wiley & Sons, Inc., Hoboken New Jersey, 2008.
- ❖ Riesenfeld F. C., C. L. Biohm, Petroleum Refiner, Vol. 29, No. 4, p. 141, 1950.
- ❖ Roberge, P.R. "Handbook of Corrosion Engineering", McGraw-Hill, 1999.

- ❖ Robert G., Kelly and J. R. Scully, D. W. Shoesmith, and R. G. Buchheit "Electrochemical Techniques in Corrosion Science and Engineering", Marcel Dekker, Inc. New York, 2003.
- ❖ Rodriguez A. Garnica, J. Genesca, M. J. Flores, and R. Duran-Romero, "Electrochemical Evaluation of Aminotriazole Corrosion Inhibitor under Flow Conditions", J. Appl. Electrochem., vol.39, pp.1809-1819, 2009.
- ❖ Ross T. K., G. C. Wood, & I. Mahmud, "The Anodic behaviour of Iron-Carbon Alloys in Moving Acid Media", J. Electrochem. Soc., vol. 113, pp. 334-345, 1966.
- ❖ Scheers P.V., "The Effects of Flow Velocity and PH on the Corrosion Rate of Mild Steel in a Synthetic Mine Water", J. S. Afr. Inst. Min. Metall., No. 10, vol. 92, pp. 275-281, 1992.
- ❖ Schmitt G.," Fundamental aspects of CO₂ corrosion", in: R.H. Hausler, H.P. godard (Eds.), Advances in CO₂ corrosion, NACE, Houston, Texas, 1984.
- ❖ Schwenk w., W. von Baeckmann, H. Bohnes, G. Franke, D. Funk, C. Gey, "Handbook of cathodic corrosion protection" theory and practice of electrochemical protection processes, third edition, 1997.
- ❖ Selman J.R.,"AICHE", Vol.77, No.204, P.88, 1981.
- ❖ Shreir L.L., Jarman R.A., and Burstein G.T., "Corrosion Control" Vol 2, 3rd edition, 1994.
- ❖ Shreir L.L., R.A. Jarman and G.T. Burstein," Corrosion Metal / Environment Reactions" third edition, Butterworth-Heinemann Volume I, Great Britain, 2000.
- ❖ Simison S.N., D.A. Lopez, S.R. de Sanchez, "The influence of steel microstructure on CO₂ corrosion. EIS studies on the inhibition efficiency of benzimidazole", Electrochim. Acta 48, 2003.
- ❖ Slaiman Q. J. M. and B. O. Hasan "Study on Corrosion Rate of Carbon Steel Pipe under Turbulent Flow Conditions" The Canadian Journal of Chemical Engineering, Vol. 88, pp. 1114- 1120, 2010.
- ❖ Slaiman Qasim J. M., Basim O. Hasan, and Hussein A. Mahmood," Corrosion Inhibition of Carbon Steel Under Two-Phase Flow (Water–Petroleum) Simulated by Turbulently Agitated System" Chemical Engineering Department, Nahrain University, The Canadian Journal OF Chemical Engineering, Volume86, April 2008.
- ❖ Steigerwald, R. F.," Corrosion", No.24, p. 1, 1968.
- ❖ Stern, M. Corrosion-NACE, Vol. 13, pp. 97, 1957.

- ❖ Sun W., K. Chokshi, S. Netic, D.A. Gulino, A Study of protective iron carbonates scale formation in CO₂ corrosion, in: AICHE annual meeting, 2004.
- ❖ Sun Y., K. George, and S. Netic, “The Effect of Cl⁻ and Acetic Acid on Localized CO₂ Corrosion in Wet Gas Flow”, Corrosion 2003 NACE, pp.28, 2003.
- ❖ Takabe H., M. Ueda, “the Formation Behavior of Corrosion Protective Films of Low Cr Bearing Steels in CO₂ Environments”. Corrosion 2001, Paper 1066, NACE International, Houston, TX, 2001.
- ❖ Tayaperumal D., S. Muralidharan, G. Venkatchari, N.S. Rengaswamy, Anti-corros. Method Mater, 2000.
- ❖ Tretheway, K. R. and Chamberlain, " Corrosion Science and Engineering", 2nd Edition. , Longman, London, 1996.
- ❖ Turkee H. M., “Investigation of the Performance of Some Corrosion Inhibitors in Aerated Acid Solutions” M.Sc. Thesis, Dept. of Chem. Eng., University of AL-Nahrain, Baghdad, 2009.
- ❖ Wan R., Advanced well completion engineering: “Oil and Gas Well Corrosion and Corrosion Prevention”, third ed., Elsevier Inc., Oxford, UK, 2011.
- ❖ Wang, S. and S. Netic, “On Coupling CO₂ Corrosion and Multiphase Flow models,” Corrosion, 2003.
- ❖ Wanga M., A. Lawal, P. Stephenson, J. Sidders, C. Ramshaw, Post-combustion CO₂ capture with chemical absorption: a state-of-the-art review, Chem. Eng. Res. Des. 89, 2011.
- ❖ West, J. M., "Electrode position and Corrosion Processes", Van Nostrand Reinhold Company, 2nd ed., vol.1, (1976).
- ❖ Whitman G.W., R.P. Russel, V.J. Altieri, Effect of hydrogen-ion concentration on the submerged corrosion of steel, Ind. Eng. Chem. 16 (1924) 665–670.
- ❖ Williams, B.B., Nierode, D.E., Design of acid fracturing treatments, paper presented at Trans SPE of AIME, 1972.
- ❖ Zehbour Panossian, Neusvaldo Lira de Almeida , Raquel Maria Ferreira de Sousa , Gutemberg de Souza Pimenta , Leandro Bordalo Schmidt Marques “Corrosion of carbon steel pipes and tanks by concentrated sulfuric acid” Corrosion and Protection Laboratory, 2 February 2012.
- ❖ Zheng Donghong, Defu Che, Yinhe Liu, “Experimental investigation on gas–liquid two-phase slug flow enhanced carbon dioxide corrosion in vertical upward pipeline”, Corrosion Science 50, 3005–3020, 2008.

الخلاصة

تم اجراء تجارب تأكل الفولاذ الكربوني في طور احادي وثنائي المحلول من السوائل غير الممتزجه (محلول كاربونات الكالسيوم وزيت الغاز) وغاز مع السائل (محلول كاربونات الكالسيوم وغاز ثنائي اكسيد الكربون) تحت ظروف تشغيل مختلفة من درجة حرارة، وسرعة جريان سائل، معدل تدفق الغاز، والزمن باستخدام طريقة فقدان الوزن وتقنية الاستقطاب الكهروكيميائي. حيث تم استخدام خلاط متكون من قرص وشفرات لخلط الطور الثنائي. تم اجراء التجارب تحت سرع خلط تتراوح بين ٠-١٢٠٠ دورة/ دقيقة، ودرجة حرارة بين ٢٥- ٥٥ م^٥، ونسبة حجم زيت الغاز (١- ١٠ %). تم دراسة تأثير وجود الحوامض مثل حامض الهيدروكلوريك وحامض الكبريتيك على معدل التآكل في مرحلتين امتزاج الخليط ايضا تحت ظروف مختلفة. تم قياس معدل التآكل في محلول مشبع بغاز ثنائي اكسيد الكربون في ظروف تشغيل مختلفة من درجات الحرارة، وجريان الخليط بين ٠- ٨٠٠ دورة/ دقيقة، وتركيز الاملاح (٢.٥-١٠^{-٢} - ٩.٩-١٠^{-٣} مولاري)، معدل تدفق غاز ثنائي اكسيد الكربون (٠.١٤٢-١.١٣٢ م^٣/ساعة)، والوقت بواسطة حساب كثافة التيار المحدد. أجريت القياسات الأساسية المختلفة التي تساعد في تفسير النتائج التي تم الحصول عليها مثل قيم درجة الحمضية، ذوبان الاوكسجين، والموصلية الكهربائية تحت ظروف مختلفة. واطهرت النتائج ان زيادة سرعة الخلط ودرجة الحرارة الى زيادة معدل التآكل لطور أحادي المحلول وفي طور ثنائي المحلول (ملح كاربونات الكالسيوم وزيت الغاز بوجود الحوامض). كان معدل التآكل في خليط محلول الملحي وزيت الغاز يتجه الى كونه غير مستقر مع تركيز زيت الغاز وسرعة الخلط. في محاليل الملح كاربونات الكالسيوم كثافة التيار المحدد يزداد مع زياده سرعة الخلط، وتركيز الملح، ودرجة الحرارة. أما معدل التآكل في طور الثنائي المتكون من خليط ملحي وغاز ثنائي أكسيد الكربون يناقص مع زياده سرعة الخلط اعتمادا على معدل تدفق الغاز ثنائي اكسيد الكربون، ودرجة الحرارة، والزمن. بشكل عام زياده معدل تدفق غاز ثنائي أكسيد الكربون يسبب انخفاض واضح في معدل التآكل خصوصا في حال سرعة الخلط العالية. تم قياس فرق الجهد تأكل لكاربون الفولاذي تحت ظروف مختلفة ومناقشتها.

تم استخدام الحماية الكاثودية لحماية الفولاذ الكربوني في خليط محلول ملحي وغاز ثنائي أكسيد الكربون باستخدام الزنك كقطب مضي تحت ظروف تشغيل مختلفة كمعدل تدفق غاز ثنائي اكسيد

الكاربون، سرعة الخلط، ودرجة الحرارة عن طريق قياس فرق جهد التآكل وطريقة فقدان الوزن. وقد حققت النتائج حماية جيدة للتآكل تحت ظروف وصلت الى ٩٣.٦%. وبالإضافة الى ذلك ، تم تحديد فرق الجهد للتآكل مع مرور الوقت (المعادن الفولاذ الكاربوني وزنك) وكذلك الفقدان في الوزن لكل معدن.